ACOUSTIC BEHAVIOR OF FLOW FROM FRACTURE TO WELLBORE

A Thesis

by

KYLE CHEN

Submitted to the Office of Graduate and Professional Studies of
Texas A&M University
in partial fulfillment of the requirements for the degree of

MASTER OF SCIENCE

Chair of Committee,	Ding Zhu
Co-Chair of Committee,	A. Daniel Hill
Committee Member,	Yong-Joe Kim
Head of Department,	A. Daniel Hill

May 2015

Major Subject: Petroleum Engineering

ABSTRACT

Acoustic sensing technology has a long history of being implemented in the oil and gas industry; from the early days of measuring seismic activity to determine oil and gas reserve to the present day technology such as fiber optic Distributed Acoustic Sensing (DAS) in the near wellbore measurement. The newly adapted DAS technology is capable of measuring the acoustic signature in the near wellbore fracture region and analyzing the measured data to predict important downhole parameters such as active producing zone, flow rate, etc. However, DAS is still a new technology partially due to the complexity of the acoustic phenomenal it tries to analyze.

In this study, how different parameters influence the acoustic behavior is investigated. The study is conducted on a laboratory setup that simulates the downhole condition when fluid flows from the fracture and perforation tunnel to the wellbore. To better simulate the downhole condition, a fracture cell and wellbore assembly are designed and built to conduct the experiments. The laboratory setup and experimental procedure are described in detail in the experimental setup section. The result of the experiments conducted under different conditions is shown in the experimental result section. Based on the experimental result, different parameters change the acoustic signal differently. An empirical correlation is concluded from the experimental result to relate flow rate and acoustic signal. The study also concludes that important downhole parameters such as flow rate can be estimated from the distributed acoustic sensing data.

NOMENCLATURE

SPL = sound pressure level in dB

N_{600}^{*} = peak to peak noise level above 600 Hz in millivolts

ρ = density in pounds per cubic foot

A_s = pipe cross sectional area in square feet,

q = is volumetric flow rate in thousand cubic feet per day

C'' = a constant coefficient

μ = viscosity in cp

D_p = the perforation diameter in inch.

TABLE OF CONTENTS

LIST OF FIGURES

LIST OF TABLES

1. INTRODUCTION

1.1 Acoustic Sensing Background

Acoustic is defined as generation, transmission and reception of energy as vibrational wave (Kinsler et al. 2000). Indeed sound plays a vital role in people's lives today; from being engaged in a conversation with other people to listening and playing music. For the average young person, a vibrational disturbance is interpreted as sound if its frequency lies in the interval from 20 Hertz (Hz) to 2000 Hz (Kinsler et al. 2000). Other examples of technologies impact people's daily lives occupy other part of the frequency spectrum are ultrasonic, wireless network, infrared remote control, etc. Acoustic sensing technology has a long history of being implemented in the oil and gas industry; from the early days of measuring seismic activity to determine oil and gas reserve to the present day technology such as fiber optic Distributed Acoustic Sensor (DAS) (Molenaar et al. 2011). Regardless of the advancement in acoustic measuring system, the goal is still to characterize hydrocarbon flow. Typically in the oil and gas industry, scientists and engineers measure the acoustic signal ranging between 20 Hz to 2000 Hz and apply Digital Signal Processing (DSP) techniques in both time and frequency domain to the measured data to obtain an acoustic characteristic of the measured phenomenal. The processed data is then merged with mathematical interpretation model to predict critical information for crude oil exploration and production.

In the oil and gas industry, a major breakthrough comes from the research and development work done by McKinley et al. around 1973. In his publication, he credited Enright for being the first one had the idea of noise logging in 1955 and qualitatively described a procedure for locating downhole (McKinley et al. 1973). McKinley et al. performed experimental work on both signal phase fluid and two phase fluid leaks, he observed frequency peaks from experimental results and established mathematical model to relate noise amplitude and flow rate (McKinley et al. 1973). Since his original work, there has been implementation of his technique in field cases in the area of production logging throughout the years (Hill 1990). Due to the technology limitation at the time, no major scientific breakthrough in acoustic logging has been developed over the years until late 1990s. Partially fueled by the telecommunication boom, fiber optic cable was being developed to offer more data bandwidth and speed to its competitor copper cables. Fiber optic cables were then being adapted to use as passive sensors based on the discovery that the backscatter light intensity in the fiber cable changes if the cable experiences external disturbance such as temperature and vibration.

The fiber optic sensing technology in the oil and gas application has grown exponentially over the years. It's currently being used in a variety of applications such as pipeline leak monitoring (Cannon and Aminzadeh 2013). The passive fiber optic sensing offers clear advantage to other sensing technologies. Perhaps some of the most attracting pieces of the distributed fiber optic sensing are no electrical power required connecting the sensor, lower cost of sensing over a long distance; high data resolution and bandwidth, reliability in high temperature environment, etc. There is an increasing

number of major oil and gas companies deploying or testing distributed fiber optic sensing technology in a couple of their wells in the last 10 years. The most developed technology in the distributed fiber optic sensing family is Distributed Temperature Sensing (DTS) at this point. The DTS technology uses the same fiber optic distributed sensor measuring the vibration and acoustic effect to measure temperature. Compare to DTS, the DAS technology is still in the research and development phase.

1.2 The Principle of Acoustic Sensing

Sound wave is a complex phenomenal to measure in space; the wave varies its characteristic in real-time. The characteristic of the wave include many parameters such as amplitude, phase, dynamic range, sensitivity, etc. It's a difficult task to reproduce two of the same exact sound. The two main acoustic measuring system in the oil and gas industry are electroacoustic and fiber optic devices. The electroacoustic devices such as hydrophone has been the standard for measuring sound for years; it basically converts acoustical energy into electrical energy. Electroacoustic device contains a diaphragm or moving surface that is excited by the acoustical wave, and the device outputs electrical signal that represents the acoustic input (Ballou 2006). Fiber optic sensing system works very differently. Fiber Bragg Grating (FBG) and Backscattering Reflectometer are the two main types of fiber optic sensors. Backscattering Reflectometer is used more commonly in the oil and gas industry. A FBG sensor utilizes periodic variation in the refractive index that purposely introduced in the optic fiber core to cause a shift in the light wavelength when external disturbance such as temperature occurs (Pal 2006). The

Backscattering Reflectometer uses either a single mode or multi-mode fiber optic cable without any grating in the core of the fiber. The Reflectometer measures the backscatter of the light when it travels through the fiber optic cable. When the light travels through the external disturbance region, certain frequency component of the backscatter light shifts and changes amplitude on the spectrum. Both types of fiber optic sensing system utilize a laser diode that generates modulated laser pulses, as the light travels though the fiber cable optical decoder converts the light signal back to electrical signal for data recording and processing.

Distributed fiber optic sensing is a unique architecture of the fiber optic sensor. As the light travels through the entire fiber optic cable, optical decoder repeats the measurement of intensity of the backscatter light at a sampling rate. The sample rate can be correlated with the velocity of light travels in fiber optic cable to obtain the distance interval of the measured data. From this distance interval along with time domain information, one can predict the location and type of external disturbance region.

1.3 Research Objectives

There are three main research objectives. The first one is to determine how different parameters such as flow rate, fracture geometry, perforation impact the acoustic behavior through laboratory study. After understand the relationship between downhole parameter and acoustic behavior change, the next step is to develop a model that takes DAS measurement data as input, after processing the DAS measurement data through advanced algorithm the model outputs important downhole unknown properties.

Important downhole unknown properties include but not limited to gas/oil flow rate, producing/non-producing zones, Gas Oil Ratio (GOR), fracture location, and fracture geometry. The final objective is to use the DAS model to diagnose and optimize the hydraulic fracture operation. The full potential of the DAS system is still unknown today, but there are a handful of proven DAS system capability based on field case DAS measurements and analyses (Molenaar and Cox 2013).

In order to achieve the research goal, multiple phases of the project in a sequence are taken. The first phase involves the study of possible parameters affect the acoustic behavior of flow from fracture to wellbore in a controlled laboratory environment. The outcome of this phase of the project will ease the difficulty level of future mathematical modeling by effectively reduce the number of parameters influence the change of acoustic behavior. The first phase involves running a matrix of experiments to collect acoustic data; the acoustic data will then be analyzed using DSP techniques to determine if acoustic signal patters can be seen in the experimental outcomes. The second phase utilizes the results of measured DAS lab data to develop a quantitative analysis model to simulate the acoustic behavior of flow through a single fracture and wellbore. Once the model for single fracture and wellbore model is established, an upscaling procedure will take the single facture and perforation model to field scale. After completion of the field scale model, case studies will be performed utilizing the developed model to diagnostic and optimize hydraulic fracture operations.

This thesis only attempts to achieve the first goal of the research. It's attempted to study how different parameters change the acoustic behavior of flow from a fracture

to a wellbore in a controlled laboratory setup. A detailed description on the laboratory setup and how the experiments are conducted is provided. Following the setup description, experimental results and the significant findings are presented. Finally, the conclusions are drawn from all of the experimental results.

2. EXPERIMENTAL SETUP

2.1 System Overview

A fracture cell is designed and machined to simulate a typical fracture geometry caused by hydraulic fracturing. Proppant are evenly placed inside the fracture cell. The experimental apparatus consists of a fracture cell and a pipe. The fracture cell is connected to the pipe through perforation tunnels. Nitrogen, compressed air, water, and mixture of gas/liquid are injected at different pressure and flow rate to the inlet of the fracture cell. A hydrophone is suspended off an L-bracket, and the measuring head is placed above the perforation tunnel with distance adjusting capability to the perforation tunnel. A data acquisition system collects all of the sound samples and saves measured data into a Comma-Separated Values (CSV) text file format. The CSV data file then undergoes post experiment analysis utilizing signal processing techniques. The data acquisition system collects multiple sets of 10 seconds and 30 seconds of continuous audio signal at 50 kHz sampling rate and 24-bit resolution for single hydrophone measurement setup. A Computer-Aided Design (CAD) picture of the experimental setup schematic is shown in Figure 1.

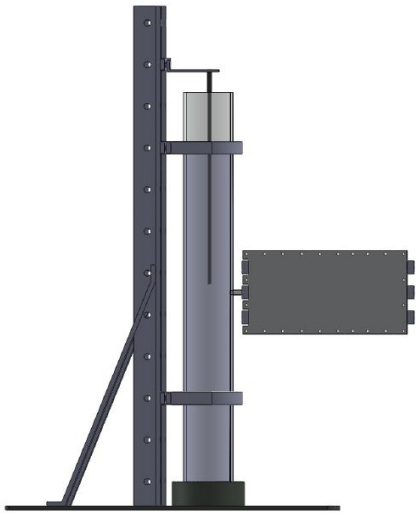

Figure 1: Example of Fracture Cell Experimental Setup

2.2 Mechanical Component

Experimental mechanical components consist of a wellbore assembly, fracture cell assembly, data acquisition assembly, and supporting base. Most of the experimental setup parts are screwed together except a few welded pieces. The system is flexible to be taken apart and reassemble together when the experiment setup changes. Supporting base and rail are made out of steel and structurally tested to withhold all of the load exerted by the experimental setup.

2.2.1 Fracture Cell

A fracture cell assembly simulating typical long and thin fracture geometry is designed and machined to study how different downhole parameters affect the acoustic behavior. A CAD drawing of the fracture cell is shown in Figure 2. The fracture cell has

outer dimension of 18-in (length) x 10-in (height) x 1.7-in (thickness). The entire fracture cell is made out of aluminum. All of the parts are assembled together using various sizes of screws and nuts.

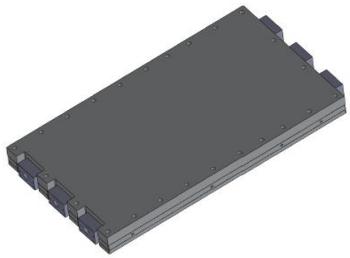

Figure 2: Fracture Cell Assembly-Isometric View

Dimension of the inner fracture cell is 16-in (length) x 8-in (height) x 0.2-in (thickness). A transparent view of the inside of fracture cell is shown is Figure 3. Inside the fracture cell, there are rows of small threaded holes for 2 detachable rails. The purpose of those rails is to simulate the effect of multiple fracture and different perforation height behavior. Those threaded holes reserved for detachable rails are plugged with screws when rails are not in use. Outlet opening of the cell has a geometry of 0.5-in (height) and 0.2-in (thickness). This geometry simulates the shape of the fracture at the connection point to a circular shaped perforation tunnel. This fracture opening is then connected to a circular shaped perforation tunnel through an adapter piece. The geometry change from the fracture cell outlet to perforation tunnel simulates the connection between the fracture to the wellbore through perforation.

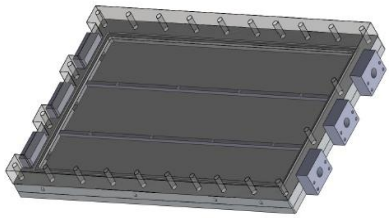

Figure 3: Fracture Cell Assembly-Transparent View

The detailed design of the fracture cell is shown in Figure 4. To assemble the entire fracture cell, the center piece is screwed into the bottom piece with appropriate O-ring placed to prevent leak. The next step is to put rails in for different fracture height or screw the plugging screws into threaded holes reserved for rails if rails are not need for the experiment. Next step is to screw in L-shaped screen to the threaded hole on the inner wall of the cell to prevent proppant coming out of the outlet opening during experiment. Fully pack the proppant into the cell and screw in the cover piece with O-ring in place following a specific pattern to prevent leak is the next step. After main part of the cell is assembled, Screw in the inlet and outlet adapter pieces with O-ring in the designed groove. The final step is to test for leaks by inject gas at the highest pressure point of the experiment intends to run for a continuous period of time.

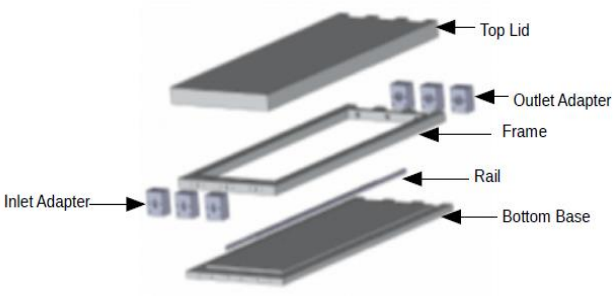

Figure 4: Fracture Cell Assembly-Explode View

The top cover of the cell is made of 1 inch aluminum to prevent deformation. Another configuration of the cell is a transparent top cover piece made of of acrylic; this configuration of the cell allows researchers to see the flow pattern inside of the cell. However, the pressure rating of the acrylic cover is significant lower than the aluminum top cover. After some experiments, pressure rating of the acrylic cover is 30 psi and aluminum pressure is at least 160 psi. All of the experiments in this thesis is based on aluminum top cover due to the high injection pressure and flow rate requirement.

2.2.2 Vertical Wellbore

A single fracture vertical wellbore setup is shown in Figure 5. The platform and wellbore pipe are both built with steel. The wellbore pipe simulates a field production string with a standard 5.5 inch outer diameter (OD) found in typical well operation. The wellbore pipe and fracture cell are connected through standard National Pipe Thread (NPT) pipe. By changing the wellbore pipe hole, fracture cell outlet adapter piece, and NPT pipe connecting the two; different sizes of perforation tunnel can be tested.

A hydrophone is suspended off an L-bracket. By adjusting the location of the L-bracket, typical oil field operation such as raising and lowering of the sensor system during production logging procedure is simulated. Nitrogen, compressed air, water, and mixture of gas/liquid are injected at different known pressure and flow rate to the inlet of the fracture cell. Sound is measured at the perforation tunnel in the wellbore to study the acoustic behavior of flow from facture to wellbore.

The hydrophone used in the experiment is made by Bruel & Kjaer. The manufacture part number is 8103. The hydrophone has sensitivity of 1 V/mPa. In the distributed sensor array setup, 3 additional microphone is added as measurement device. The microphone is manufactured by GRAS Sound & Vibration. The manufacture part number of the microphone is 40PH. The 40PH microphone has sensitivity of 50 mV/Pa. Both hydrophone and microphone are sufficient to measure single phase nitrogen gas flows from fracture cell to wellbore. When measuring multiphase flow, acoustic signal can only be measured with hydrophone.

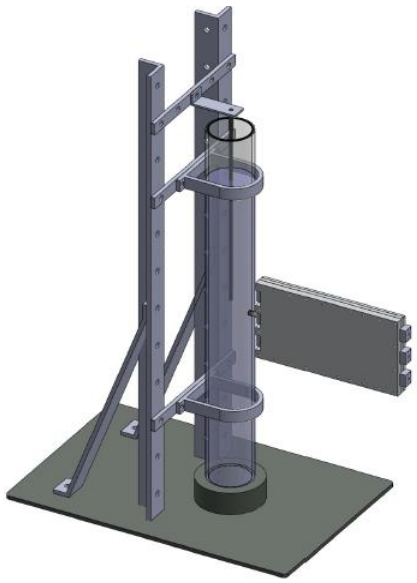

Figure 5: Vertical Wellbore Single Fracture Setup

2.2.3 Horizontal Wellbore

The flexibility of the experimental setup design allows to convert the vertical wellbore setup to a horizontal wellbore setup. A 90 degree bend steel pipe is used to connect the vertical and horizontal section of the wellbore pipe. Flange is welded to the end of the pipe and pipes are connected using bolts and nuts. With this horizontal wellbore design, fracture cell can be connected to the horizontal wellbore in any angle through the perforation tunnel. Also, multiple fractures can be added to the horizontal wellbore by machine out more fracture cells. A CAD drawing of a single fracture and single stage horizontal wellbore setup is shown in Figure 6.

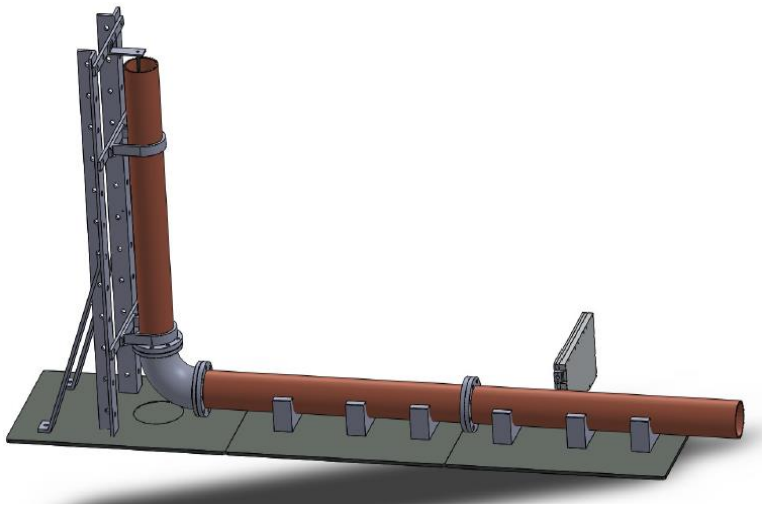

Figure 6: Horizontal Wellbore Single Fracture and Single Stage Setup Example

Not only can multiple fractures be incorporated into the horizontal wellbore, multiple stages of the horizontal wellbore can be assembled as well. By adding another wellbore pipe with 2 flanges welded at both ends, the single stage setup becomes a two stage horizontal wellbore setup. The horizontal wellbore setup can become multiple fracture and multiple stage design by adding more fracture cell assembles and sections of wellbore pipes. Figure 7 shows a possible multiple horizontal stage configuration.

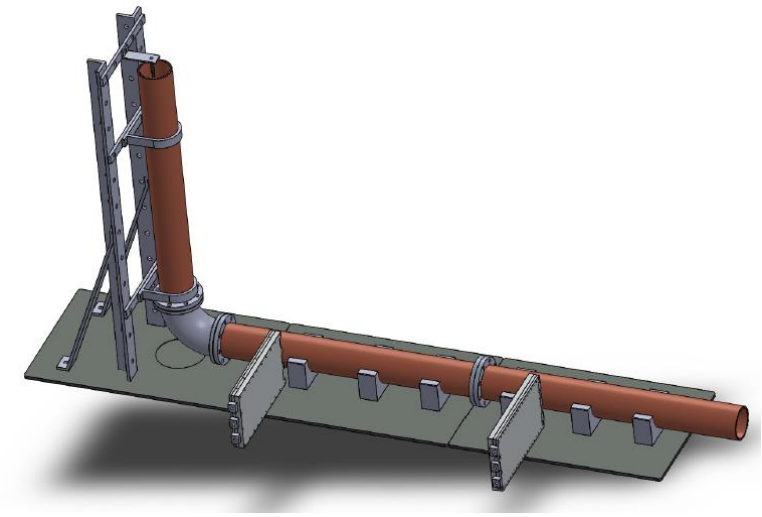

Figure 7: Horizontal Wellbore Two Stage Setup Example

2.3 Electrical Component

The electrical component of the system consists a hydrophone, amplifier/signal conditioning unit, quad-channel data logger, and Personal Computer (PC) running the data acquisition software. A flow chart of the electrical system is shown in Figure 8. Sound samples are recorded at the hydrophone, and are send through an amplifier/signal conditioning unit that contains amplification and analog front end circuitry. The unit converts and amplifies hydrophone acoustical vibration input signal to analog voltage output signal within -5V and +5V rail range. The amplifier/signal conditioning unit also provides hardware bandpass filtering from 10 Hz to 20000 Hz to the audio samples collected by the hydrophone. A shielded Bayonet Neill-Concelman (BNC) cable connects hydrophone and amplifier/signal conditioning unit to reduce electromagnetic interference. Only one channel of the quad-channel data logger is used connecting the output of the amplifier/signal conditioning unit to input of the data logger. The cable

connecting amplifier/signal conditioning unit and data logger is also a shielded cable with BNC connector termination to minimize electromagnetic noises. The output of the data logged is cabled to a PC running data acquisition software through a Universal Serial Bus (USB) cable.

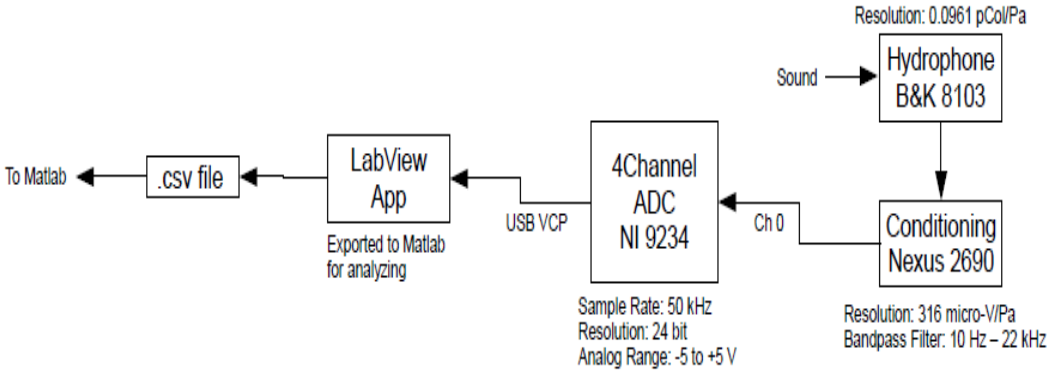

Figure 8: Electrical Component Block Diagram

2.4 Software Component

The experimental system software component consists of a data acquisition software application and signal processing software application. The data acquisition application runs to collect audio samples and save the collected samples into a CSV formatted text file. After the CSV file is obtained from experiments, an evaluation application software is used to analyze the collected audio data. Both software application runs on a PC and has a graphical user interface (GUI).

2.4.1 Data Acquisition Application

A GUI based data acquisition software application is developed in LabVIEW to control the data logger. The flexibility of the data logger allows most of the features to be software defined. The data acquisition software application is designed to collect multiple sets of 10 seconds and 30 seconds of continuous audio signal at 50 kHz sampling rate and 24-bit resolution. The collected audio file is saved into a CSV formatted text file. The GUI of the data acquisition software application allows user easily select name and directory of the CSV file to save to. All of the saved files are time stamped for better data management purpose. The data acquisition software application also displays plots of information about audio sample collected such as amplitude in time domain, peaks in frequency domain, and phase in frequency domain in real time. Thus, an instant feedback of the experimental result is shown to determine the quality of the measurement data.

2.4.2 Signal Processing Application

A data evaluation software application is developed in MATLAB to analyze the measured audio file. The evaluation application is designed specifically for this research project. It allows user to enter data file directory path and a couple amplifier/signal conditioning unit settings to start the analysis on the graphical user interface. Once all of the required information is entered, user has the option to choose how to analyze the audio data. The software application allows user to apply different filter type and cutoff value to the data file for further analysis. User can analyze in both time and frequency

domains by examining the signal components such as amplitude and phase. The application is also capable of plotting waveform in time domain, generating of both amplitude and phase of Fast Fourier Transform (FFT) plot, and showing spectrogram of the audio file. The application also allows plotting of multiple waveforms on a single plot. It has a quick view window to preview before full-blown plots are generated. It also calculates important signal parameters such as Sound Pressure Level (SPL) and Signal Noise Ratio (SNR). A screen shot of the evaluation software application is shown in Figure 9.

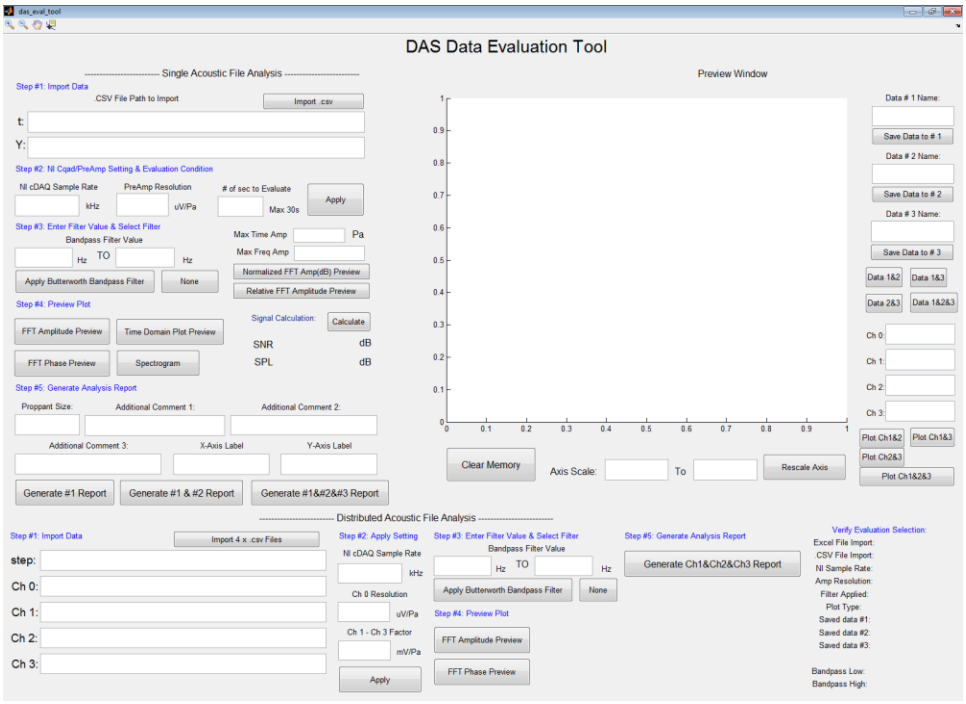

Figure 9: Screen Shot of DAS Evaluation Software Application

DAS evaluation software application is used exclusively to analyze the measured audio files. All of the time and frequency domain plots in the thesis is generated using the DAS evaluation software application.

2.5 Experimental System and Laboratory Environment Verification

A list of experimental system verification steps are taken to ensure the accuracy and precision of the experimental system and laboratory environment. The 1st step is to measure the background "lab noise". This experiment starts with assembling the facture cell experimental setup as the experimental condition. Multiple sets of 10 second audio sample are taken to measure the background noise. Without injecting any fluid, the result is plotted on a spectrogram as shown in Figure 10 and Figure 11.

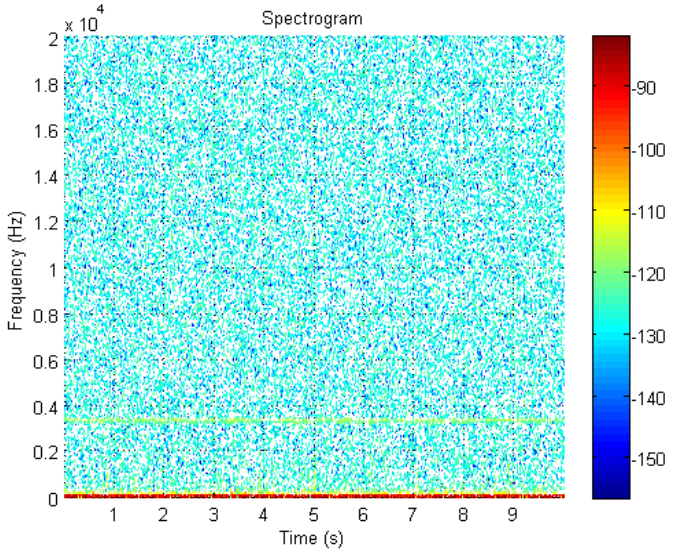

Figure 10: Spectrogram of Laboratory Background Noise from DC-20 kHz

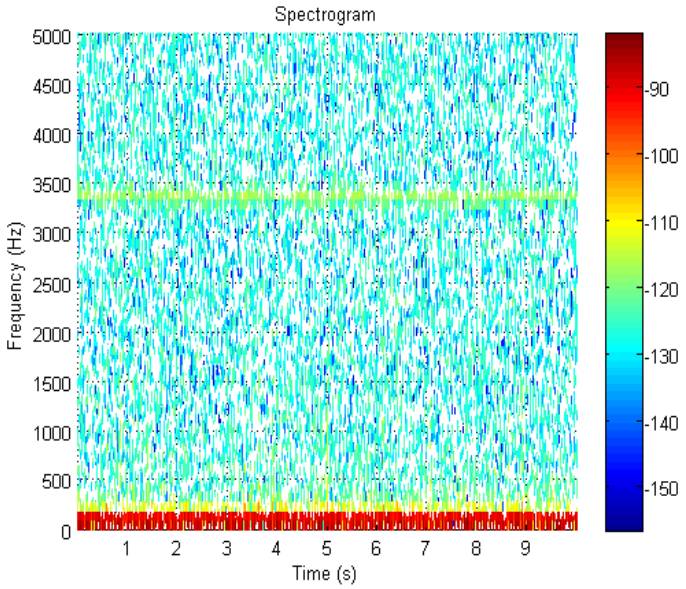

Figure 11: Spectrogram of Laboratory Background Noise from DC-5 kHz

As the results shown from Figure 11, laboratory spectrum is very noisy below 200 Hz and less noisy around 300 Hz and 3400 Hz. Perhaps, the noise below 300 Hz is caused by the 60 Hz Alternating Current (AC) power sources and its harmonics in the lab. There is also some noise at around 3400 Hz; the amplitude of this noise changes among the different audio files being analyzed. A possibility of the cause of this noise is air conditioning in the lab, but it's not confirmed. Other than below 300 Hz and 3400 Hz, laboratory spectrum is cleaned up to 20 kHz as shown in Figure 10. The plotting upper limit is set at 20 kHz because data sampling rate is at 50 kHz. Applying Nyquist's Theorem; sampling rate has to be at least twice the rate of signal of interest. Since the data logger has a Sigma-Delta Analog Digital Converter (ADC) in it, excellent 24 bit sampling resolution is obtained from the audio sample.

Experimental system undergoes another system verification test of a known signal to check the correctness of both data acquisition and signal processing software application. A couple of known monotone 1 kHz audio is played outside the wellbore; audio samples are taken to test if the system plots the 1 kHz signal as expected. The testing result of experimental system measuring and plotting a known 1 kHz monotone signal is shown in Figure 12. The experimental system successfully identified the known signal and graphed signal peak at 1 kHz on the FFT plot. Similar verification procedure also performed at other known monotone frequencies such as 500 Hz. The result validates the experimental system.

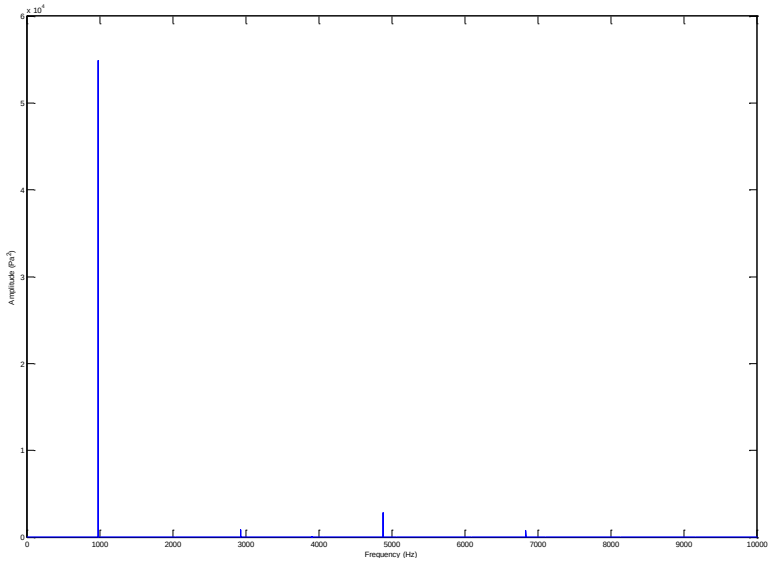

Figure 12: FFT Plot of a Known 1 kHz Monotone Signal

Data acquisition system implements a scalable amplitude resolution setting. Similar sound is measured at multiple amplitude resolution settings such as 316 uV/Pa

and 1 mV/Pa. Sound level in Pa is being calculated using measured analog data in Volts divided by selected resolution in mV/Pa. The reason for such scalable amplitude resolution implementation is to avoid signal clipping on the -5V to +5V ranges of the ADC input channel when the sound level is very high. The purpose of this verification experiment is to show sound level in Pa of similar audio samples is the same at different measuring amplitude resolution settings. The result is shown in Figure 13.

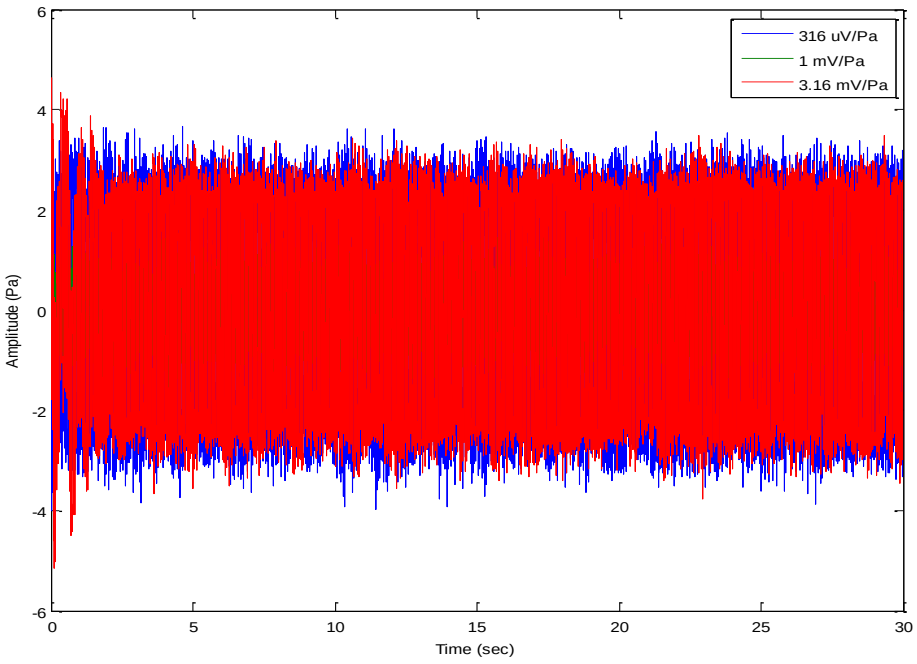

Figure 13: Comparison of Different Amplitude Resolution Settings

As Figure 13 shown, measuring sound under similar conditions at different amplitude resolution settings obtains the same sound amplitude range. Due to acoustic signal generated to conduct this set of experiments is not exactly the same, the time

domain plots of different amplitude resolution settings do not overlay. Amplitude resolution setting verification only checks if the amplitude range is similar when amplitude resolution setting changes. This verification step shows that the correctness of the scalable amplitude resolution setting is validated.

2.6 Summary of Experimental Setup

A fracture cell is designed and machined to simulate a single fracture. The fracture cell is connected to different vertical and horizontal wellbore setup through perforation to mimic the field case. Gas and liquid flow through the fracture cell to wellbore at controlled pressure and flow rate to simulate fluid flows from fracture to wellbore. During time fluid flows from the fracture to wellbore, audio samples are taken to study the acoustic behavior of flow from fracture to wellbore under different conditions. A hydrophone based measurement system is setup to measure the audio data. Sampling rate and resolution are carefully selected based on Nyquist's theorem. The flexibility of the experimental setup allows different experiments to take place under different conditions and configurations of the experimental station.

A list of verification steps is performed to valid the precision and accuracy of the experimental setup. The verification result shows that the experimental setup is valid. The result also shows that the testing laboratory is not noise free; there are background noises at below 300 Hz and 4300 Hz on the spectrum from DC to 20 kHz.

3. EXPERIMENTAL RESULTS

3.1 Acoustic Behavior of Vertical Wellbore

An experimental matrix is developed to study how different parameters affect the acoustic behavior of flow from fracture to a vertical wellbore. The experimental matrix contains a baseline measurement setup condition; the acoustic signature of the baseline measurement is being compared to other measurements taken with change of experimental parameters. A list of the possible downhole parameters might cause acoustic behavior change is tested using the vertical wellbore experimental setup to simulate fluid flows from fracture to a completed vertical wellbore.

3.1.1 Experimental Baseline Characteristic

A baseline measurement is taken using the 16/30 HSP proppant filled fracture cell, and the acoustic signature of the baseline setup is used as a reference to acoustic behavior change from other experimental conditions. During the baseline experiment, 2 sets of data with a constant of injection flow rate increment are recorded. The first set of data collected has half the flow rate increment than the second dataset. Thus, the 1st dataset has twice the data resolution than the 2nd dataset. Nitrogen gas is injected from 0 psi to 160 psi with increment of 5 and 10 psi to the fracture cell inlet. Nitrogen with controlled pressure and flow rate travels across the 16/30 HSP filled fracture cell through the perforation tunnel to the vertical wellbore. 10 seconds of audio samples are recorded

at each injection increment point. A typical time domain of the acoustic signal at a gas flow rate of 300 standard cubic feet per hour (scf/hr) is shown in Figure 14.

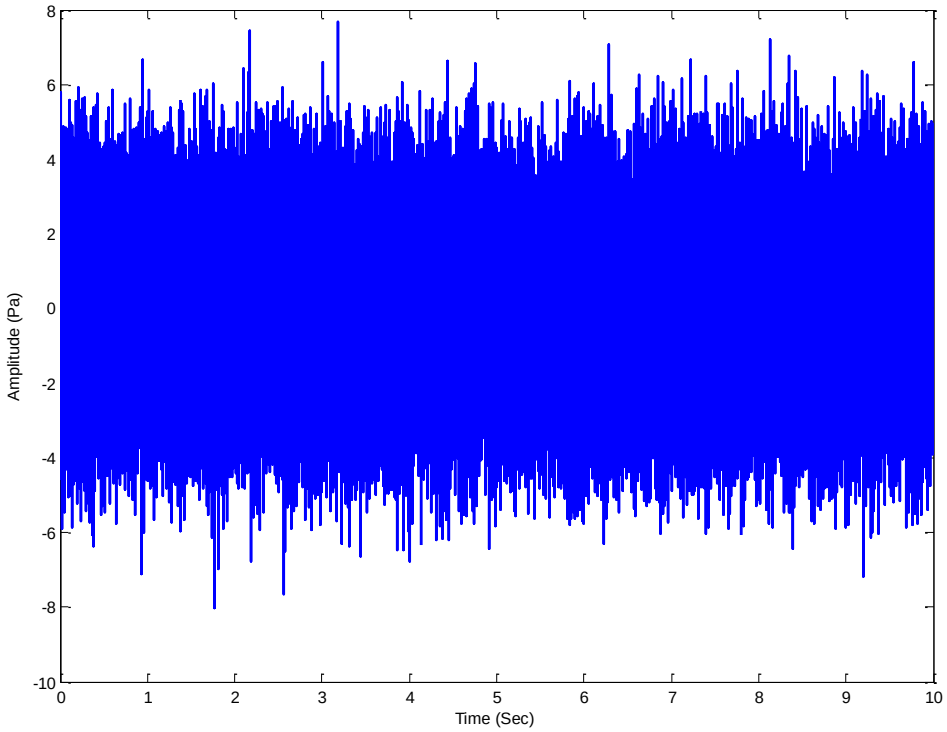

Figure 14: Example of Baseline Acoustic Signal without Filtering in Time Domain

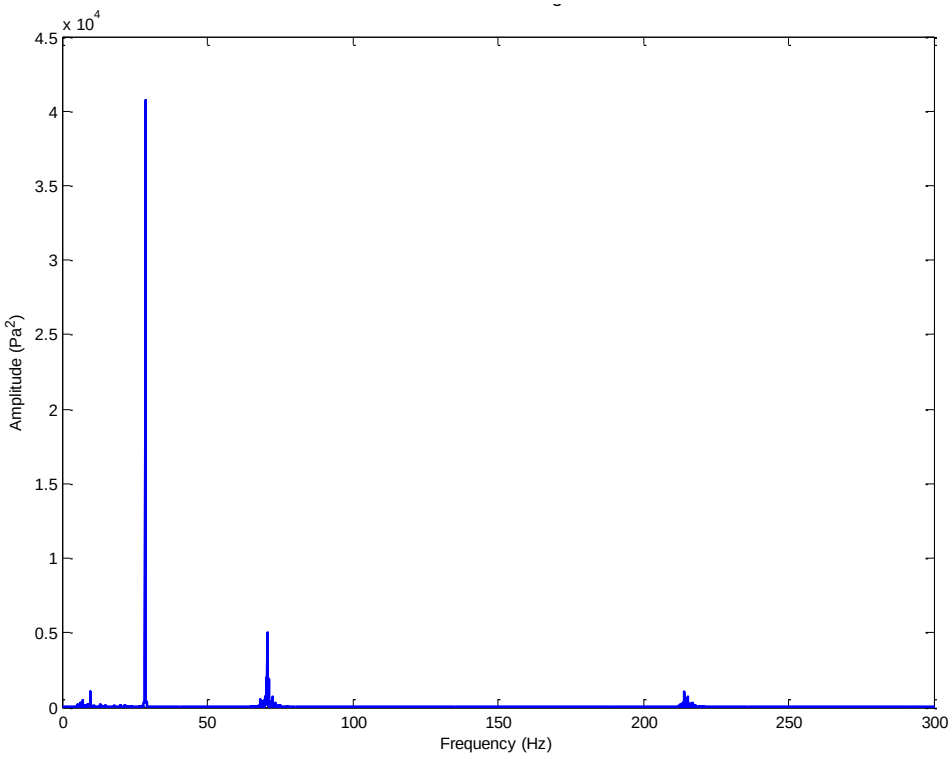

Figure 15: Example of Baseline Acoustic Signal without Filtering in Frequency Domain

From the Figure 14, information such as signal amplitude can be found. Observation from Figure 14 is that sound amplitude is around 6 Pa and the sound recorded is not a monotone. In order to further understand the acoustic behavior generated by the flow through porous space, a frequency domain analysis needs to be performed on the recorded sound signal. In the last chapter, significant lab noise is found at below 300 Hz. In order to preserve the signal integrity, filtering is applied to extract portions of the signal above 300 Hz.

Figure 15 shows the same acoustic signal at 300 scfh gas flow rate in frequency domain without filtering. A Fast Fourier Transform (FFT) is applied to the measured

audio signal (Martinez et al. 2014a, 2014b). Since the data is plotted without filtering, significant noise can be seen at below 200 Hz in Figure 15. The amplitude of the lab noise is significantly higher than the actual sound generated by fluid flows from fracture to perforation tunnel; therefore filtering needs to be applied to remove this unwanted background noise.

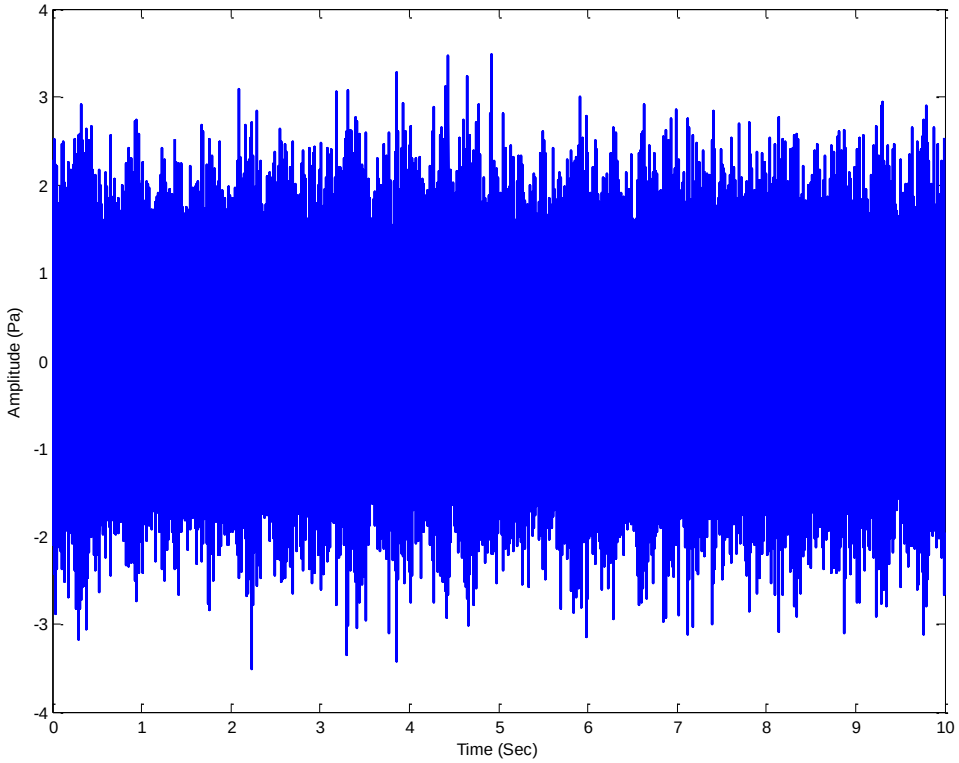

Figure 16: Example of Baseline Acoustic Signal with Filtering in Time Domain

Figure 16 shows an example of baseline acoustic signal with filtering in time domain. By filtering, background noise can be eliminated and integrity of the signal is preserved. A bandpass filter with a cutoff frequency range of 1 kHz to 7 kHz is applied

to the audio signal collected. From the figure, the amplitude is reduces to 3 Pa and the shape of signal is changed as well. However, there is not much critical acoustic behavior information can be found by analyzing the signal in time domain. Thus, a transformation of the signal from time domain to frequency domain is needed to further analyze the data set.

After removing the lab noise by applying a bandpass filter with cutoff frequencies of 1 kHz and 7 kHz, Figure 17 shows the same audio signal with filtering in frequency domain. From the figure, a couple of observations can be made. The signal of interest is between 1 kHz to 7 kHz with most of the dominate peaks in the 3400 Hz to 4000 Hz range. The acoustic signal of fluid flows from the fracture to the wellbore has many frequency components and it is not a monotone sound being generated by the fluid flows from the fracture to the wellbore.

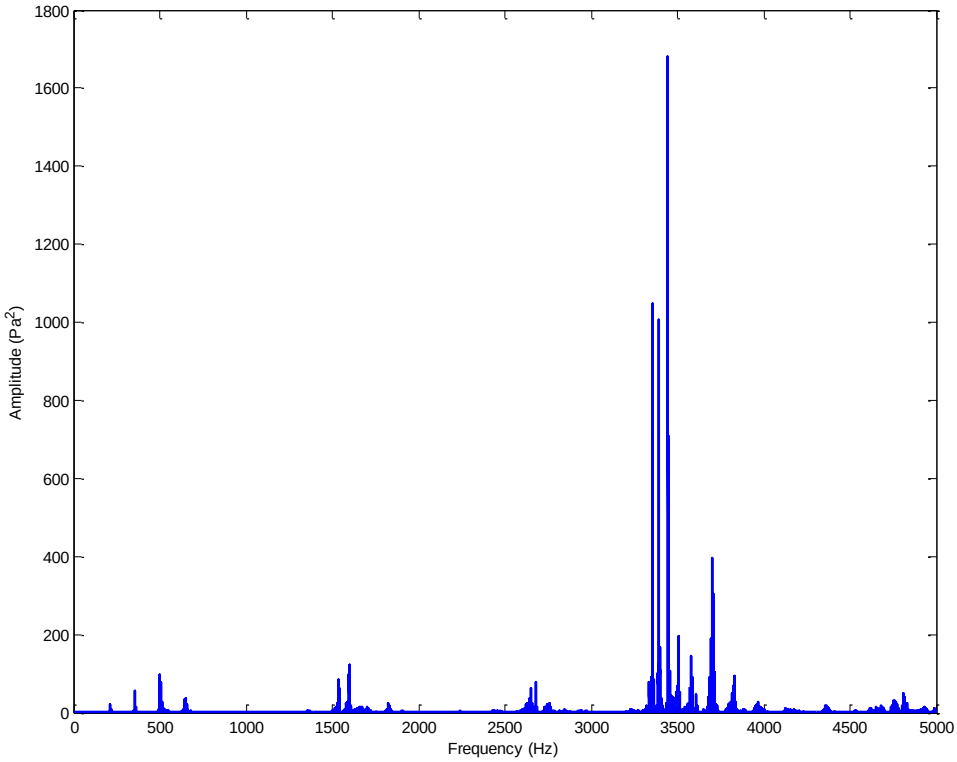

Figure 17: Example of Baseline Acoustic Signal with Filtering in Frequency Domain

By analyzing the baseline acoustic behavior of flow from the fracture to the wellbore, a general idea of the acoustic characteristic is understood. Once a baseline experimental condition is established, different downhole parameters can be changed to further understand the acoustic behavior under different downhole conditions. From baseline acoustic behavior, the frequency range of signal of interest is observed. More extensive analysis will be performed in those frequency ranges when different downhole parameter changes.

3.1.2 Flow Velocity Effect

Flow velocity contributes significantly to the acoustic behavior. As flow rate increases, Sound Pressure Level (SPL) increases in the fracture cell experimental setup. A plot of SPL vs flow rate curve of 2 different data sets is shown in Figure 18. The experimental setup used 16/30 size proppant, the inner fracture cell dimension of 16 inch (Length) x 8 inch (Height) x 0.2 inch (Width), the perforation dimension of 5.2 inch (Length) x 0.493 inch (Diameter), and single perforation tunnel. A hydrophone is placed 2.5 in above the perforation tunnel inside of the casing and single phase gas is injected through the proppant packed fracture cell. The first data set is taken at 5 psi incremental and second data set incremental step is at 10 psi. By examining Figure 18, both data sets suggest the same SPL vs flow rate trend. Thus, measurement precision and accuracy are improved by plotting 2 different datasets.

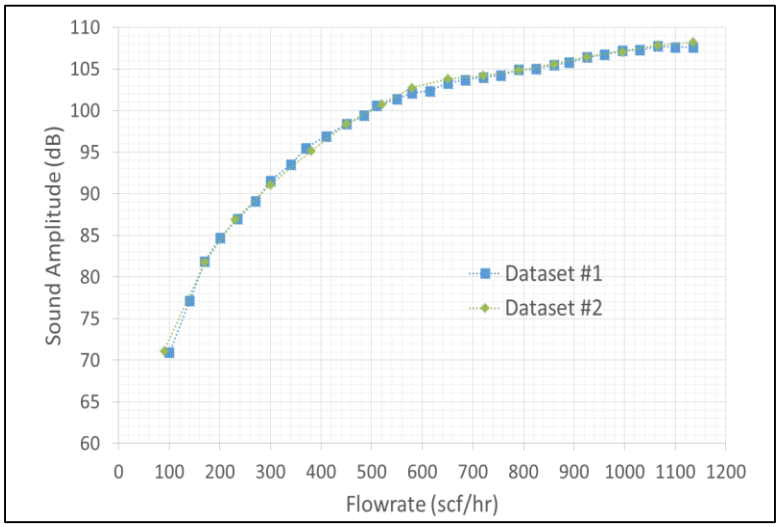

Figure 18: Baseline Experimental Setup SPL vs Flow Rate Curve

Looking at the slopes of the SPL vs flow rate curve, the figure suggests that SPL curve slope is steeper in the lower flow rate region than higher flow rate region. In order to verify this observation, figures of the same experimental data are analyzed in both time and frequency domain. Results are shown in the figures below.

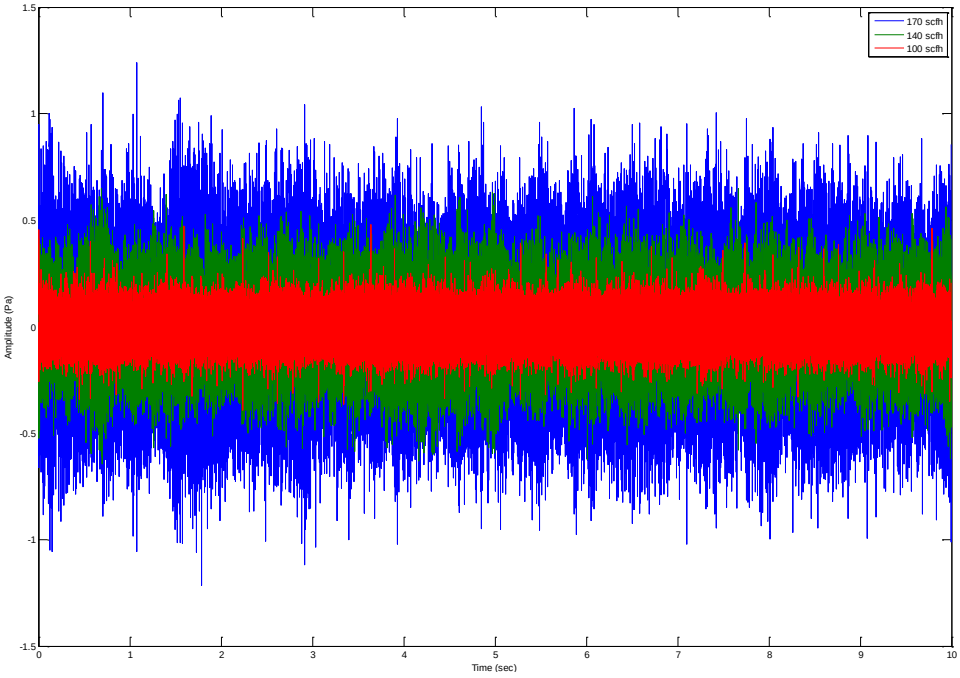

Figure 19: Flow Velocity Effect from 100-170 scf/hr in Time Domain

In Figure 19, observation is made that amplitude of the acoustic signal is increased significantly at 3 different flow rates 100 scf/hr in red, 140 scf/hr in green, and 170 scf/hr in blue. The significant acoustic signal amplitude increasing can also be seen in Figure 18 on the dB scale. In the 100 SCFH to 170 SCFH region of the SPL curve, sound amplitude increment is more than any other region. Thus, the steeper slope on SPL curve in the low flow rate region can be verified with the time domain plot. Again,

a detailed time domain analysis can be performed to verify this observation. In Figure 20, 10 seconds of acoustic signal is plotted.

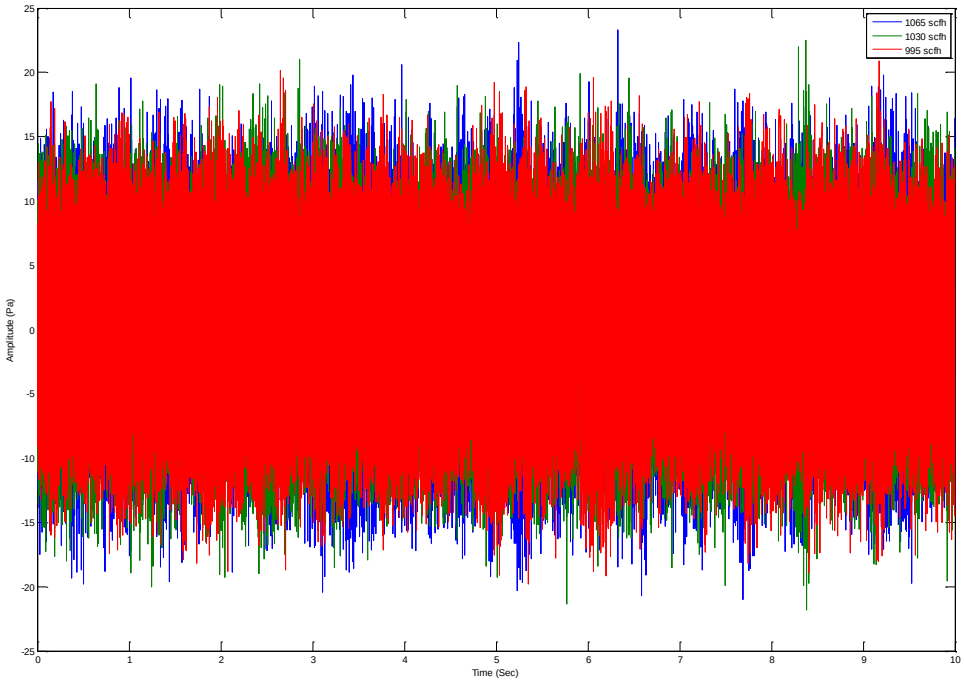

Figure 20: Flow Velocity Effect from 995-1065 scf/hr in Time Domain

From Figure 20, a different acoustic amplitude behavior is observed compare to Figure 19. In Figure 20, amplitude of the acoustic signal remains the same at 3 different flow rates at 995 scf/hr, 1030 scf/hr, and 1065 scf/hr. The same level of acoustic signal amplitude can also be seen in Figure 18. In the 995 scf/hr to 1065 scf/hr region of the SPL curve, sound amplitude increment remains relatively the same.

By analyzing the acoustic signal in time domain, the shape of the SPL vs flow rate curve is determined. However, time domain analysis doesn't provide enough

information on the causes of the SPL increasing. Thus, frequency domain analysis is needed to understand the phenomenal further.

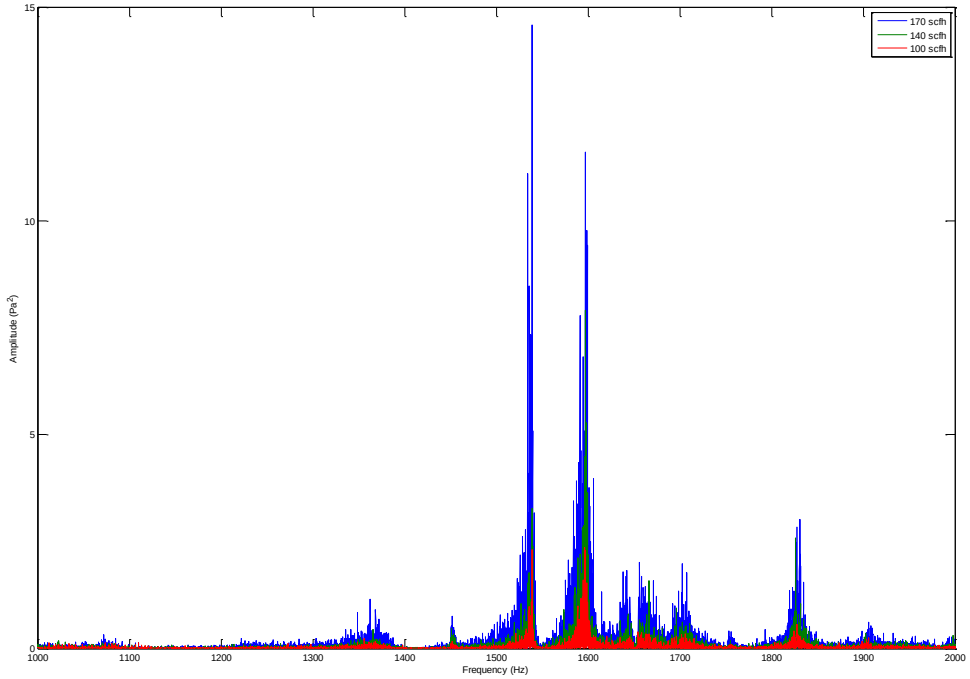

Figure 21: Flow Velocity Effect from 100-170 scf/hr in Frequency Domain

In Figure 21, observation can be made that as flow rate increases from 100 scf/hr to 170 scf/hr, the location of acoustic signal frequency component remains the same but frequency component amplitude increases as flow rate increases. In Figure 21, acoustic signal at all 3 different flow rates shows the same pattern. If the flow rate is increased to the 270 scf/hr to 340 scf/hr region, same acoustic behavior can be observed in Figure 22.

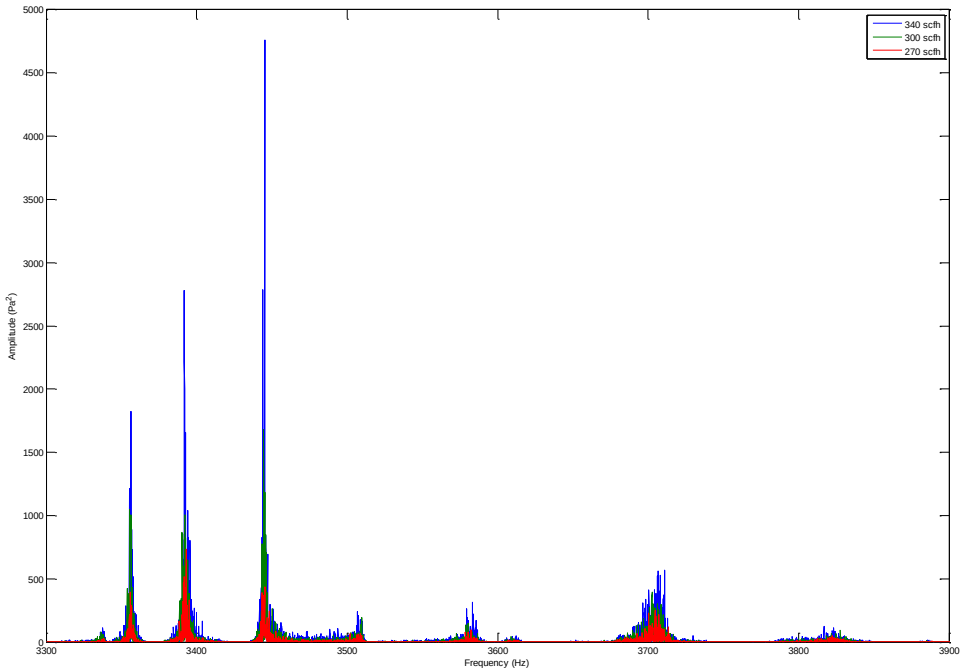

Figure 22: Flow Velocity Effect from 270-340 scf/hr in Frequency Domain

Same pattern can be observed in the 270 scf/hr to 340 scf/hr flow rate range. The Amplitude vs Frequency plot is shown in Figure 22. From Figure 22, all 3 flow different flow rates show the same acoustic behavior pattern in frequency domain. As the flow rate increases, the amplitude of the frequency components increases.

Acoustic behavior for flow rate in the 100 scf/hr to 340 scf/hr range is shown in Figure 21 and Figure 22. In Figure 23, flow rate is increased to the range of 995 scf/hr to 1065 Scf/hr; the frequency peaks of the 3 different flow rates still remain at the same location. The amplitude of the frequency peaks increases slowly at a given frequency location.

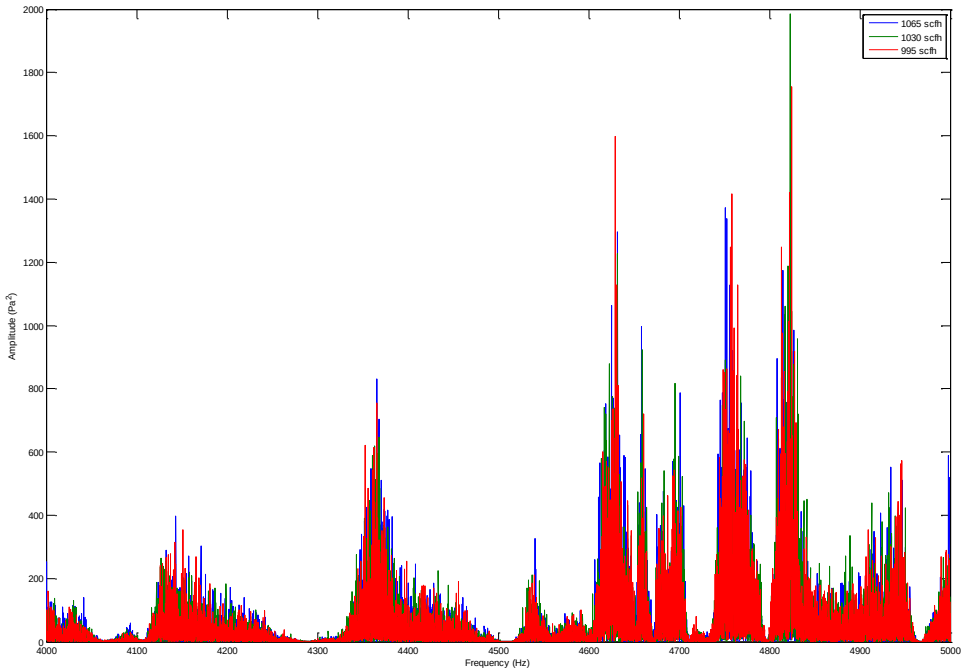

Figure 23: Flow Velocity Effect from 995-1065 scf/hr in Frequency Domain

To summarize the flow rate effect on acoustic signal behavior, as flow rate changes, frequency peaks remain at the same location on the spectrum. As flow rate increases, SPL increases. Amplitude of the frequency peaks increase as flow rate increases.

3.1.3 Proppant Effect

A proppant filled fracture cell makes different sounds compare to an empty fracture cell. Also, the size of proppant changes acoustic behavior as well. Experiments have been conducted to exam the proppant effect. Every other parameters in the experiment are held the same as the baseline measurement, the only parameter changes in this experiment is the proppant size. The baseline setup is based on 16/30 proppant.

Experimental result shows that when proppant size changes, amplitude of the frequency peaks changes. Also, when no proppant fills the fracture cell, acoustic signature is completely different than proppant filled fracture cell.

In Figure 24, both the amplitude and location of the no proppant frequency component peaks change from the proppant filled fracture cell acoustic frequency peaks. Thus, the result shows that fracture contains proppant has a different acoustic signature than fracture without proppant in it.

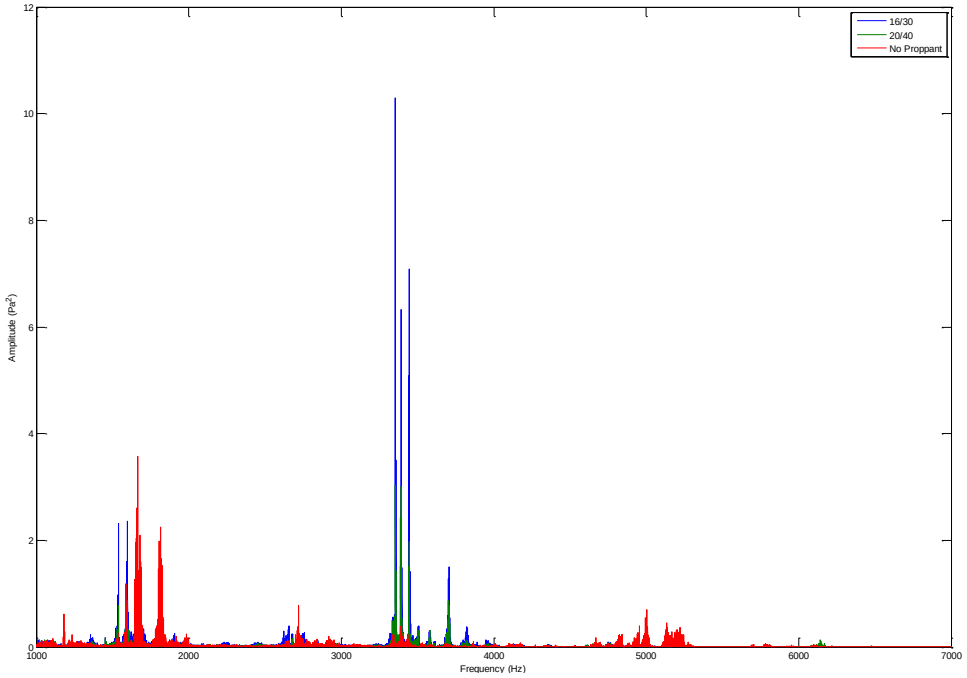

Figure 24: Proppant Effect from 1-7 kHz at 100 scf/hr

Not only no proppant filled fracture changes the acoustic signature compare to the baseline 16/30 size proppant filled fracture, the size of proppant changes the acoustic

behavior as well, but in a different way. In Figure 25, fracture contains 16/30 proppant has a larger sound amplitude than the 20/40 proppant at a particular frequency location at a fixed flow rate. Shown in Figure 25, there is no shifting of the frequency components; only the amplitude of the frequency peaks change when proppant size changes.

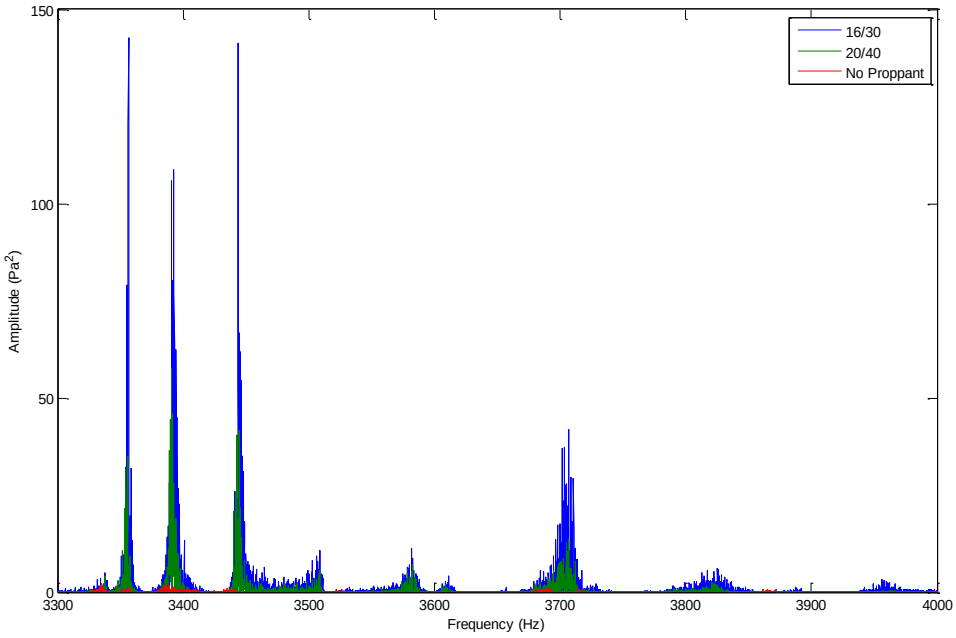

Figure 25: Proppant Effect from 3.3-3.9 kHz at 170 scf/hr

To verify the experimental result in the frequency domain, a SPL curve is plotted and shown in Figure 26. From SPL vs flow rate curve, observation can be made that at a given flow rate, 16/30 proppant makes louder sound than 20/40 proppant. Also, the proppant effect SPL curve shows that the fracture contains no proppant has lower sound

amplitude than proppant filled fracture. The shape of the no proppant filled fracture SPL curve is different than proppant filled fracture SPL curve.

For the no proppant experimental result below 200 scf/hr, the slope of the SPL vs flow rate curve is different than the proppant filled fracture cell experimental result. In the flow rate above 1100 scf/hr region, the sound amplitude of 20/40 proppant filled fracture cell converges with the no proppant experimental result. In the above 900 scf/hr region, 16/30 proppant filled fracture cell experiments show larger sound amplitude than 20/40 filled fracture cell experimental result.

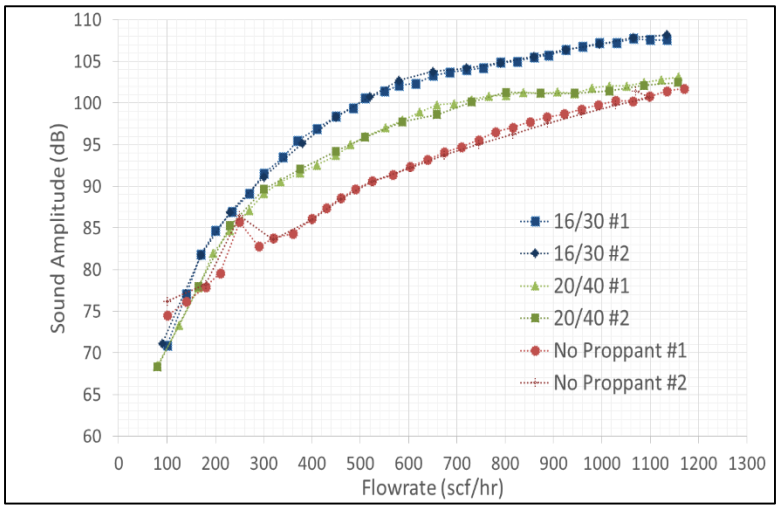

Figure 26: Proppant Effect SPL vs Flow Rate Curve

To summarize the proppant effect, fracture filled with proppant has a different acoustic signature than fracture contains no proppant. Proppant size only changes the amplitude of the acoustic frequency components. At a given flow rate, 16/30 proppant

has higher sound amplitude than 20/40 proppant. The shape of the SPL curve is the same when the size of proppant filling the fracture changes.

3.1.4 Fracture Width Effect

In this experimental setup, the width of the fracture cell is changed. The fracture cell width change attempts to mimic the fracture geometry change in the downhole environment. All of other parameters are kept the same as the baseline experiment. The result of experiment shows that when fracture width changes, only the amplitude of the frequency component changes.

In Figure 27, the frequency domain plot of 3 different fracture width is shown. In Figure 27, as the fracture width decreases, the amplitude of the frequency component increases. Also can be seen from Figure 27, location of acoustic frequency components remain at the same, the only acoustic behavior change when fracture width changes is the amplitude of frequency component. In the fracture width effect experiment, due to the change of fracture cross section area, volumetric flow rate across the fracture cell changes as well. Thus, only injection pressure can be held constant when comparing different fracture width acoustic signatures under the same testing conditions in the fracture cell width experiment.

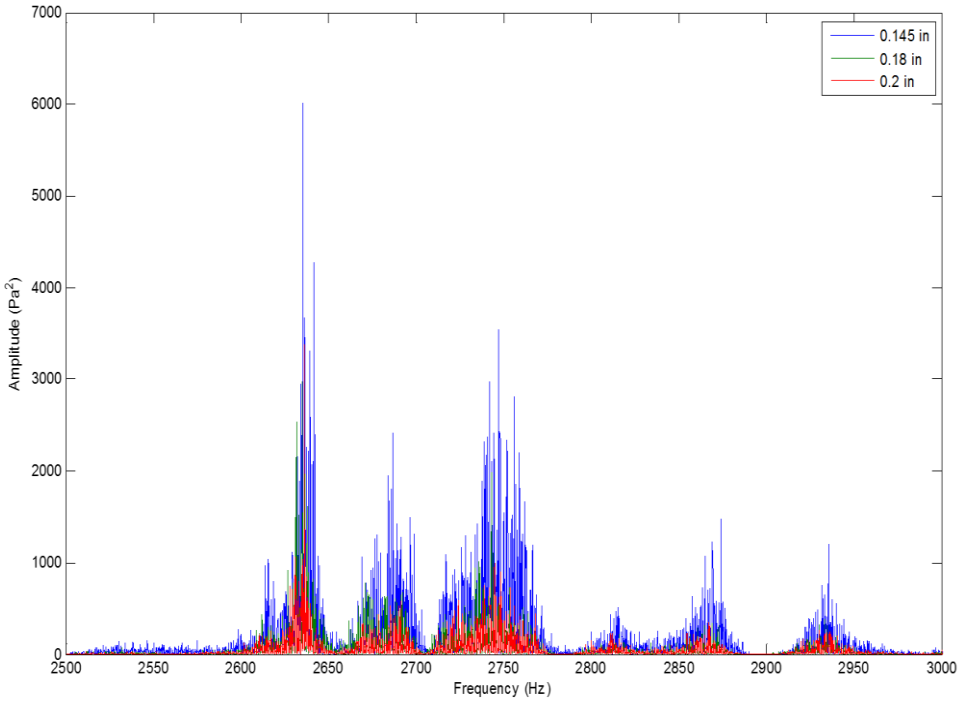

Figure 27: Fracture Width Effect from 2.5-3 kHz at 30 psi

To summarize the fracture width effect, acoustic frequency component changes only the amplitude when fracture width changes. As fracture width decreases, amplitude of the acoustic frequency components increases. Location of the frequency components remains at the same on the frequency spectrum.

3.1.5 Perforation Tunnel Length Effect

In the perforation tunnel length effect experiment, all other parameters are held the same as the baseline experiment expect the length of perforation tunnel pipe length. Perforation tunnel length of 5.2 inch is used in the baseline setup. In perforation tunnel length experiment, perforation tunnel length is increased to 9.2 inch and 15.2 inch. The

result shows that perforation tunnel length changes the frequency signature of the acoustic signal; acoustic signal frequency components shifts and changes amplitude on the frequency domain plot. On the SPL curve, the baseline experimental setup has the largest sound amplitude; perhaps it is caused by the additional sound generated in the fracture propagates to the hydrophone.

In Figure 28, the default perforation tunnel at 5.2 inch length has a different acoustic signature than the perforation tunnel length at 9.2 in and 15.2 in. The dominate frequency peaks at baseline setup are at different locations than the frequency peaks when the perforation length is increased to 9.2 inches and 15.2 inches. The acoustic signature is also different between the 9.2 inch and 15.2 inch perforation tunnel length data sets as shown in Figure 28.

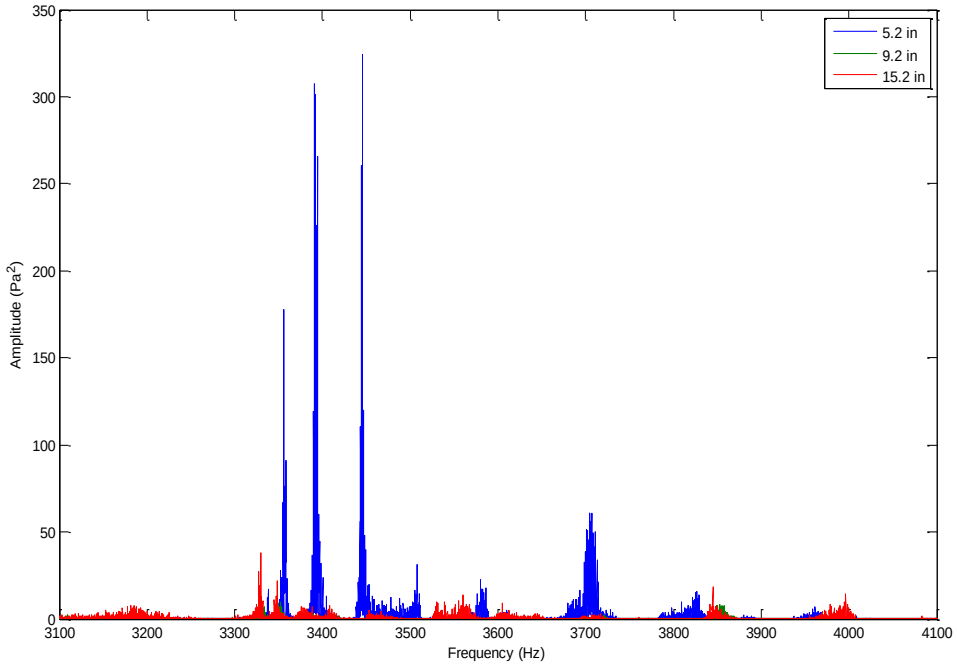

Figure 28: Perforation Tunnel Length Effect from 3.1-4.1 kHz at 200 scf/hr

The perforation tunnel length changes the acoustic behavior in a different way than other parameters such as proppant size and flow rate, which only change the amplitude of frequency components. Perforation length changes the acoustic signature of audio samples collected in the experiment.

In Figure 29, the shortest perforation tunnel data set has largest sound amplitude compare to the other two. Perhaps this is caused by additional sound generated in the fracture propagates through the shorter perforation tunnel. The shape of SPL curve above 300 scf/hr region is different when comparing the longer perforation tunnel length data sets to the baseline data set.

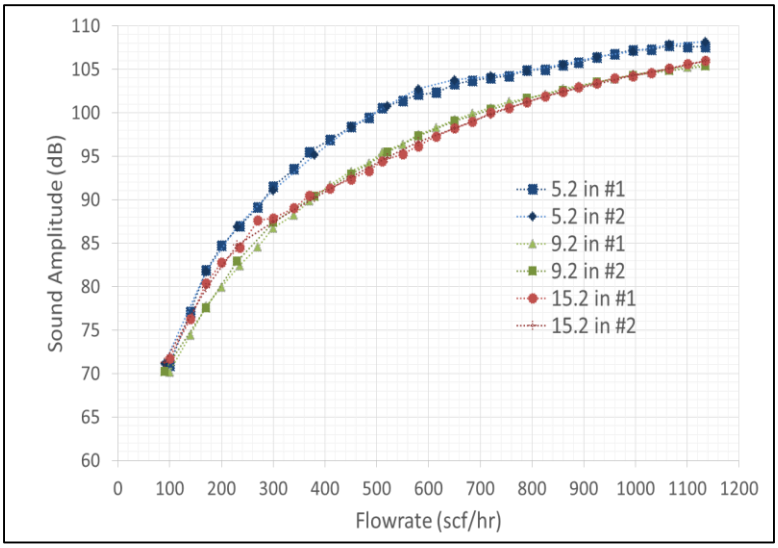

Figure 29: Perforation Length Effect SPL vs Flow Rate Curve

To summarize the perforation tunnel length effect, acoustic signal signature is changed when perforation tunnel length changes. As perforation tunnel length decreases, the sound amplitude increases.

3.1.6 Perforation Tunnel Diameter Effect

In this experiment, perforation tunnel diameter effect is studied. All of the parameters are held the same as the baseline experimental setup except perforation tunnel diameter. The baseline setup has perforation tunnel pipe diameter of 0.493 inch; the perforation tunnel diameter is changed to 0.364 inch and 0.622 inch running the same experimental procedure as the baseline experiment. Perforation diameter effect changes both amplitude and location of the acoustic signal frequency component. As

perforation diameter decreases, amplitude of the acoustic signal frequency component increases and frequency peaks shifts to the left.

In Figure 30, the acoustic behavior in the frequency domain is shown for three different perforation diameters. The smallest perforation diameter 0.364 inch has the largest frequency component amplitude and the largest perforation diameter 0.622 inch has the smallest frequency component amplitude. The shifting of the frequency peaks can also be seen in Figure 30, as the perforation diameter decreases, the peaks shift to the left. Therefore, the perforation diameter shifts acoustic frequency peaks as well as changes the amplitude of those frequency peaks.

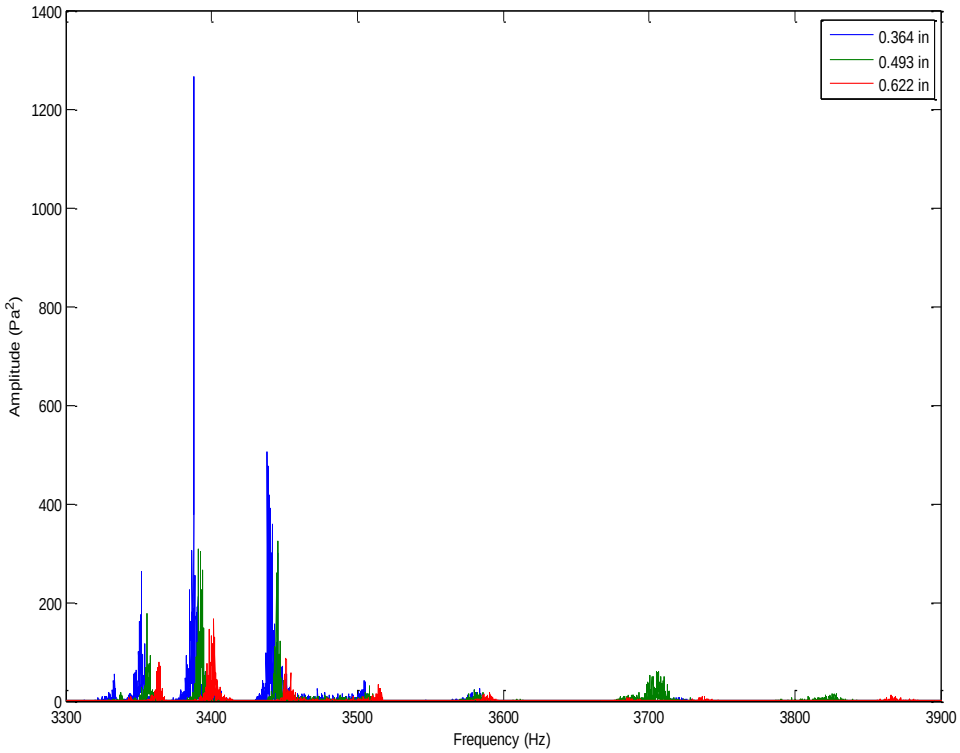

Figure 30: Perforation Tunnel Diameter Effect from 3.3-3.9 kHz at 200 scf/hr

In Figure 31, three different perforation tunnel diameters generate relatively the same sound amplitude since 3 different perforation diameter curves mesh together on the plot. By only comparing the sound amplitude at a given flow rate, size of the perforation diameter cannot be identified.

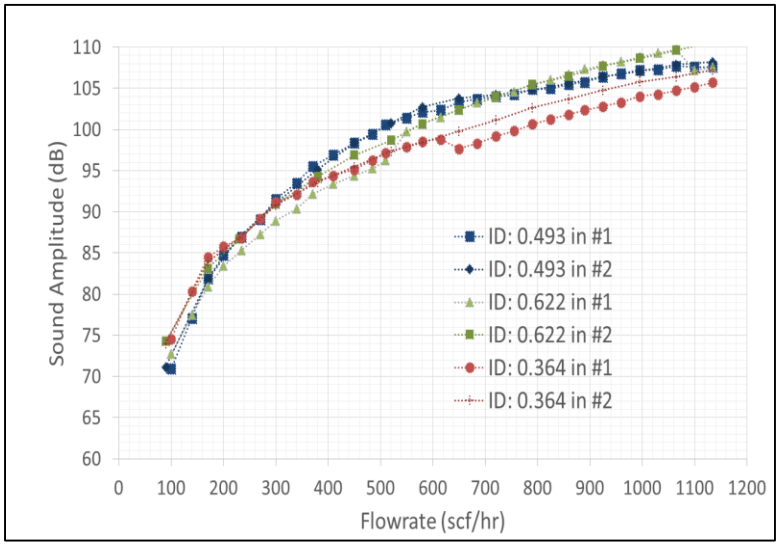

Figure 31: Perforation Tunnel Diameter Effect SPL vs Flow Rate Curve

To summarize the perforation diameter effect, acoustic signal frequency components decrease amplitude and shifts to right as perforation diameter increases. Perforation diameter changes both amplitude and frequency peak location of the acoustic signal. From the sound amplitude curve, there is not much information can be obtained when perforation diameter changes because 3 different curves bunch together on the plot.

3.1.7 Perforation Tunnel Smoothness Effect

After perforating the producing zone, each perforation tunnel has a different inner wall smoothness, experiments have been conducted to study the perforation tunnel smoothness effect on acoustic signal behavior. The experiment utilizes a rusty pipe with visible rough inner surface and a brand new smooth inner wall pipe.

In Figure 32, rough perforation tunnel inner surface has higher sound amplitude at a given flow rate within a portion of the flow rate range. One of the reasons of this observation could be the additional flow turbulence caused by rough inner surface of the pipe makes a louder sound. In Figure 32, both rough perforation tunnel and smooth perforation tunnel have the same SPL below 300 scf/hr. Once flow rate increases above 300 scf/hr, rough perforation tunnel acoustic signal has higher SPL than the smooth perforation tunnel. From the experimental result, the acoustic signal of both rough perforation tunnel and smooth perforation tunnel converges to the same sound amplitude level when the gas flow rate reaches 100 scf/hr.

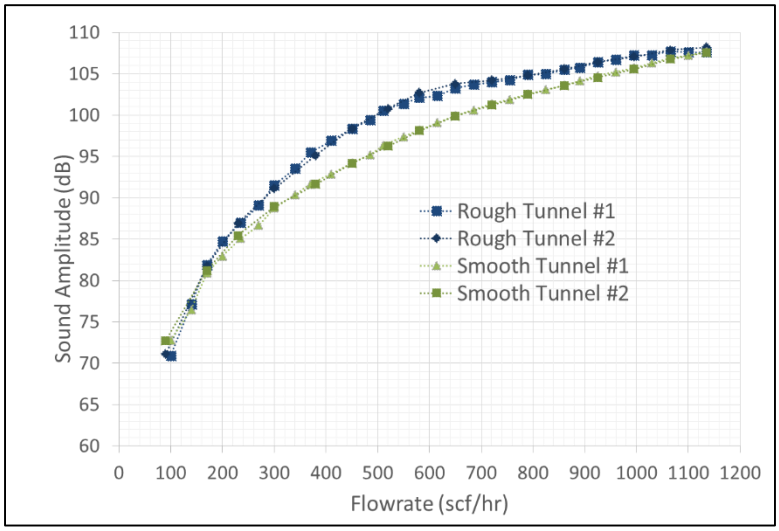

Figure 32: Perforation Tunnel Smoothness SPL vs Flow Rate Curve

In the frequency domain, smoothness of the perforation tunnel changes the acoustic signal signature. In Figure 33, most of the peaks in the 3.3 kHz to 3.9 kHz range belong to the rough perforation tunnel. Smooth perforation tunnel causes smaller frequency peaks in the 3.3 kHz to 3.9 kHz range. However, in Figure 32, the SPL curve of the smooth perforation tunnel is similar to rough perforation tunnel. The similar sound amplitude is because SPL calculation is based on all of the frequency components with cutoff frequency at 1 kHz and 7 kHz. Rough perforation tunnel acoustic frequency peaks dominates the 3.3 kHz to 3.9 kHz range. In another frequency range, smooth perforation tunnel acoustic frequency peaks dominates.

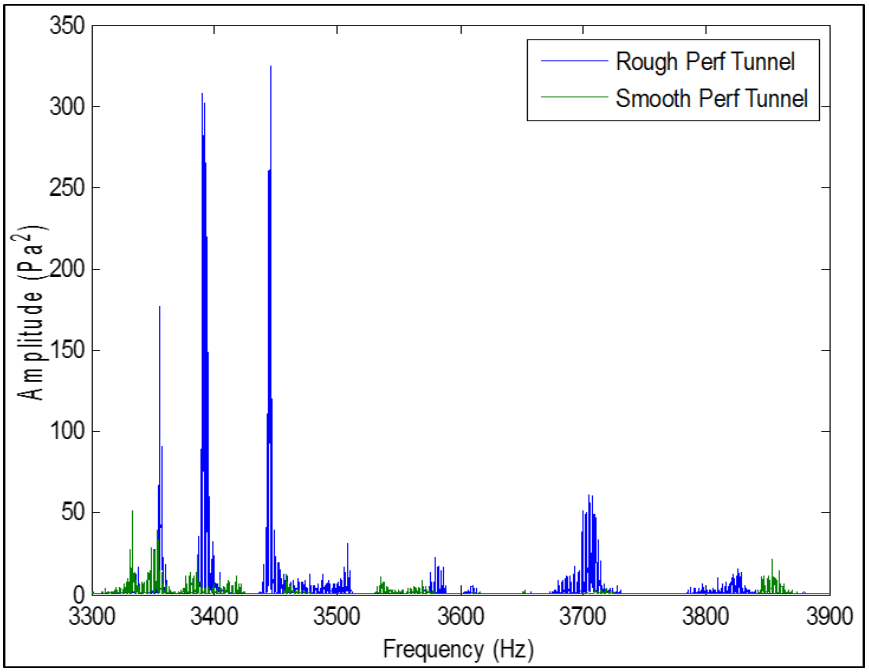

Figure 33: Perforation Tunnel Smoothness Effect from 3.3-3.9 kHz at 200 scf/hr

In Figure 34, smooth perforation tunnel dominates the 1.2 kHz – 2.0 kHz range. This explains the effect of similar SPL value between smooth perforation tunnel inner surface and rough perforation tunnel inner surface acoustic signal. The SPL calculation taken account into all of the frequency peaks in a specified frequency range. In certain frequency range, rough perforation acoustic signature dominates the spectrum; smooth perforation acoustic signature dominates other ranges of the spectrum.

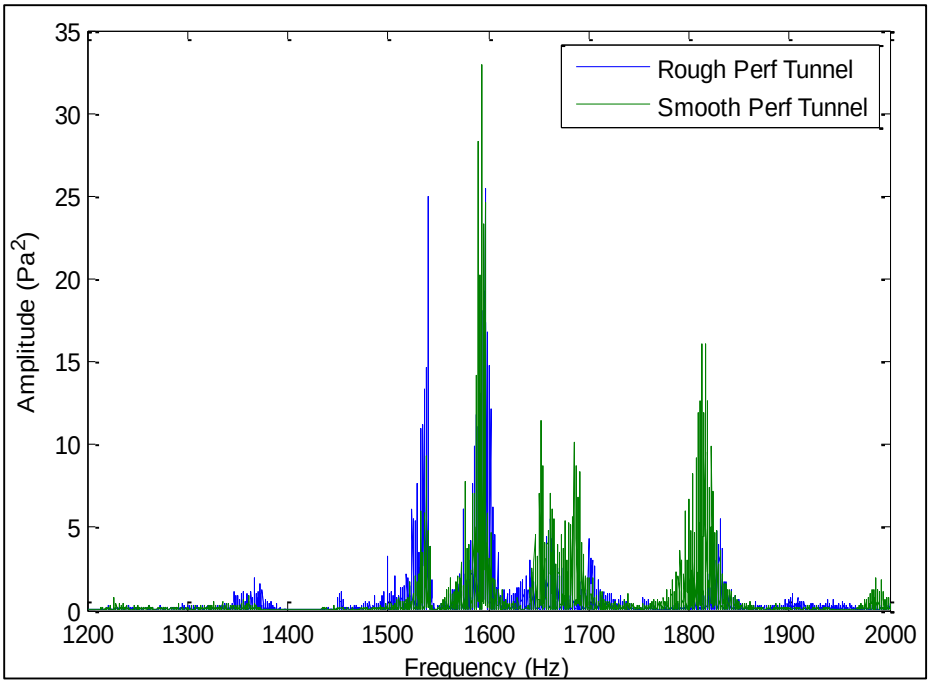

Figure 34: Perforation Tunnel Smoothness Effect from 1.2-2 kHz at 200 scf/hr

To summarize the perforation tunnel inner surface smoothness effect, the increase of the perforation tunnel inner surface roughness causes SPL to increase. The sound amplitude increasing is caused by acoustic signature change. The perforation tunnel inner surface smoothness changes the acoustic signature of the signal.

3.1.8 Multiple Perforation Tunnel Effect

Perforation tunnel typically occurs in clusters, the acoustic signal generated by different perforation tunnel within the perforation cluster can change the characteristics of the acoustic signal recorded by the sensor. In this experiment, multiple perforation tunnel is connected to the wellbore. Experiments are conducted in a 3 perforation tunnel

and 2 perforation tunnel setup. Result of the multiple perforation tunnel is compared to the baseline single perforation tunnel experiment result. The purpose of this multiple perforation tunnel experiment is to determine how perforation clusters affect the acoustic signal. Hydrophone location is fixed at 2.5 inch above the top perforation tunnel in both single and multiple perforation tunnel experiments. A picture of the 3 perforation tunnel experimental setup is shown in Figure 35.

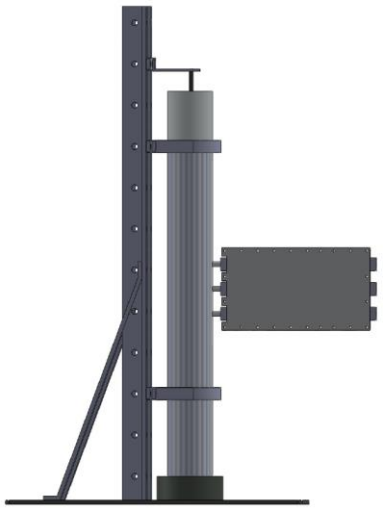

Figure 35; Multiple Perforation Tunnel setup

In Figure 36, SPL curve of 3 different multiple perforation experimental setups is plotted with flow rate in scf/hr on the x-axis and sound amplitude in dB on the y-axis. In the single perforation case, the flow rate is the flow meter measurement reading; in the multiple perforation case, the flow rate used on the plot is the sum of all perforation tunnel flow rate. In Figure 36, observation can be made that acoustic sound amplitude is much higher in a single perforation setup compare to multiple perforation setup. The

cause might be the much higher flow rate in an individual perforation tunnel. All of the individual perforation flow rate comparing to single perforation flow rate is recorded in Table 1.

Table 1: Individual Perforation Flow Rate in Multiple Perforation Experiment

3 Perforation Tunnel Experiment				2 Perforation Tunnel Experiment			Single Perf Tunnel Exp
Top	Middle	Bottom	Sum	Middle	Bottom	Sum	
Flowrate (scf/hr)	Flowrate (scf/hr)	Flowrate (scf/hr)	Flowrate (scf/hr)	Flowrate (scf/hr)	Flowrate (scf/hr)	Flowrate (scf/hr)	Flowrate (scf/hr)
36	24	24	84	60	42	102	100
48	36	42	126	84	63	147	140
66	54	54	174	102	84	186	170
78	66	66	210	120	99	219	200
90	78	78	246	144	120	264	235
108	90	90	288	162	132	294	270
120	99	102	321	180	150	330	300
132	111	111	354	192	162	354	340
144	123	120	387	216	180	396	370
156	132	132	420	228	198	426	410
168	147	144	459	252	216	468	450
180	156	156	492	264	228	492	485
192	168	168	528	288	240	528	510
204	180	177	561	303	252	555	548
216	192	186	594	324	264	588	582
228	198	141	567	336	282	618	616
240	210	207	657	360	300	660	651

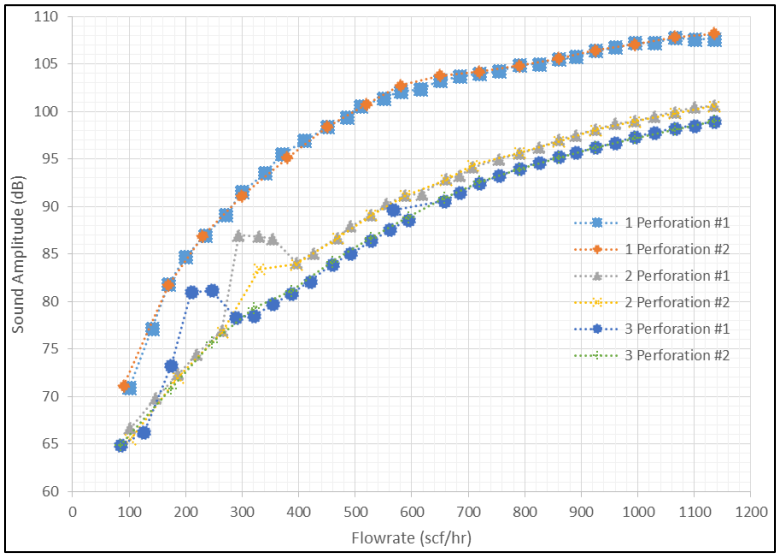

Figure 36: Multiple Perforation Tunnel SPL vs Flow Rate Curve

In Figure 36, a couple of data points are off the general trend curves; in the 3 perforation experiment from 200 scf/hr to 300 scfh/hr range and 2 perforation experiment from 270 scf/hr to 390 scf/hr range. A possible explanation is that the experimental system might display natural coupling resonant frequency at those particular flow rate. Further investigation is performed to understand such phenomena. In the 2 perforation tunnel experiment, acoustic signal at 354 scf/hr and 396 scf/hr are used to study the natural coupling resonant frequency effect. Measurement at 354 scf/hr is the abnormal data point and data point at 396 scf/hr is the normal one fits the trend line.

In Figure 37, the acoustic peaks at 396 scf/hr dominate the frequency spectrum in the plotted range. However, the abnormal acoustic signal frequency at 354 scf/hr has a

higher SPL value compare to acoustic signal at 396 scf/hr. To further understand the root cause of higher SPL at 354 scf/hr, frequency spectrum below 1 kHz is plotted.

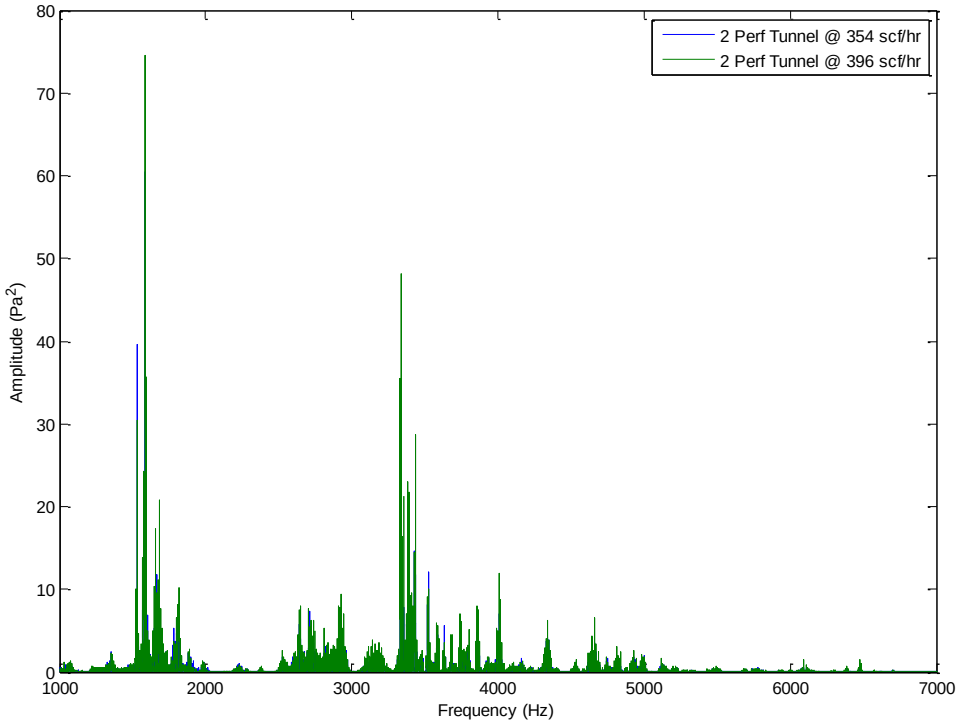

Figure 37: 2 Perforation Tunnel Effect from 1-7 kHz at 359 & 396 scf/hr

In Figure 38, observation can be made that large frequency peaks occur at 320 Hz and 640 Hz at flow rate 354 scf/hr in the 2 perforation experiment. Amplitude of below 1 kHz frequency peaks at 354 scf/hr is too large that after applying band pass filter at cutoff frequency 1 kHz and 7 kHz, large frequency peak still occurs. It's possible that the frequency peak at 640 Hz is the 2nd harmonic of the 320 Hz resonant frequency. From the result shown in Figure 38, the larger SPL at flow rate 354 scf/hr compare to

396 scf/hr is caused by a resonant frequency generated by running the experiment at a particular condition.

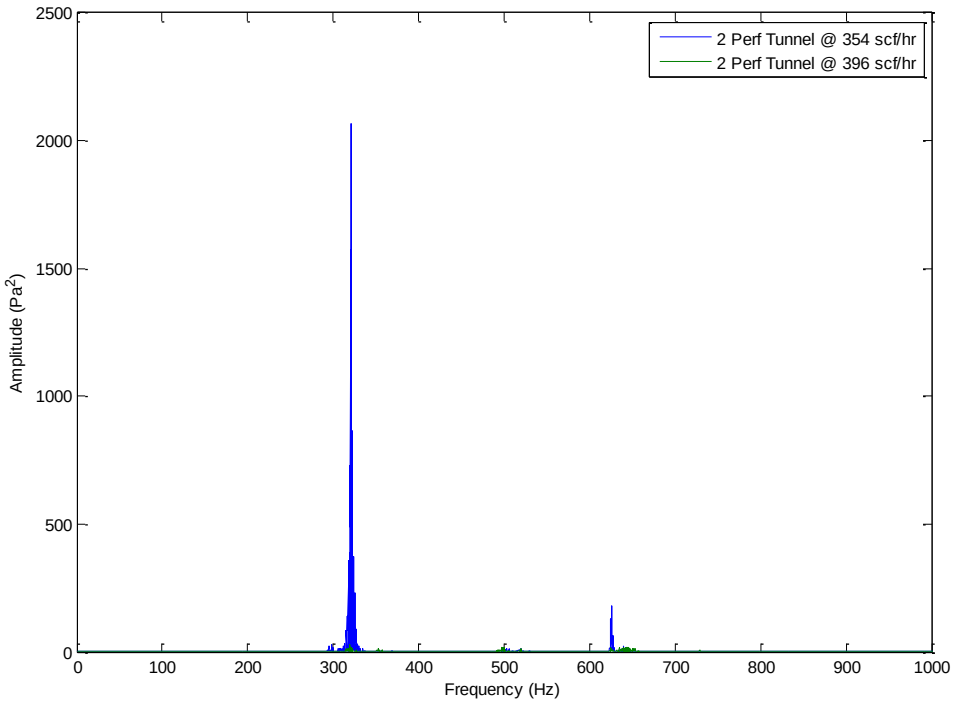

Figure 38: 2 Perforation Tunnel Effect from DC-1 kHz at 359 & 396 scf/hr

In Figure 39, frequency signature for multiple perforation effect is plotted. Some of the frequency signature is persevered when the number of perforation tunnel is increased from one to three. There are frequency peaks associated with multiple perforations only comparing to the acoustic signature of a single perforation tunnel. The measured flow rate for single perforation tunnel is 200 scf/hr, sum of 2 perforation tunnels is 210 scf/hr, and sum of 3 peroration tunnels is 219 scf/hr.

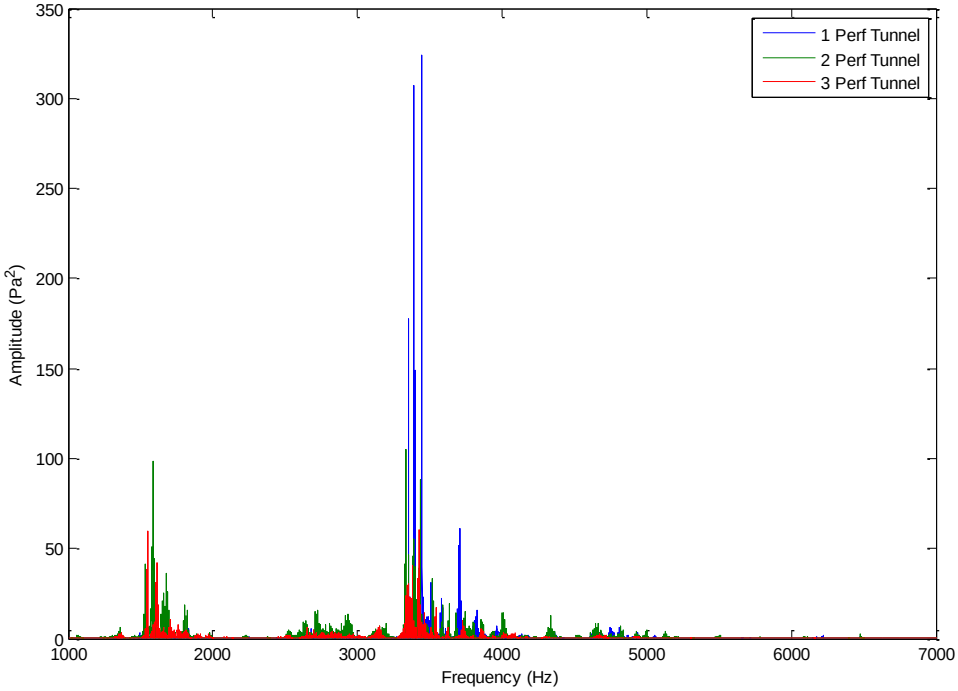

Figure 39: 3 Perforation Tunnel Effect from 1-7 kHz at 210 scf/hr

A plot for higher flow rate with only 2 perforation and 3 perforation tunnels is shown in Figure 40. The measured flow rate of the sum of 2 perforation tunnels is 520 scf/hr and sum of 3 perforation tunnels is 528 scf/hr. In Figure 40, some of the frequency pattern is preserved when the number of perforation tunnels increased from 2 to 3. However, there are a number of distinct acoustic signature difference when the perforation tunnel increases from two to three.

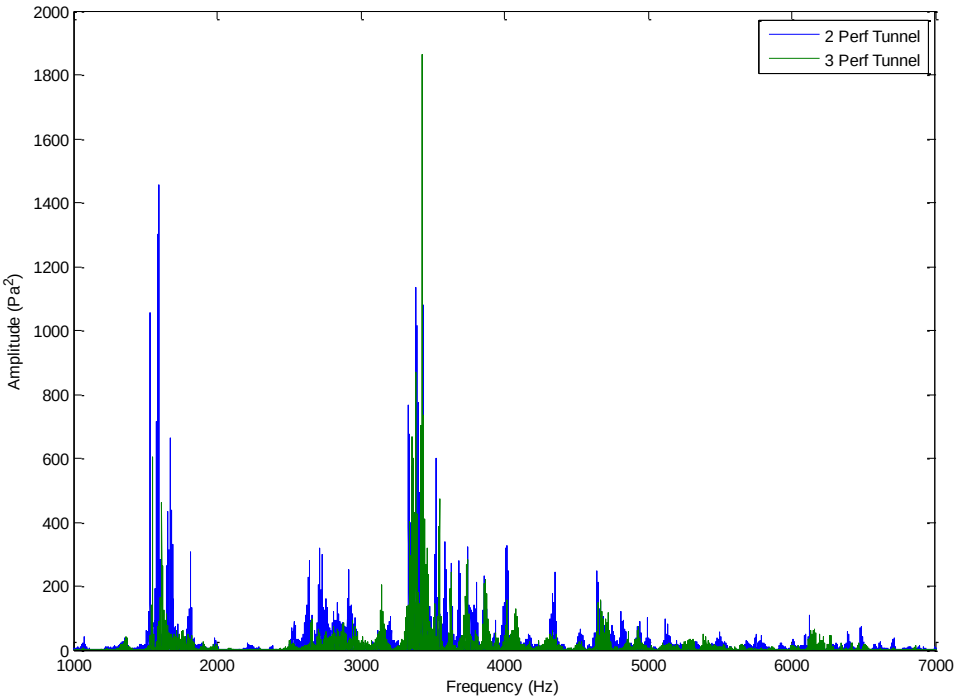

Figure 40: 2 Perforation Tunnel Effect from 1-7 kHz at 525 scf/hr

In the earlier part, experimental data shows only the amplitude of the frequency peak increases when flow rate increases in the single perforation experimental setup. A similar analysis is performed on the 3 perforation setup showing the same result. In Figure 41, frequency domain information of 3 different flow rates in the 3 perforation tunnel experiment is plotted. As the flow rate increases, only the amplitude of the frequency components increases and the location of frequency peaks remain the same. The flow rate effect result of the 3 perforation experiment confirms the conclusion of earlier section.

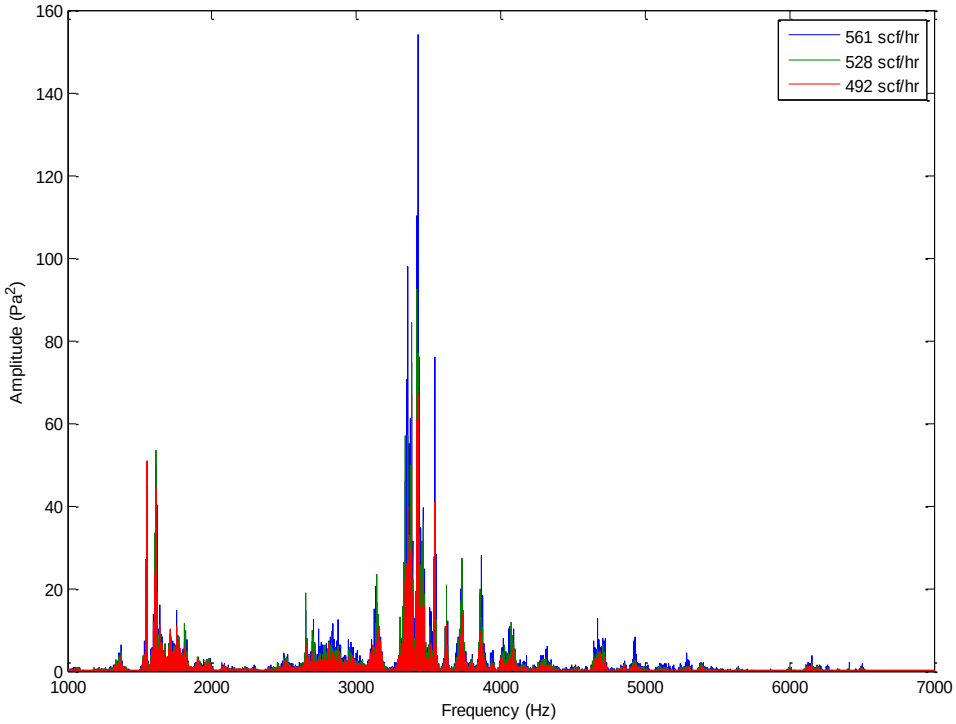

Figure 41: 3 Perforation Tunnel Effect from 1-7 kHz at 492, 528, and 561 scf/hr

To summarize the multiple perforation tunnel effect, when the hydrophone location is fixed at a distance from the top perforation tunnel and number of perforation tunnel is increased, some of the acoustic signature is preserved and other acoustic signature changes. The single perforation tunnel has the largest SPL caused by higher flow rate through the perforation closest to the hydrophone. In the multiple perforation experiment, when flow rate increases only the amplitude of the frequency component increases and location of frequency peaks remain the same.

3.1.9 Flow Distribution Effect

In the first part of this experiment, 2 dividing rails are placed down inside of the fracture cell. The 2 dividing rail screwed in experimental setup is shown in Figure 42. With dividing rail in place, the center perforation and the bottom perforation are producing at different rates. A table of the flowrate data is shown in Table 2.

Table 2: Two Perforation Tunnel with Different Flow Rate

Different Flow Rate (2 Perforation)			Similar Flow Rate (2 Perforation)			Single Perf Tunnel Exp
Middle	Bottom	Sum	Middle	Bottom	Sum	
Flowrate (scf/hr)	Flowrate (scf/hr)	Flowrate (scf/hr)	Flowrate (scf/hr)	Flowrate (scf/hr)	Flowrate (scf/hr)	Flowrate (scf/hr)
90	0	90	60	42	102	100
125	25	150	84	63	147	140
160	40	200	102	84	186	170
190	70	260	120	99	219	200
230	100	330	144	120	264	235
260	110	370	162	132	294	270
300	130	430	180	150	330	300
330	140	470	192	162	354	340
370	155	525	216	180	396	370
410	170	580	228	198	426	410
440	180	620	252	216	468	450
480	200	680	264	228	492	485
520	210	730	288	240	528	510

In the second part of this experiment, no diving rails are in place. The center and bottom perforation tunnels have relatively the same flowrate. The flowrate measurement data is shown in Figure 42. The results of two parts of experiments are compared to

understand the acoustic signal of multiple perforation tunnels at different producing rates. Baseline measurement condition is applied to both parts of the experiments. Hydrophone is placed 2.5 inch above the center producing perforation tunnel. The sound amplitude comparison result of the first and second part of the experiment is shown in Figure 43. Acoustic behavior in frequency domain is shown in Figure 44.

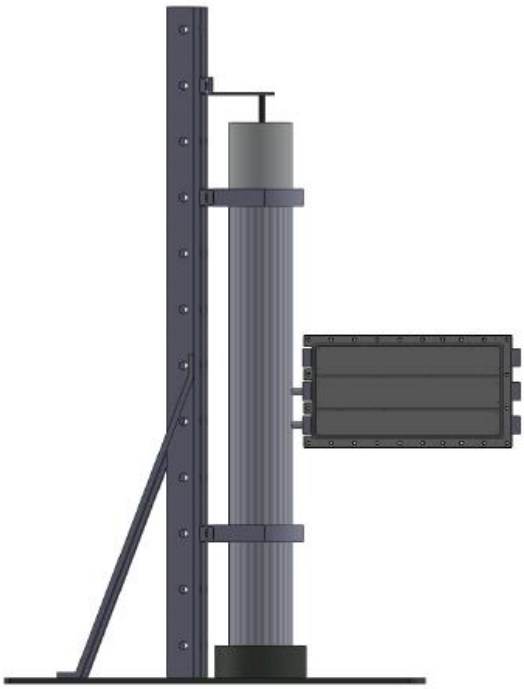

Figure 42: Two Perforation Tunnel with Different Flow Rate Setup

In Figure 43, sum of the 2 perforation tunnel flow rate in scf/hr is plotted on the x-axis and calculated SPL in dB is plotted on the y-axis. On the plot, the data set labeled “2 perforation equal flowrate” represents experimental result with no dividing rails in place; the data set with the name “2 perforation diff flowrate” represents experimental

result with 2 dividing rails in place. When the experiment is conducted with 2 dividing rails in place, larger ratio of flowrate of the top perforation tunnel to the bottom perforation tunnel is shown. In other words, the top perforation tunnel has significant larger flowrate compare to the bottom perforation tunnel.

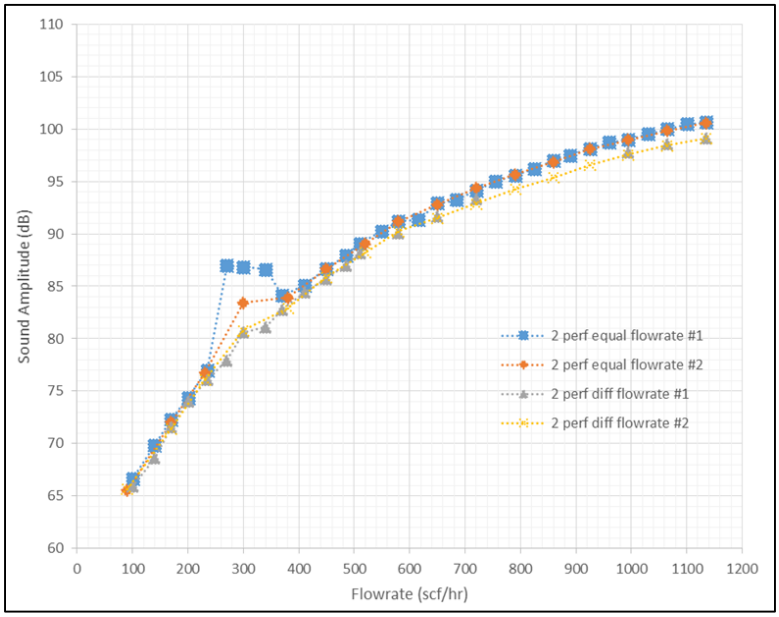

Figure 43: Different Flowrate in Multiple Perforation SPL vs Flow Rate Curve

In Figure 44, acoustic signature is shown in the range from 1 kHz to 7 kHz. The data set with label “equal perforation flowrate” has a top perforation flow rate of 84 scf/hr, a bottom perforation flow rate of 63 scf/hr, and a sum of 2 perforation tunnel flow rates at 147 scf/hr. Another data set on the same plot named “different perforation flowrate” has a top perforation flow rate of 125 scf/hr, a bottom perforation flow rate of 25 scf/hr, and a sum of 2 perforation tunnel flow rates at 150 scf/hr. The value of the

sum of 2 perforation tunnel flow rate data sets is very close with only 3 scf/hr difference. However, the ratio of top perforation tunnel flow rate to the bottom perforation tunnel flow rate is very different. Therefore, the 2 experiment conditions have different flow distributions. A detailed comparison of the 2 experiment conditions is shown in Table 3.

Table 3: Two Perforation Tunnel with Total Flow Rate of 150 scf/hr

Different Flow Rate (2 Perforation)				Similar Flow Rate (2 Perforation)			
Middle Flowrate (scf/hr)	Bottom Flowrate (scf/hr)	Sum Flowrate (scf/hr)	Ratio Middle/ Bottom	Middle Flowrate (scf/hr)	Bottom Flowrate (scf/hr)	Sum Flowrate (scf/hr)	Ratio Middle/ Bottom
84	63	147	1.33	125	25	150	5

In Figure 44, most of the acoustic signatures match between relatively equal perforation flow rate and different perforation flowrate datasets. At certain frequency locations, the amplitude of the frequency peaks are different. This behavior might be caused by the different flow rate in each perforation tunnels.

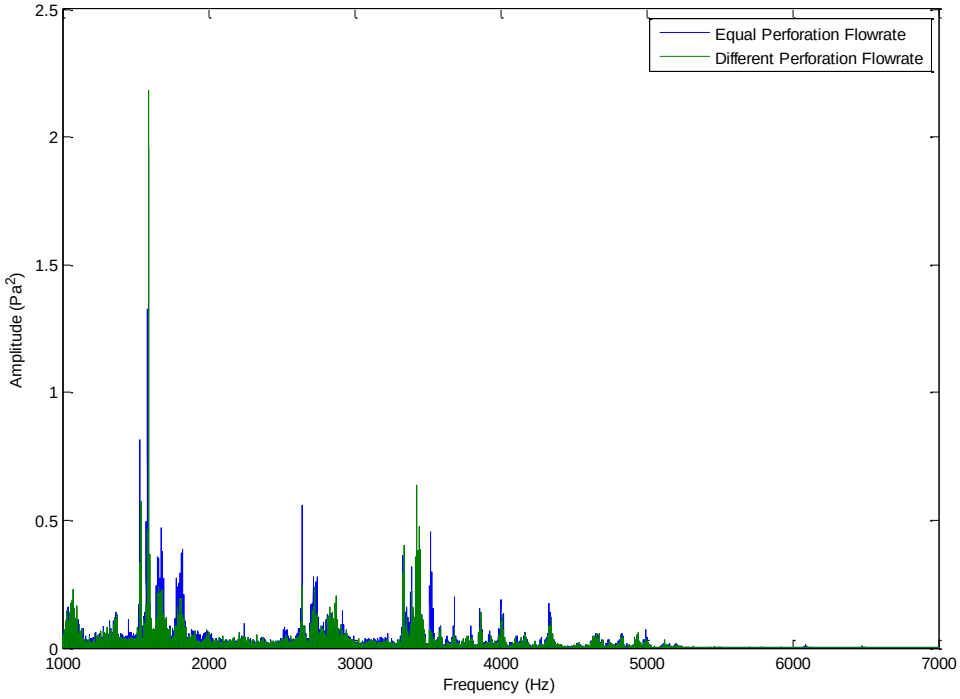

Figure 44: Different Flowrate in Multiple Perforation from 1-7 kHz at 150 scf/hr

To summarize the different flow rate in multiple perforation effect, analysis is performed on 2 data sets with top to bottom perforation tunnel flow rate ratio of 25 and 1.33. Both data sets show similar SPL along different flow rate when hydrophone is fixed 2.5 inch above the top perforation tunnel. On the frequency spectrum, acoustic signature of the high and low top to bottom perforation tunnel flow rate ratio experiments show similar pattern. Only the amplitude of some particular frequency components change when flow distribution changes and hydrophone location is fixed at a distance above the top perforation.

3.1.10 Hydrophone Location Effect

Measurement sensor placement plays a vital role in measuring sound amplitudes of acoustic signals. The closer the sensor to the sound source, the higher sound amplitude the sensor records. To verify this effect, an experiment is conducted to determine the hydrophone location effect by moving the hydrophone 6.5 inch and 10.5 inch above the perforation tunnel. The result from the new hydrophone location is compared with the baseline setup, which fixes the hydrophone 2.5 inch above the perforation tunnel.

In Figure 45, the data sets with the name “2.5 in”, “6.5 in”, and “10.5 in” represent measurements taken when hydrophone is placed 2.5 inch, 6.5 inch, and 10.5 inch above the perforation tunnel. In Figure 45, as the hydrophone moves away from the sound source or perforation tunnel SPL decreases. The largest SPL is recorded when the sensor is placed closest to the perforation tunnel at 2.5 inch.

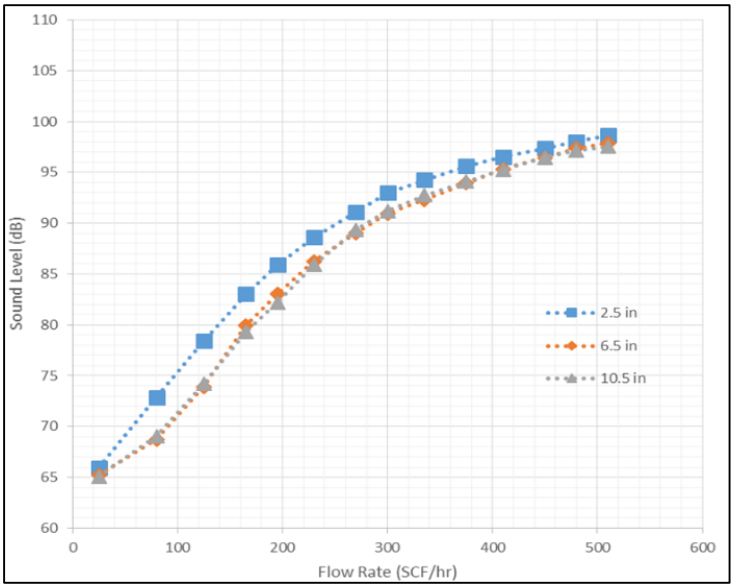

Figure 45: Hydrophone Location SPL vs Flow Rate Curve

In the Frequency Domain, acoustic behavior is shown in Figure 46. The locations of the dominate peaks of the acoustic signals are relatively the same. The acoustic signal when the hydrophone is 2.5 in above the perforation tunnel has larger amplitude of some particular frequency components.

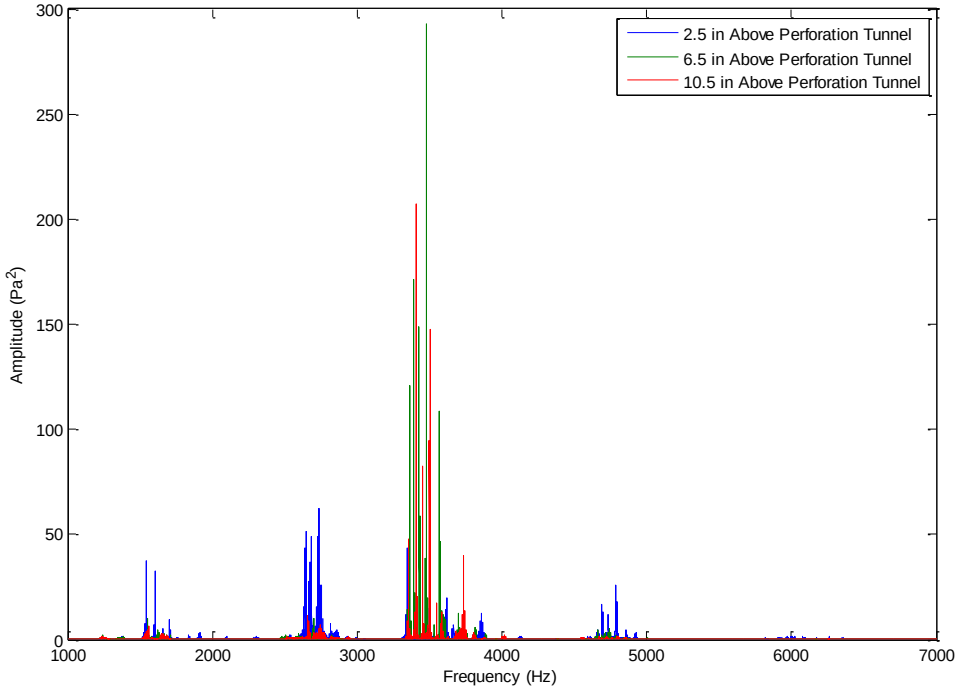

Figure 46: Hydrophone Location Effect from 1-7 kHz at 195 scf/hr

To summarize the effect of hydrophone locations, as hydrophone moves away from the sound source SPL decreases. Acoustic measurement is affected by the location of the measurement device. Amplitude of certain frequency component changes as hydrophone moves away from the sound source.

3.1.11 Sampling Interval Effect

The baseline measurement data set is based on 10 second of the audio samples collected at 50 kHz sampling rate. This experiment investigates if the sampling time interval has any effect on the data collected by the hydrophone. A single dataset is being

studied at 10 second, 5 second, and 1 second. A sampling interval effect SPL vs flowrate plot is generated to compare the results from 3 different time sampling intervals.

SPL vs flow rate of 10 seconds, first 5 seconds, and first second of the baseline data set is plotted in Figure 47. From Figure 47, the first second, first 5 seconds, and the entire 10 seconds of data show the same sound amplitude in dB.

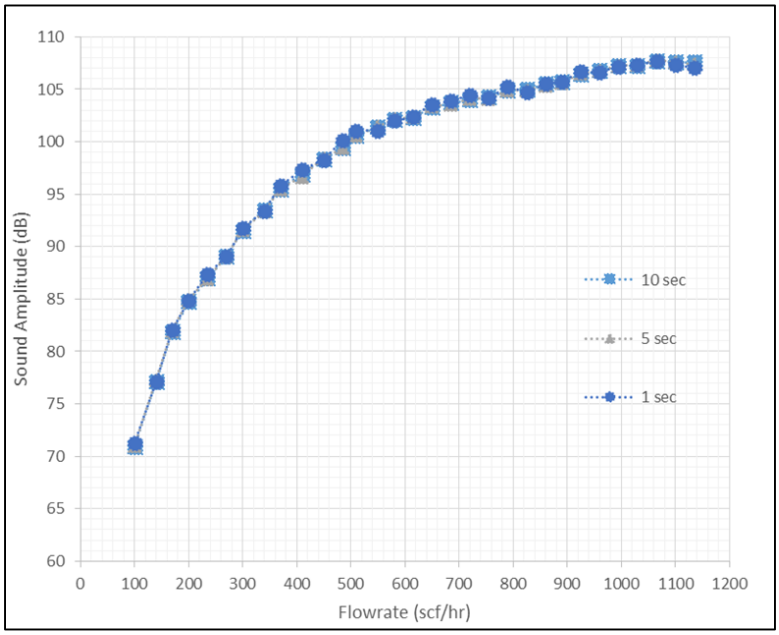

Figure 47: Sampling Interval Effect SPL vs Flow Rate Curve

In Figure 48, frequency domain plot of the sampling interval effect shows acoustic signature is the same among 1 second, 5 seconds, and 10 seconds of the same data set. There is frequency component amplitude difference at a few particular frequencies. The sampling interval does not have noticeable effect on the measurement result.

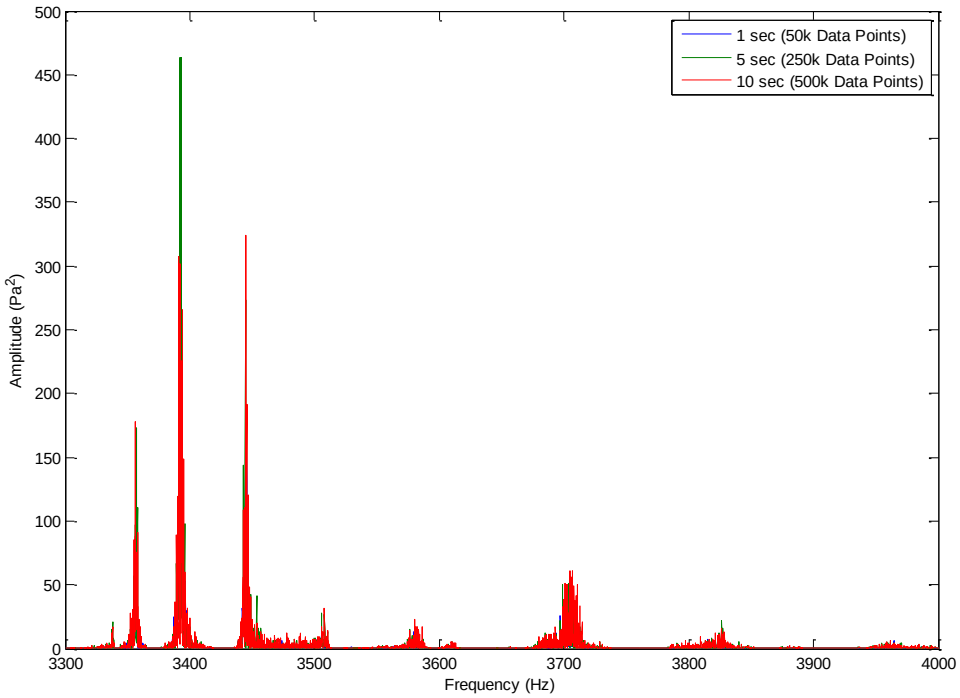

Figure 48: Sampling Interval Effect from 3.3-4 kHz at 200 scf/hr

To summarize the sampling interval effect, acoustic signature remains the same when sampling interval changes. There are a few peaks only the amplitude changes as sampling interval changes. SPL calculation shows the same result for 3 different sampling intervals. Sampling interval has not much effect on measurement and analysis results.

3.1.12 Two Phase Wet Proppant Effect

In this experiment, the effect of water in the fracture cell is investigated. Prior to blowing single phase gas through the fracture cell, water is injected through the fracture cell by a displacement pump. After the injection of the water through the fracture cell,

single phase gas is then running through the fracture cell in the same condition as the baseline experimental setup. The purpose of the experiment is to compare the acoustic behavior of high gas oil ratio (GOR) fluid to single phase gas flows through the fracture cell.

The results of water wet proppant experiments are shown in Figure 49, the sound amplitude of water wet proppant in the fracture cell is different from the dry proppant, which is used in the baseline experimental condition. The overall shape of the sound amplitude vs flowrate remains the same. 2 wet proppant measurement datasets are used in the analysis. Both datasets show similar results of the sound amplitude vs flow rate curve.

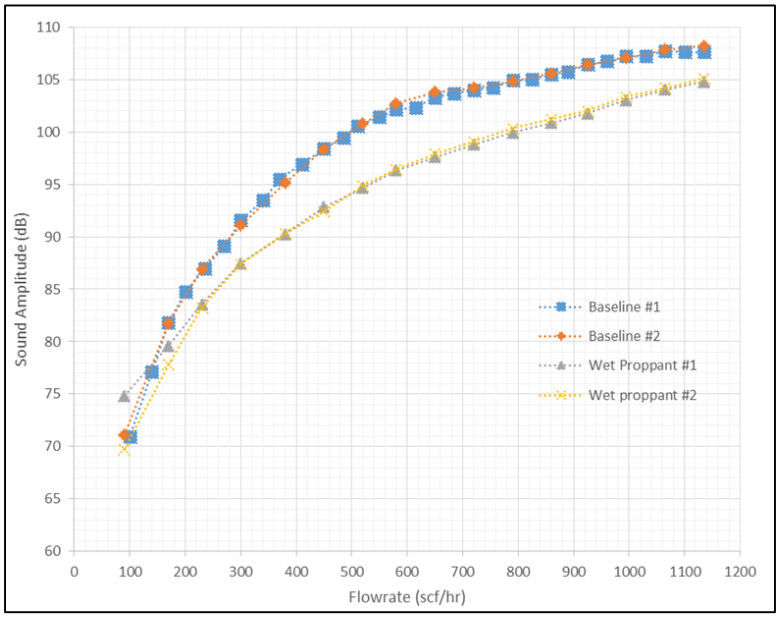

Figure 49: Water Wet Proppant SPL vs Flow Rate Curve

Frequency domain information is shown comparing the acoustic behavior difference between water wet proppant and dry proppant is shown in Figure 50. Multiple water wet proppant data sets are plotted in Figure 50. Some of the frequency signature information is preserved in water wet proppant comparing to the dry proppant experiment. However, other acoustic information is changed in the water wet proppant. In Figure 50, the frequency information from 3.3 kHz to 3.4 kHz is preserved in the water wet proppant fracture cell experiment. Acoustic signature is changed in other frequency ranges on the plot.

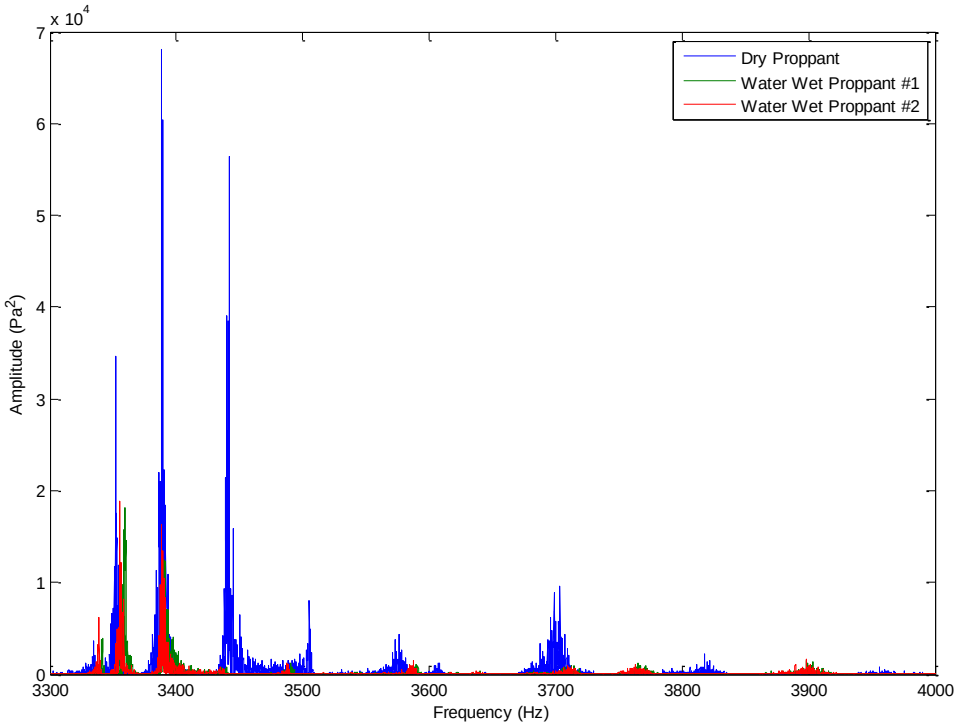

Figure 50: Water Wet Proppant Effect from 3.3-4 kHz at 1065 scf/hr

The plot in Figure 51 shows frequency plot ranges from 2 kHz to 3 kHz of water wet proppant and baseline single phase dry proppant. From the 2.5 kHz to 3 kHz range, acoustic signature is preserved in the water wet proppant experiment data compare to the baseline dry proppant experiment data. In the 2 kHz to 2.5 kHz range, acoustic signal is different for the 2 experimental conditions.

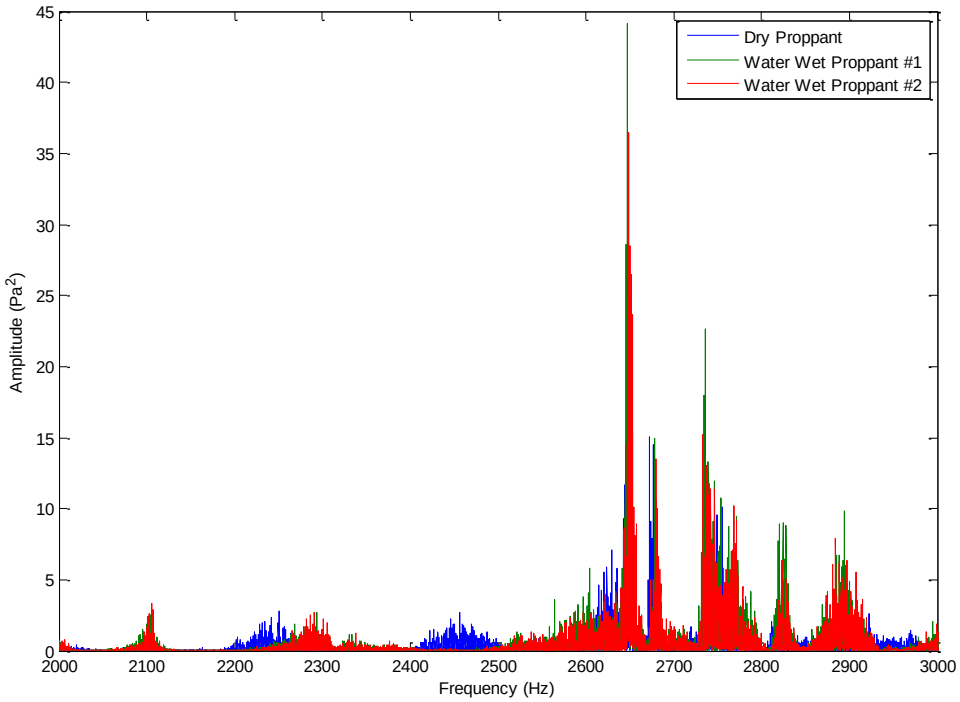

Figure 51: Water Wet Proppant Effect from 2-3 kHz at 230 scf/hr

To summarize the water wet proppant effect, SPL curve changes when water is introduced to the baseline single phase gas experiment. In the frequency domain, some of the acoustic signature is preserved in the wet proppant experiment compare to dry

proppant experiment. Other frequency information is changed when water is introduced in the system.

3.1.13 Two Phase Liquid Column Effect

The effect of liquid column in the wellbore on acoustic signal change is investigated in this experiment. The baseline experimental setup condition is applied to this experiment with a water filled wellbore. Hydrophone is placed 2.5 inch above the perforation tunnel. Liquid used in this experiment is water with the room temperature. Water level is kept at 20.5 inch below the perforation, 2 inch below the perforation, and at the perforation level. Effect of acoustic signal change is studied under different water column level conditions. Figure 52 displays the results.

In Figure 52, there is not much sound amplitude difference among different water levels in the wellbore. All water column level experimental data sets show relatively the same sound amplitude at a given flow rate. The shape of SPL curve remains the same when the water column level increases in the wellbore. In order to further understand the difference, detailed frequency domain analysis is performed.

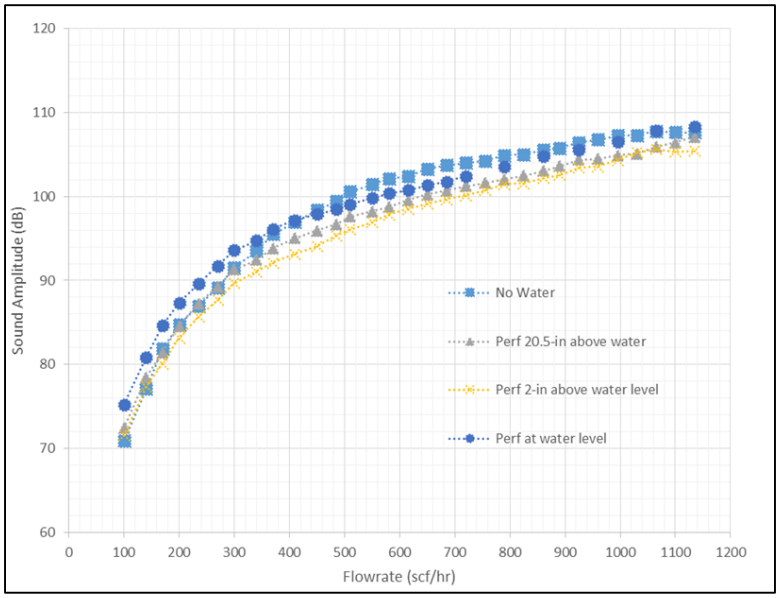

Figure 52: Liquid Column Effect SPL vs Flow Rate Curve

In Figure 53, acoustic signal is compared between perforation tunnel 20.5 inch above the water level and 2 inch above the water level. Figure 53 plots acoustic signature in the 1 kHz to 7 kHz at flow rate of 510 scf/hr. Most of the frequency signature remains the same when water level is increased 18.5 inch from 20.5 inch below the perforation tunnel to 2 inch below the perforation tunnel level in the wellbore. However, there are distinct differences on certain frequency ranges when the water level is increased significantly in the wellbore. Acoustic signature changes when the water level is increased closer to the perforation tunnel.

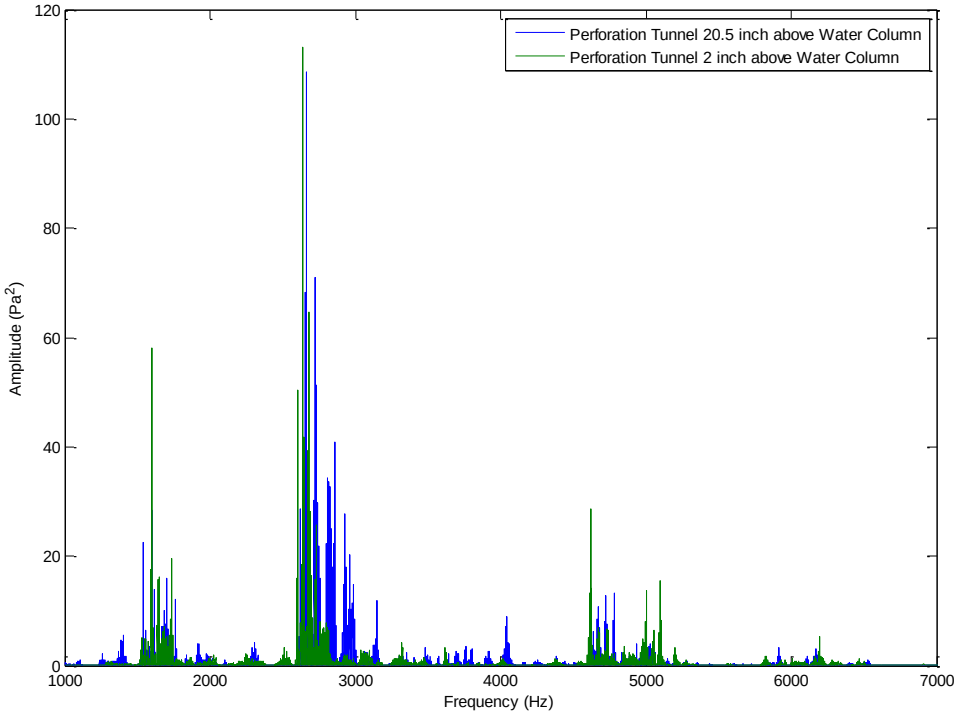

Figure 53: Liquid Column below Perforation Effect from 1-7 kHz at 200 scf/hr

In Figure 54, a similar trend can be seen compare to Figure 53. The water level is increased another 2 inch to reach right below the perforation tunnel. The acoustic behavior of water level at the perforation tunnel is compared to the water level of 2 inch below the perforation tunnel. Similar to Figure 53, most of the frequency signature remains the same between the 2 data sets. Certain frequency characteristics change was observed when the water level is increased to the perforation tunnel level compare to water level 2 inch below the perforation tunnel.

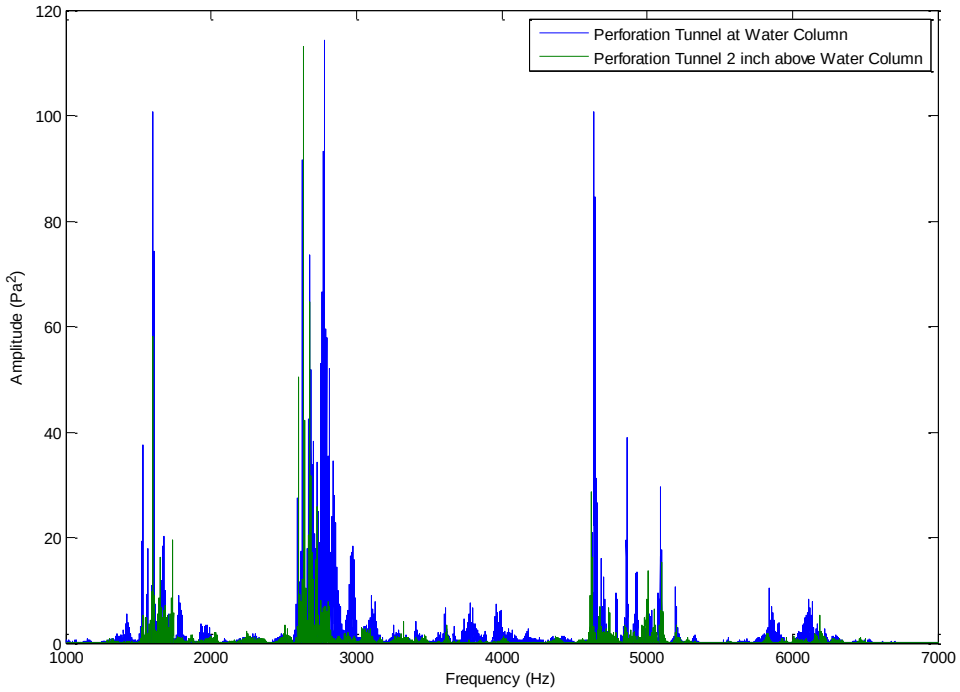

Figure 54: Liquid Column at Perforation Effect from 1-7 kHz at 200 scf/hr

Figure 55 plots the acoustic behavior of perforation tunnel 2 inch above the wellbore water level when flow rate changes. The purpose of this experiment is to verify if the conclusion from earlier flow rate effect experiment is still valid when a liquid phase is introduced to the system. The experimental result shows that only the amplitude of frequency component increase when flow rate increase when a column of liquid is introduced to the experiment. The conclusion from earlier flow rate effect with single phase gas experiment is validated in this 2 phase experimental setup result.

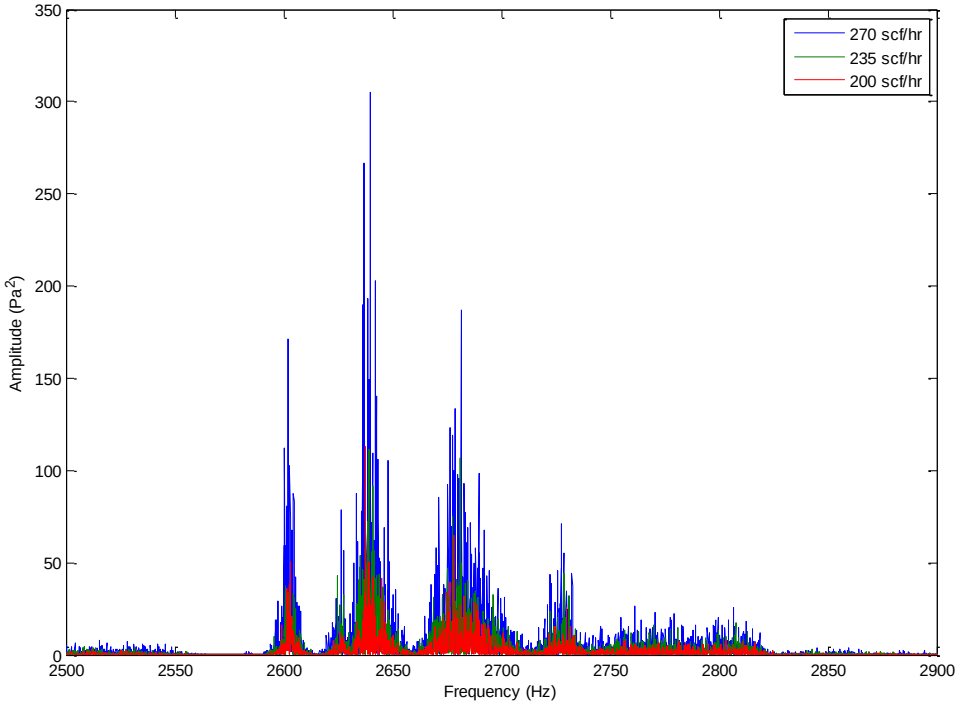

Figure 55: Perforation Tunnel 2 inch above Water Level at 200, 235, and 270 scf/hr

To summarize the effect of a column of water in the wellbore, the sound amplitude level curve remain almost the same when water level in the wellbore is increased. Also the shape of SPL curve remain the same when water level in the wellbore changes. In the Frequency domain, some of the acoustic signature remains the same while others are changed when the water level is changes in the wellbore.

3.1.14 Fracture Cell Effect

In the fracture cell effect experiment, the acoustic signature of a perforation tunnel compare to a combination of a fracture cell and a perforation tunnel is studied. The same injection gas hose is used in both experiments. The purpose of this experiment

is to determine how dominate the perforation tunnel affects the overall acoustic signal generated by flow from fracture to wellbore system. Also, it serves as a feasibility study of if fracture information can be extracted from the acoustic signal generated by the fluid flows from a fracture to a wellbore through perforation tunnels.

In this experiment, the fracture cell is removed. Perforation tunnel is directly connected to the injection connection. All other experimental condition is kept the same as the baseline experimental setup. The perforation flow rate is measured and SPL is calculated at each measured flow rate.

In Figure 56, SPL of the acoustic signal generated by only the perforation tunnel is compared to the acoustic signal made by a combination of perforation tunnel and fracture cell. The acoustic signal of perforation only has significantly larger SPL than the baseline fracture cell experiment SPL at any given flow rate. The shape of the SPL curve remains the same for the perforation tunnel only experiment. To further understand the acoustic behavior difference, a frequency domain analysis is performed.

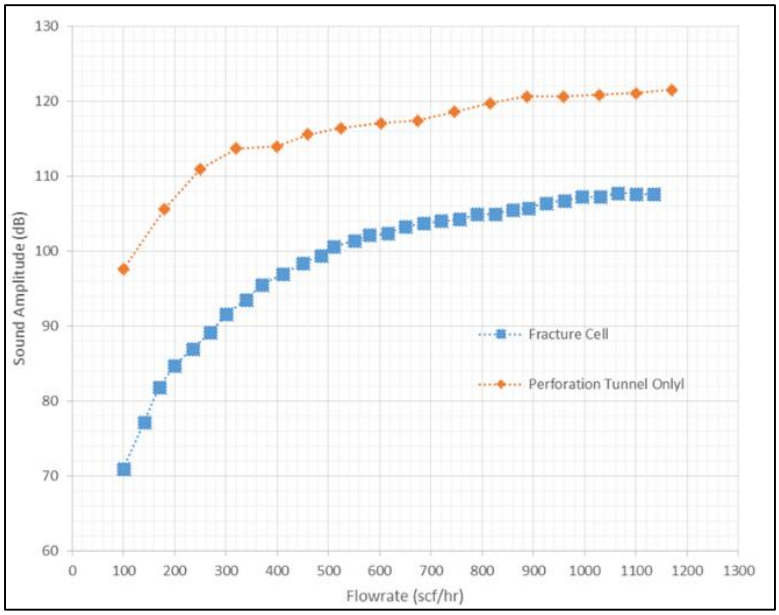

Figure 56: Fracture Cell Effect SPL vs Flow Rate Curve

In Figure 57, the acoustic signal of perforation only experiment at a flow rate of 180 scf/hr is compared to the baseline fracture cell experiment at flow rate of 170 scf/hr from 4 kHz to 5 kHz range. Due to the large sound amplitude difference, the amplitude of the perforation only acoustic signal is significantly larger than the baseline fracture cell experiment at any given flow rate. The baseline fracture cell acoustic signal is fully covered by the perforation only acoustic signal. Thus, the acoustic behavior of the overall baseline fracture cell is dominated by the perforation tunnel parameters.

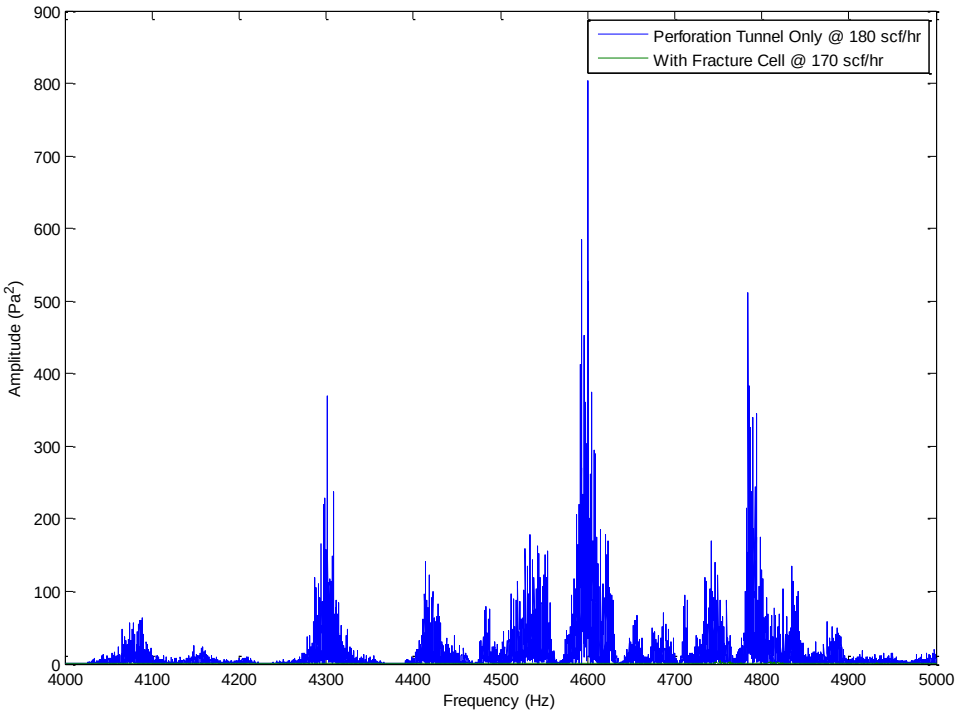

Figure 57: Fracture Cell Effect from 4-5 kHz at 180 & 170 scf/hr

In order to visibly compare the acoustic behavior of perforation only and baseline fracture cell experimental setup, a baseline fracture cell data set with higher flow rate is used for the analysis. In the earlier section, the experimental result shows that only the amplitude of frequency components increases when the flow rate increases. A baseline fracture cell experiment data set at 510 scf/hr is used to compare with the perforation only experiment at 180 scf/hr result. In the same frequency range from 4 kHz to 5 kHz as shown in Figure 57, the acoustic signature changes in perforation only compared with the baseline fracture cell experiment. Therefore, although perforation tunnel acoustic effect dominates the overall fracture to wellbore system acoustic signal, the fracture does affect the acoustic signal collected by the hydrophone in the wellbore.

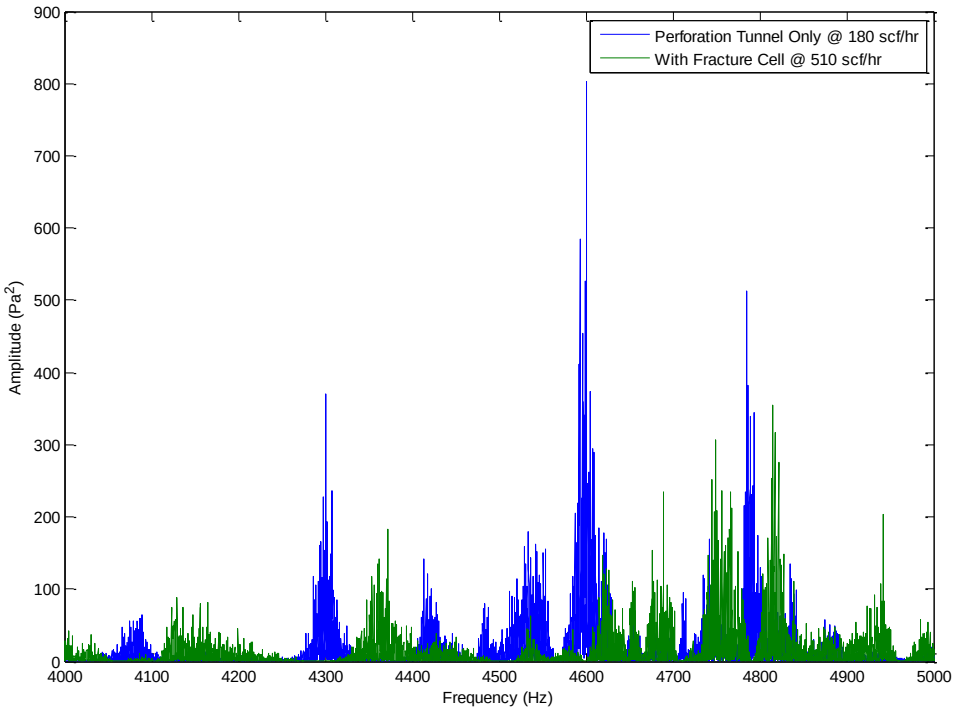

Figure 58: Fracture Cell Effect from 4-5 kHz at 180 & 510 scf/hr

Although facture cell changes the acoustic behavior of the overall system, the combined perforation and fracture cell system still shows the same pattern as the acoustic signals for the perforation only setup. In Figure 59, flow rate of the baseline fracture cell is again increased to view the plot better. The plot in Figure 59 shows similar frequency component pattern of the acoustic signals between the perforation tunnel only and the fracture cell. Although the pattern of acoustic peaks is similar, shifting of the frequency peaks still occurs on the plot.

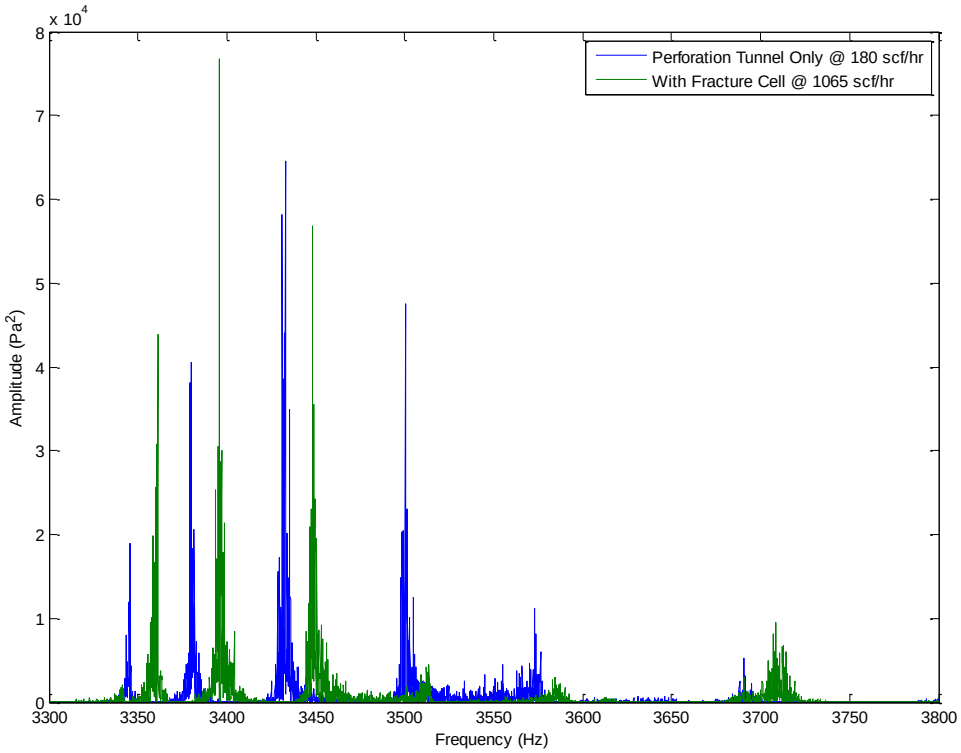

Figure 59: Fracture Cell Effect from 3-3.8 kHz at 180 & 1065 scf/hr

To summarize the fracture cell effect, sound amplitude of perforation only system is significantly larger than a combination of fracture cell and perforation. In the frequency domain, acoustic behavior of the combined system of fracture cell and perforation is dominated by the perforation tunnel. However, fracture cell does change the acoustic signature of fluid flows from fracture to wellbore system. As long as the portion of the acoustic signal affected by the fracture is extracted, information about the fracture can be obtained.

3.2 Acoustic Behavior of Horizontal Wellbore

An experimental matrix is developed to study the acoustic behavior of flow from fracture to a Horizontal wellbore. A baseline experiment condition is established to serve as the experiment reference point. The baseline horizontal wellbore experimental setup a total horizontal distance of 8.5 ft long. The fracture cell and facture to perforation connection is the same as the vertical wellbore setup. The hydrophone system is connected through flex conduit to the L-bracket mounted on the top of vertical wellbore. Addition supporting legs push against the inner wall of horizontal pipe to hold the sensor in the center of the pipe. The location of the hydrophone is visually inspected to ensure centering of the sensor system. The experimental procedure on the horizontal experimental setup is the same as the established procedure on the vertical setup. A list of parameters are investigated in the horizontal setup to study if similar acoustic behavior change is observed in the horizontal wellbore setup compare to the observation made on the vertical wellbore setup.

3.2.1 Horizontal Wellbore Experimental Baseline Characteristic

The horizontal wellbore baseline experimental setup uses the same fracture cell as the vertical wellbore setup experiments. The fracture cell connects to the wellbore through an adapter piece and threaded pipe to simulate fracture and perforation tunnel. The fracture cell is filled with 16/30 HSP proppant. Nitrogen flows through the fracture and perforation tunnel system to the wellbore. Acoustic data is recorded by the same hydrophone at a distance away from the perforation tunnel. The sensor system

incorporates 3 additional microphones to form an array of sensor. In order to accommodate the additional microphones in the system, sample rate is changed to 25.6 kHz per channel. The slower sample rate allows better real-time per channel performance on the quad-channel data logger utilizing the Sigma-Delta ADC technology.

In Figure 60, a similar baseline acoustic signature can be observed in the horizontal wellbore experimental setup compare to the vertical wellbore setup. The acoustic signal has complex patterns. Frequency peaks scatter across the 1 kHz to 7 kHz spectrum. Dominate peaks can also be seen on the plot in the similar range compare to the vertical wellbore baseline acoustic signal.

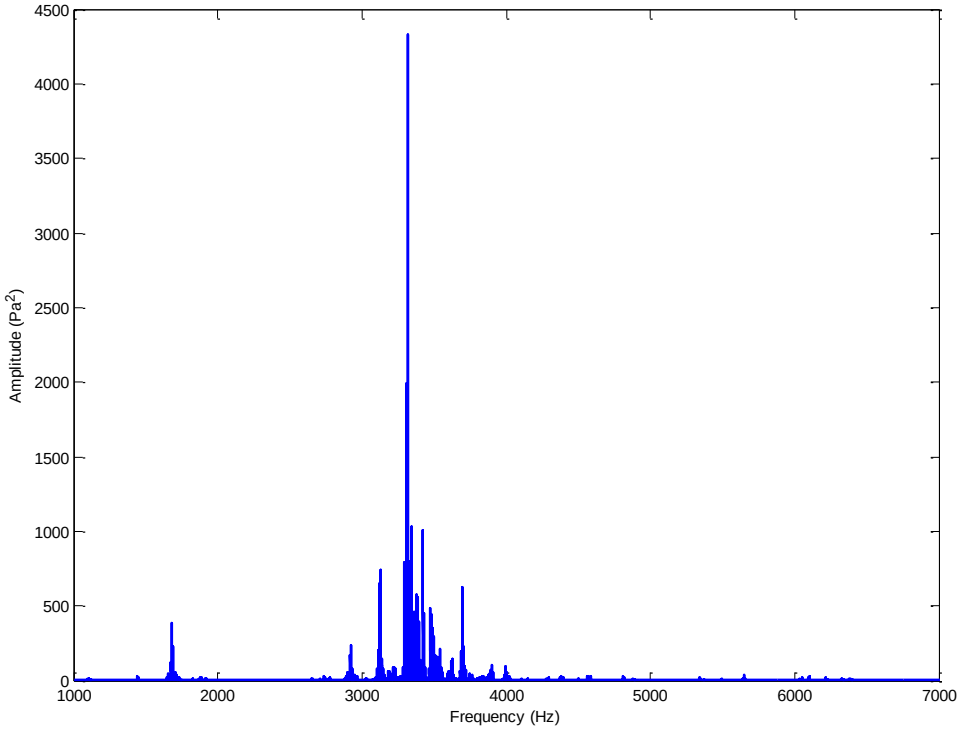

Figure 60: Horizontal Wellbore Baseline from 1-7 kHz at 520 scf/hr

In Figure 61, the frequency spectrum is zoomed in the 3 kHz to 4 kHz range. Acoustic pattern is similar to the vertical wellbore setup. Multiple main frequency peaks are seen in the 3 kHz to 4 kHz range. The dominate frequencies in the 3 kHz to 4 kHz range show that acoustic signal recorded by the hydrophone is not a single peak monotone frequency signal. The acoustic signature of fluid flows from fracture to wellbore through perforation is a complex signal with frequency peaks scattered over a range of frequencies.

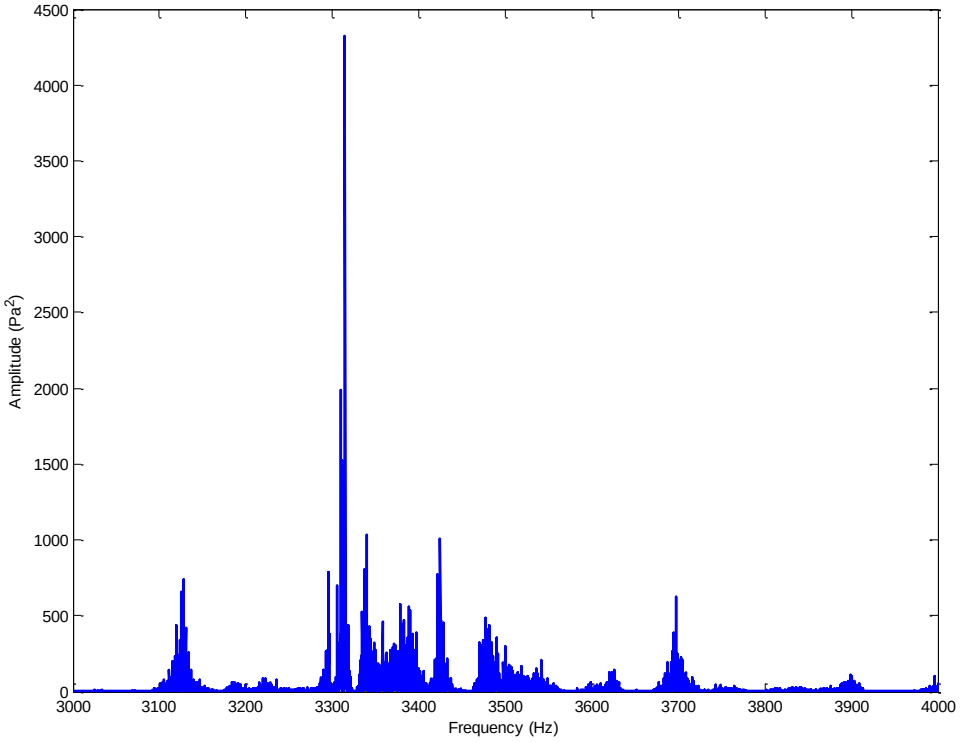

Figure 61: Horizontal Wellbore Baseline from 3-4 kHz at 520 scf/hr

3.2.2 Horizontal Wellbore Flow Velocity Effect

In this experiment, the baseline experimental condition is kept. Gas injected into the inlet of fracture cell is controlled at desired pressure and flow rate. All other parameters are kept the same with only the injection flow rate increases to determine the flow velocity effect on horizontal wellbore acoustic behavior. The same experimental procedure is carried in this horizontal wellbore experiment as in the vertical wellbore flow experiment.

In Figure 62, the acoustic behavior change as flow rate increases is plotted. In the vertical wellbore experiment, observation is made that only the amplitude of acoustic signal increases as flow rate increases. The same observation is also made on the horizontal wellbore experiment. In Figure 62, as the flow rate increases from 230 scf/hr to 380 scf/hr, only the amplitude of the acoustic signal increases.

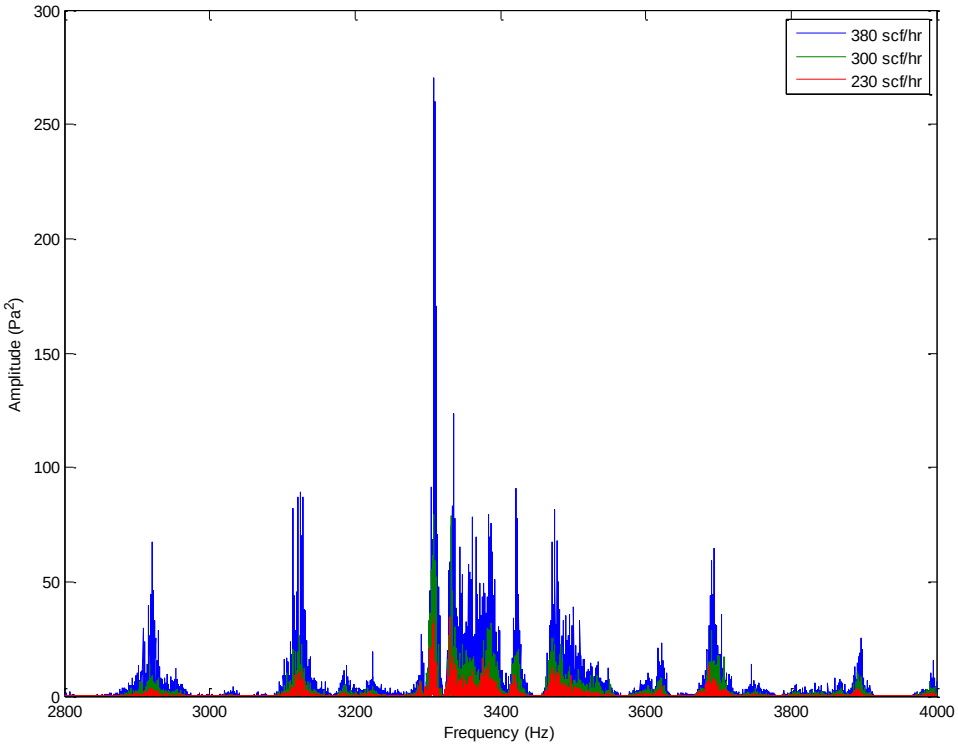

Figure 62: Horizontal Wellbore Flow Velocity Effect from 230-380 scf/hr

In Figure 63, flow rate region is bumped up to the 925 scf/hr to 1065 scf/hr region. The same observation is made that only the amplitude changes as the flow rate changes. Therefore, horizontal wellbore flow velocity effect on acoustic behavior is the same as the vertical wellbore system. Observation from the flow rate experiment is that only amplitude of the acoustic signal frequency component changes as flow rate changes. Location of the acoustic signal frequency component remains the same.

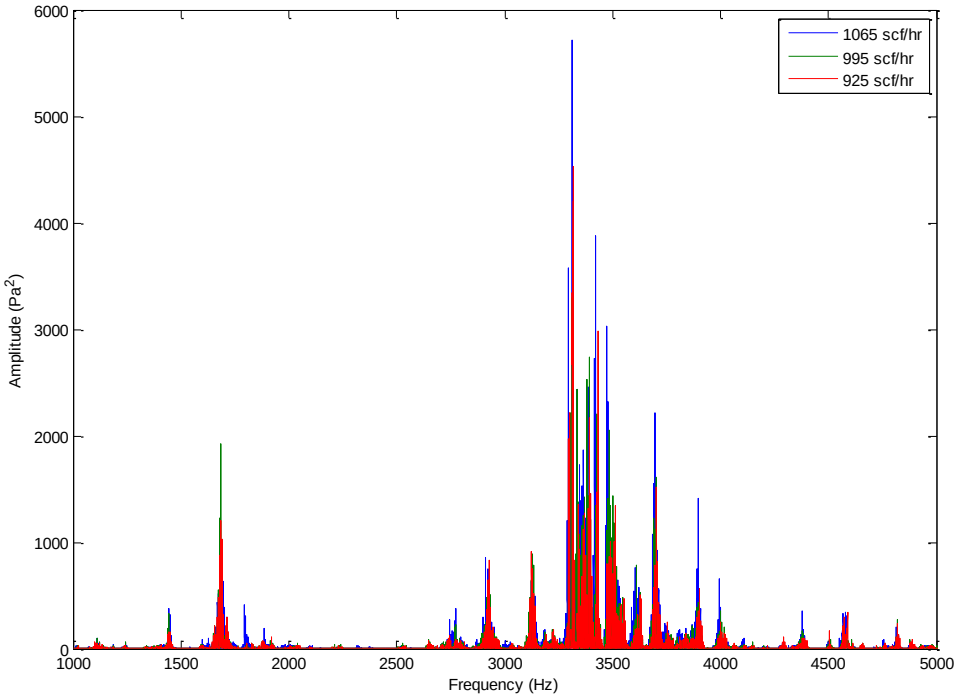

Figure 63: Horizontal Wellbore Flow Velocity Effect from 995-1065 scf/hr

Once an understanding in the frequency domain of the acoustic behavior in horizontal wellbore experiment is established, sound amplitude vs flow rate curve is plotted. The flow velocity SPL curve on the horizontal wellbore experimental setup shows the same shape as the experimental result on the vertical wellbore setup. The change in sound amplitude at different flow rates is related to the flow rate of injected gas. A different slope of the curve is observed on lower flow rate region and higher flow rate region of the SPL curve.

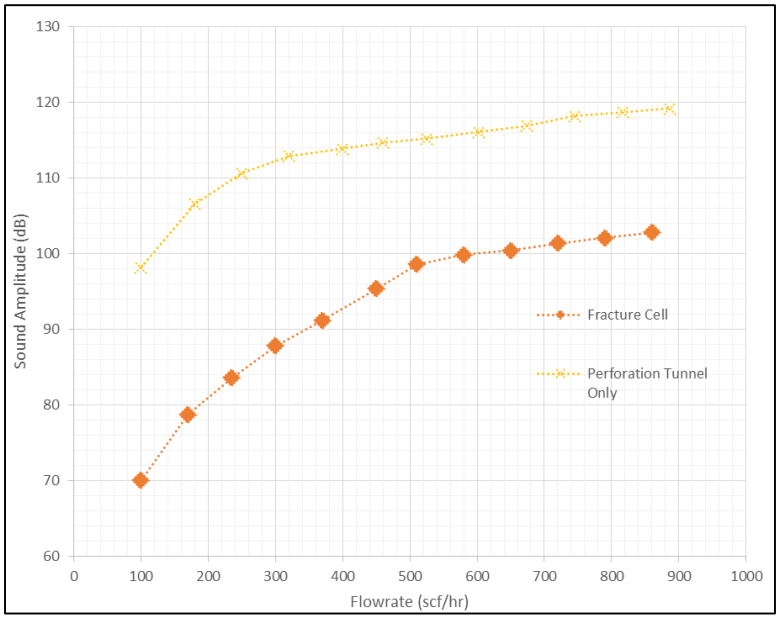

Figure 64: Horizontal Wellbore Flow Velocity Effect SPL vs Flow Rate Curve

On the horizontal experimental setup, similar acoustic behavior is observed as on the vertical experimental setup. As the flow rate increases, only the amplitude of frequency peaks increases. Location of each frequency peaks stay the same on the frequency spectrum. The shape of the SPL curve is also similar to the vertical wellbore experimental SPL result.

3.2.3 Horizontal Wellbore Fracture Cell Effect

In this experiment, we study the effect of fracture induced on acoustic signature of the fluid flows from fracture to wellbore on the horizontal wellbore. The acoustic signature of combined fracture and perforation tunnel system is compared to only the perforation tunnel. The purpose of this experiment is to study the fracture cell effects.

The experiment also serves as a feasibility study of if fracture information can be extracted from the entire system of fracture, perforation tunnel, and wellbore.

In Figure 65, the acoustic signal signature is plotted from the range of 1 kHz to 7 kHz of combined perforation tunnel and fracture cell comparing to the perforation tunnel only data set. As Figure 65 shows, perforation tunnel dominates the acoustic behavior of the entire perforation tunnel and fracture cell system. The acoustic signature of combined fracture cell and perforation tunnel system follows the trend of perforation tunnel only acoustic signature. Dominate peaks in the range of 3 kHz to 4 kHz range is observed in both data sets. The amplitude of perforation only acoustic signal is significantly larger than the combined fracture cell and perforation tunnel system.

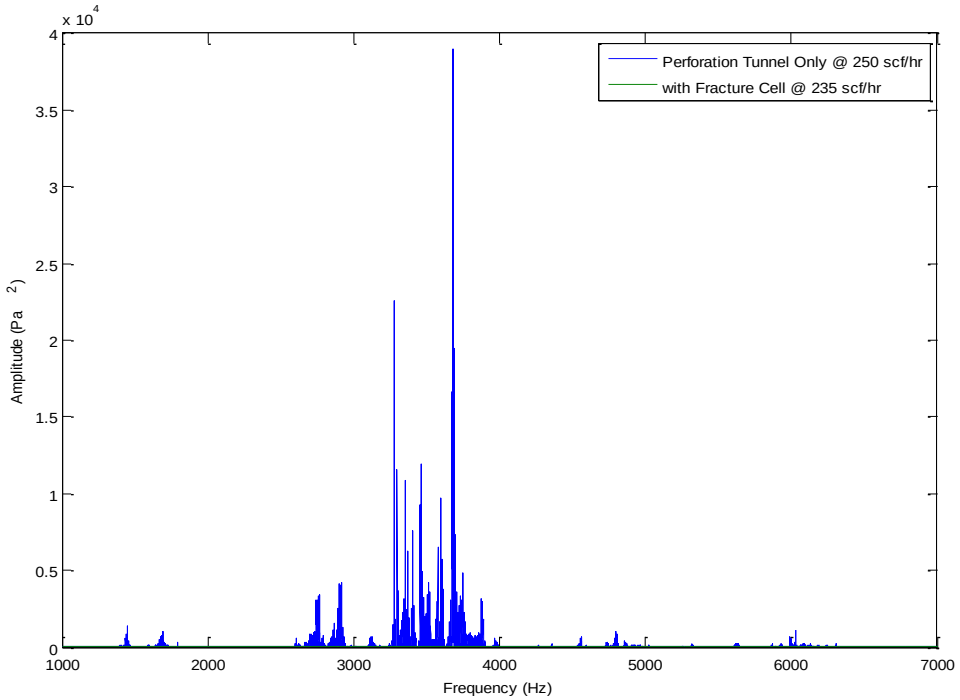

Figure 65: Horizontal Wellbore Fracture Cell Effect from 1-7 kHz at 235 scf/hr

In Figure 66, the acoustic signal is zoomed in the 4 kHz to 5 kHz range. The acoustic signals for perforation tunnel only is taken at a flow rate of 250 scf/hr, and compared with the signals for the fracture cell data set at 235 scf/hr. The two data sets picked for analysis have similar flow rate. However, the amplitude of the perforation only data set is significantly larger than the combined fracture and perforation tunnel data set. To effectively analyze the acoustic signature difference between the 2 data sets, a higher flow rate combined fracture and perforation tunnel acoustic behavior data set has to be used.

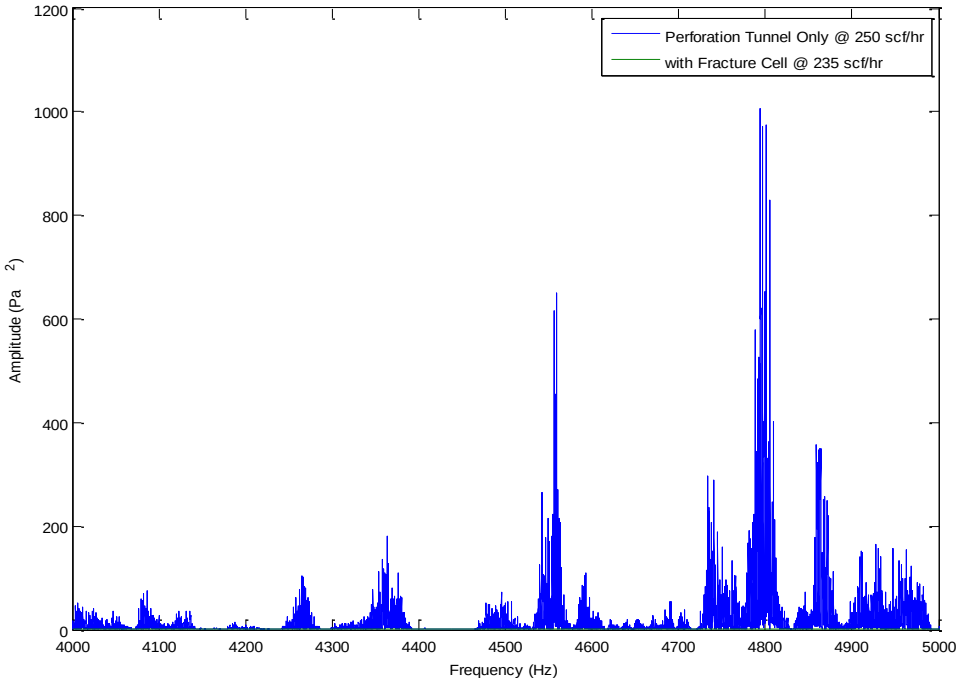

Figure 66: Horizontal Wellbore Fracture Cell Effect from 4-5 kHz at 235 scf/hr

In Figure 67, acoustic signal of combined fracture and perforation tunnel is plotted at flow rate 860 scf/hr comparing to perforation only acoustic signal at 250 scf/hr. The increase of flow rate allows better comparison between the 2 data sets. In the 4 kHz to 5 kHz range, observation is made that the acoustic behavior changes in the combined fracture and perforation tunnel setup comparing to perforation tunnel alone experiment setup. The acoustic signal frequency components in the 4 kHz to 5 kHz range have both amplitude changing and frequency peak shifting.

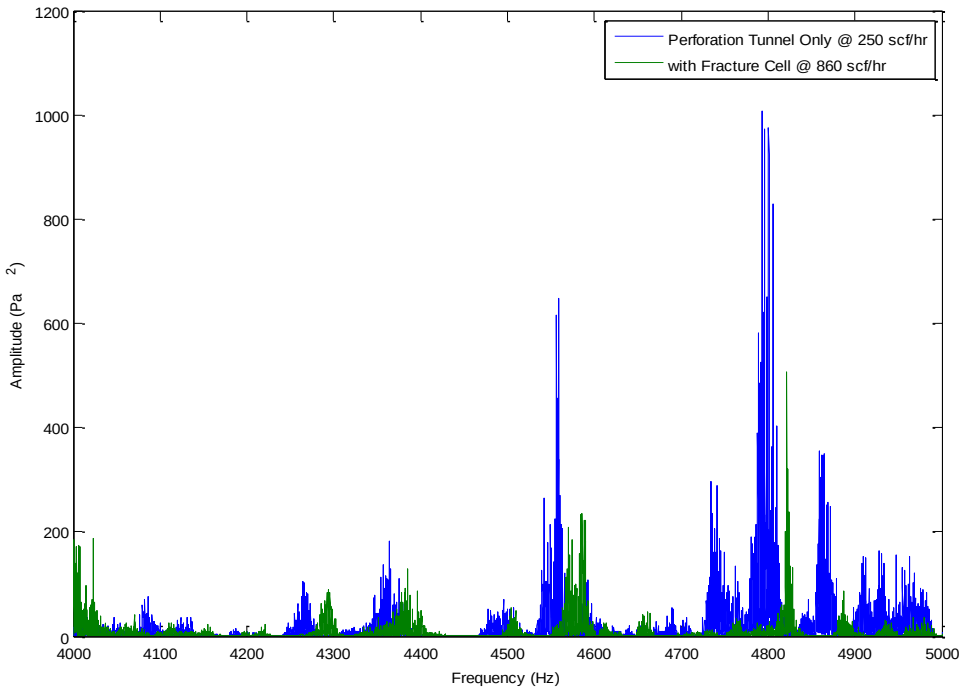

Figure 67: Horizontal Wellbore Fracture Cell Effect from 4-5 kHz at 860 scf/hr

In Figure 68, frequency spectrum is investigated in the 3 kHz to 3.8 kHz range where dominate peaks locate. The flow rate of combined fracture and perforation tunnel

data set is increased to 860 scf/hr in order to better compare the dominate frequencies of the 2 data sets. As Figure 68 shows, most of the dominate peak patterns remain the same in the 3 kHz to 3.8 kHz range. There is a shifting of the frequency peaks in the 3 kHz to 3.8 kHz range as well.

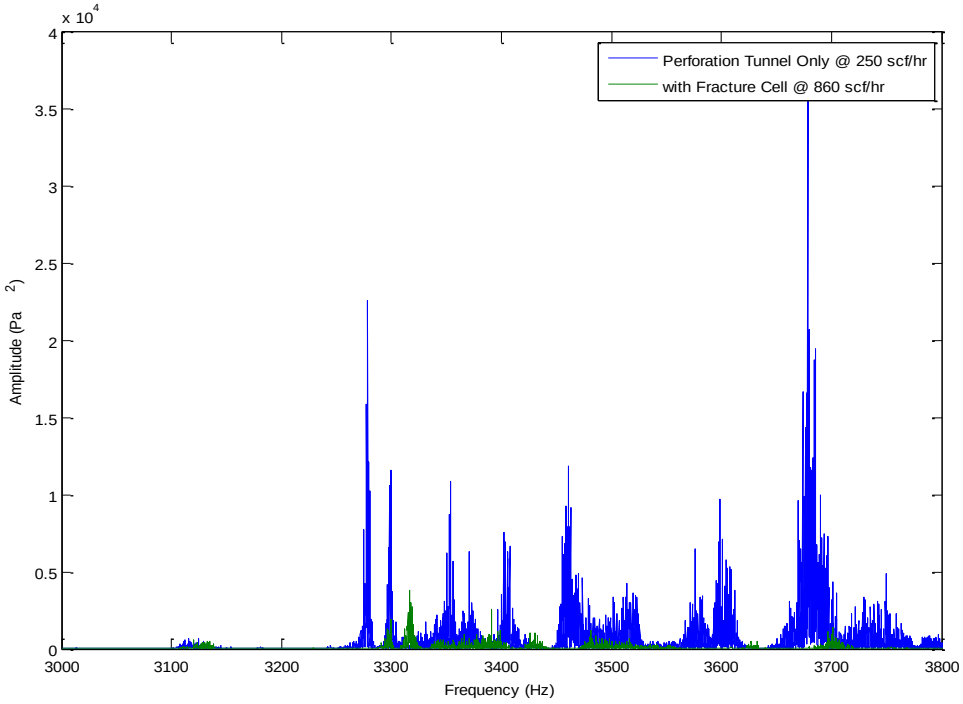

Figure 68: Horizontal Wellbore Fracture Cell Effect from 3-3.8 kHz at 860 scf/hr

To summarize the horizontal wellbore fracture cell effect, sound amplitude of perforation only system is significantly larger than a combination of fracture cell and perforation. In the frequency domain, acoustic behavior of the combined system of fracture cell and perforation is dominated by the perforation tunnel. However, fracture cell does change the acoustic signature of fluid flows from fracture to wellbore system.

3.3 Summary of Experimental Results

To better summarize the experimental results for both vertical and horizontal wellbore setups, a table of summary is created for different parameters studied in this thesis. Different downhole parameter changes the acoustic behavior differently. Due to this effect, downhole parameters can be estimated from acoustic signal collected by any downhole measurement instruments through advanced algorithm and modeling. A summary how the acoustic signal change based on different parameter change is shown in Table 4 and Table 5.

Table 4: Summary of Vertical Wellbore Experimental Result

Parameter Investigated	Frequency Component		Sound Pressure Level Change
	Amplitude Change	Peak Shifting	
Baseline	-	-	-
Flow Rate	Yes	No	Yes
Adding Proppant	Yes	Yes	Yes
Proppant Size	Yes	No	Min.
Fracture Width	Yes	No	Yes
Perforation Tunnel Length	Yes	Yes	Yes
Perforation Tunnel Diameter	Yes	Yes	Min.
Perforation Tunnel Smoothness	Yes	Yes	Min.
Multiple Perforation Tunnel	Yes	Min.	Yes
Flow Distribution	Yes	Min.	No
Hydrophone Location	Yes	Min.	Yes
Sample Interval	No	No	No
Wet Proppant	Yes	Yes	Min.
Liquid Column	Yes	Yes	Min.
Fracture Cell	Yes	Yes	Max.

Table 5: Summary of Horizontal Wellbore Experimental Result

Parameter Investigated	Frequency Component		Sound Pressure Level
	Amplitude Change	Peak Shifting	
Baseline	-	-	-
Fracture Cell	Yes	Yes	Max.
Flow Rate	Yes	No	Yes

The experimental result shows that there are patterns on acoustic signal behavior when different parameter changes. Each parameter investigated in the experiment causes different acoustic signal behavior. Some parameter changes only the amplitude of the acoustic signal, other parameter changes the location of the frequency peaks, and rest of the parameters cause both changing in amplitude and shifting in frequency peaks. A number of parameters shows similar acoustic behavior; further investigation is needed to fully understand the acoustic behavior of those parameters. The experiment result shows that acoustic signal can be used to determine downhole parameter change.

4. EXPERIMENTAL CORRELATION

4.1 Previous Correlation

Noise logging became viable for production logging application through the work performed by researchers during the 1970s. Researchers built a leak simulator to mimic the oil and gas flowing into the wellbore from the perforation tunnels. The leak simulator can also be used to measure the acoustic signal of the flow behind the casing. A correlation based on the leak simulator experimental results is established for both flow behind the casing and flow from the perforation (McKinley et al. 1973).

From the single phase gas flow behind the casing experiments, the correlation from the experimental data is $N_{600}^{*} = 4 \times 10^{-6} \frac{\rho q^3}{A_s^2}$. For the single phase gas flow from the perforations, the empirical correlation is $N_{600}^{*} = C'' \frac{\rho^4 q^3}{\mu^3 D_p^2}$. Where N_{600}^{*} is the peak to peak noise level above 600 Hz in millivolts, ρ is the density in pounds per cubic foot, A_s is the cross sectional area in square feet, q is volumetric flow rate in thousand cubic feet per day at flowing temperature and pressure, C'' is a constant coefficient, μ is viscosity in centipoise, and D_p is the perforation diameter in inch (McKinley and Bower 1977).

Based on the previous empirical correlation, the noise level is proportional to the flow rate cubed for both flow behind the casing and flow from the perforations. The correlation can be expressed in the form $N_f^{*} \sim q^3$; where N_f^{*} is the peak to peak noise level above a cutoff frequency in millivolt. If all of the constants are grouped together and a constant C' is assigned as a replacement, the empirical correlation can be

expressed as $N_f^* = C'q^3$. If the base 10 log is taken on both sides of the correlation, the new log based form is expressed as $\log N_f^* = \log(C'q^3)$. If log product rule is applied to the expression, the new form can be written as $\log q^3 = \log N_f^* - \log C'$. Whether the previous empirical correlation in either linear or log based expression, the correlation between flow rate and noise level is $N_f^* \sim q^3$ for single phase gas flows from perforations (McKinley and Bower 1977).

4.2 Empirical Correlation Based on Experimental Data

To develop a mathematical correlation based on all of the experimental data on the vertical wellbore setup, each parameter studied at different flow rate is organized as different data sets. First, a sound pressure level (SPL) is calculated using formula $SPL = 10 \log \frac{P_{rms}^2}{P_{ref}^2}$. The reference pressure level term P_{ref} is defined as 2×10^{-5} Pascal. The term P_{rms} is calculated by using the measured experimental acoustic data in millivolts. To obtain the P_{rms} value from the experimental data, first the experimental acoustic data in millivolt is divided by a unit conversion resolution number in millivolt per Pascal to convert the experimental data units from millivolt to Pascal. The unit conversion resolution number is a setting on the data acquisition system. The next step is to calculate the Root Mean Square (RMS) value from the measured experimental acoustic data in Pascal; a filter removing any lab noise can be applied to the measured data prior to calculate the RMS value. After filtering and calculating the RMS value of the experimental data, the result value is used as P_{rms} in Pascal. Once the value of P_{rms}

is calculated, SPL value can be calculated with the formula $SPL = 10 \log \frac{P_{rms}^2}{P_{ref}^2}$. Appling the same calculation procedure to all of experimental data at different flow rates, a plot can be generated with flow rate in standard cubic feet per hour (scf/hr) on the x-axis and sound pressure level in decibel (dB) on the y-axis. The plot of sound amplitude in dB and flow rate in scf/hr is shown throughout in the experimental result section. Throughout the entire document, the term sound amplitude and the sound pressure level (SPL) are used interchangeably.

If the x-axis of the SPL vs flow rate plot is changed to $\log(q^3)$, and the axis of the plot is flipped, the new plot has SPL in dB on the x-axis and $\log(q^3)$ with q in scf/hr on the y-axis. An example of the new plot is shown in Figure 69. In Figure 69, different experimental data sets are plotted with sound pressure level on the x-axis and $\log(q^3)$ on the y-axis. The correlation seems to be linear between SPL and $\log(q^3)$ as Figure 69 is shown. Thus from curve fitting the experimental data sets, a correlation in the form of $\log(q^3) = A \times SPL + B$ is concluded. Both A and B in the correlation are constants that are to be determined. Further analysis is needed to determine the exact form of A and B.

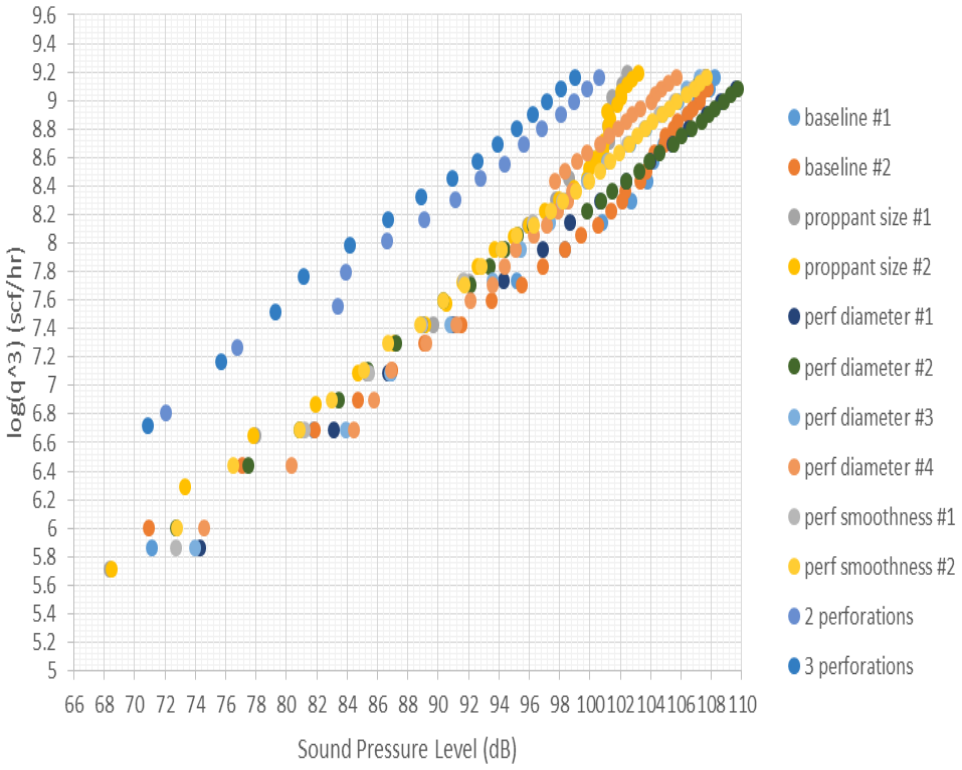

Figure 69: Logarithmic of Flow Rate Cubed vs SPL Plot

Once the basic relationship between flow rate and sound amplitude is determined. Trend line can be applied and the coefficient of determination (r^2) can be calculated. The theoretical range of r^2 is between 0 and 1. When the value of r^2 is equal to 1, the trend line and experimental data fits perfectly. If the value of r^2 is closer to 0, the trend line is a poor fit to the experimental data. For all of the data sets, a trend line is established to curve fit the experimental data. Values of coefficient A and B in the basic form $\log(q^3) = A \times SPL + B$ are calculated. The value of coefficient of determination (r^2) is also calculated to exam how closely the trend line fits the experimental data.

All of the curve fitting results is shown in Table 6. Parameters studied in the earlier sections are fitted with the equation $\log(q^3) = A \times SPL + B$. The value of A, B, and r^2 are shown in separate columns in Table 6. The value of r^2 is close to 1 for all of the single phase gas experiments. Based on the value of r^2, the conclusion can be drawn that the basic form of equation $\log(q^3) = A \times SPL + B$ closely represents the correlation between flow rate and sound pressure level. Despite the basic form of correlation between flow rate and sound pressure level is established, the coefficient A and B are still in need to be determined.

Table 6: Summary of Experimental Correlation Results

Parameter	**Log(q^3) = A(SPL) + B**		
	A	**B**	**R^2**
Baseline #1	0.0873	-0.4873	0.9827
Baseline #2	0.0867	-0.4065	0.9764
Proppant Size #1	0.0989	-1.2187	0.9713
Proppant Size #2	0.0973	-1.0764	0.974
No Proppant #1	0.1112	-1.9887	0.9632
No Proppant #2	0.1039	-1.3126	0.9814
Perforation Length #1	0.0896	-0.3709	0.9967
Perforation Length #2	0.0857	0.0092	0.9965
Perforation Length #3	0.0947	-0.8666	0.9987
Perforation Length #4	0.0936	-0.7632	0.9968
Perforation Diameter #1	0.0897	-0.7415	0.9992
Perforation Diameter #2	0.0818	0.1284	0.9896

Table 6 Continued

Parameter	Log(q^3) = A(SPL) + B		
	A	B	R^2
Perforation Diameter #3	0.1016	-1.7416	0.9981
Perforation Diameter #4	0.1106	-2.5098	0.9871
Perforation Smoothness #1	0.0943	-0.9634	0.9993
Perforation Smoothness #2	0.0901	-0.543	0.9992
2 Perforations #1	0.0844	0.6383	0.9932
2 Perforations #2	0.0845	0.6342	0.9942
3 Perforations #1	0.0908	0.2195	0.9846
3 Perforations #2	0.0888	0.3953	0.9809
2 Perforations Different Flow Distribution #1	0.0933	-0.0867	0.9952
2 Perforations Different Flow Distribution #2	0.0897	0.2422	0.9966
Hydrophone Height #1	0.0785	0.3651	0.9939
Hydrophone Height #2	0.0784	0.377	0.9909
Wet Proppant #1	0.1044	-1.7391	0.9941
Wet Proppant #2	0.093	-0.6346	0.9984
Liquid Column #1	0.0977	-1.3285	0.9895
Liquid Column #2	0.096	-1.0547	0.9945
Liquid Column #3	0.1014	-1.8883	0.986
Horizontal #1	0.0812	0.2972	0.9888

4.3 Summary of Experimental Correlation

Based on the previously established empirical correlation for single phase gas flowing from perforations, the relationship between peak to peak noise levels above a cutoff frequency in millivolt to flow rate is expressed as $N_f^* \sim q^3$. The acoustic noise level is proportional to the flow rate cubed (McKinley and Bower 1977). By taking the log base 10 on both sides of relationship $N_f^* \sim q^3$, the new relationship can be expressed as $\log N_f^* \sim \log q^3$.

The results from the experiments conducted on both the horizontal and vertical wellbore setups show the same relationship between flow rate and acoustic noise level. The RMS value of the sound pressure level is proportional to the value of peak to peak noise level in millivolt. For sinusoid wave, the RMS value of the sine wave is equal to the peak to peak value divided by square root of two. The noise level in millivolt can be converted to Pascal by dividing a data acquisition system scalar amplitude resolution factor in millivolt per Pascal. Thus, by expressing the previous correlation in the logarithmic terms, the same flow rate and noise level correlation is matched between the previous correlation and the results from the experimental studies. The basic relationship concluded from both studies is that the flow rate cubed is proportional to the acoustic noise level.

There are a couple advantages replacing the noise level with the sound pressure level to correlate with flow rate. The first one is that the sound pressure level calculation has a standard formula to calculate comparing to peak to peak noise level in millivolt. The value of peak to peak noise level in millivolt depends on the resolution setting in

millivolt per Pascal in the instruments measuring the acoustic signal. Different instruments measuring the acoustic signal have different resolution settings, dynamic range, and sensitivity. Thus the peak to peak noise level is highly dependent on the instrument setting during the acoustic measurement. The second advantage is that by calculating the RMS value of the acoustic signal in Pascal the acoustic signal over the entire spectral range is captured. As the experimental results shown, certain parameters change the acoustic signature of the measured data. When the acoustic signature changes, both the amplitude and phase of the frequency peaks are changed. By taking account into all of the frequency components and calculating the RMS value of the signal, the shifting of the frequency components is also factored into the calculation. Lastly, by calculating the sound pressure level of the measured acoustic signal, the obtained result can be compared to other common known acoustic level on the same scale. For example, a comparison can be done on the level of loudness between fluid flows from fracture to wellbore and normal human conversation. There is a physical scale applied to the measured acoustic data by calculating the sound pressure level.

The previous correlation flow rate cubed is proportional to noise level is being confirmed through the experimental studies. The conclusion is drawn that the results from experimental studies are curve fitted with the equation $\log(q^3) = A \times SPL + B$. The term A and B are constants to be determined.

5. SUMMARY AND CONCLUSION

5.1 Summary

Throughout of this thesis, the acoustic behavior of fluids flow from fracture to wellbore is studied in detail. An experimental setup is designed and built to investigate the acoustic behavior change under various conditions. The experimental setup contains a customized fracture cell with long and thin geometry to simulate a fracture, a pipe connection to simulate a perforation tunnel, a vertical and horizontal wellbore, a set of sensors and data acquisition system, and customized software to analyze the experimental results. The experimental setup can easily converted from vertical wellbore to horizontal wellbore setup. An experimental matrix is developed to guide the investigation of parameter of interest. A list of downhole parameter is simulated on the experimental setup to exam the acoustic behavior when those parameter changes. The result of the experiment shows that there is a pattern on acoustic behavior when parameter of interest changes. Similar acoustic behavior is observed between vertical wellbore setup and horizontal wellbore setup when investigating the same parameter of interest. Some parameter investigated only changes the amplitude of the frequency peaks, other parameter shifts the frequency components, and rest affects both amplitude and phase of the acoustic signal. The experimental result shows there is a correlation between certain acoustic behavior and each particular parameter investigated. The correlation based on experimental results is concluded to be $\log(q^3) = A \times SPL + B$. The term A and B are constants to be determined. The experimental result also confirms

that acoustic signal alone can be used to monitor and diagnosis the hydraulic fracture operation.

5.2 Conclusion

In this thesis, parameters influence the change of acoustic behavior is investigated when fluid flows through a simulated fracture and perforation tunnel to the wellbore. The result of the laboratory experiments conducted to study the acoustic behavior of flow from fracture to wellbore shows that important downhole parameters such as flow rate can be estimated from the distributed acoustic sensing measurement data.

Flow rate changes only the amplitude of frequency peaks. As the flowrate increases, sound amplitude increases. A proppant filled fracture cell shows different amplitude and location of frequency components comparing to an empty fracture cell. By changing the fracture width, only the amplitude of the frequency peaks changes. Perforation tunnel length, diameter, and smoothness change both the amplitude and location of frequency components. Perforation tunnel length changes sound amplitude more than perforation tunnel diameter and smoothness. Multiple perforation tunnels change the amplitude of frequency peaks with some shifting of the location of the frequency peaks. The sound pressure level decreases significantly when the number of perforation tunnels is increased to multiple from a single perforation tunnel. However, the sound amplitude decrease is small when comparing 2 perforation tunnels and 3 perforation tunnels. When changing the flow distribution in the 2 perforation tunnels, the

amplitude of the frequency peaks change and sound amplitude doesn't change. As the hydrophone moves away from the perforation tunnel, the sound amplitude decreases. The sampling interval has no effect on the acoustic behavior. The introduction of water changes both the amplitude and location of frequency components. The removing of the fracture cell also changes both the amplitude and location of frequency peaks. The sound amplitude with fracture cell removed is significantly larger than the sound amplitude with fracture cell in place. Based on a few experimental results, acoustic behavior of nitrogen gas flows from fracture to wellbore through perforation tunnel is similar in both horizontal wellbore setup and vertical wellbore setup.

The previous correlation flow rate cubed is proportional to noise level is being confirmed through the experimental studies. The conclusion is drawn that the results from experimental studies are curve fitted with the equation $\log(q^3) = A \times SPL + B$. The term A and B are constants to be determined.

Although the experimental result shows promising result toward using DAS data to diagnosis the hydraulic fracture operation, further investigation is still need toward fully understand the acoustic behavior when different downhole parameter changes. DAS is an emerging technology that has a lot of promise in various applications. Hopefully, this thesis contributes to the progress of DAS technology in the future.

REFERENCES

Ballou, G. 2006. Introduction. In *Electroacoustic Devices*, ed. G. Ballou, Chap. 1, 1-15. Burlington, MA: Elsevier Academic Press.

Cannon, R. and Aminzadeh, F. 2013. Distributed Acoustic Sensing: State of Art Paper. Presented at the SPE Digital Energy Conference and Exhibition, The Woodlands, Texas, 5-7 March. SPE-163688-MS.

Hill, A. D. 1990. Noise Logging. In *Production Logging: theoretical and interpretive elements*, Vol. 14, Chap. 10, 112-120. Society of Petroleum Engineers: Henry L. Doherty Series.

Kinsler, L., Frey, A., Coppens, A., and Sanders, J. 2000. Fundamentals of Vibration, In *Fundamentals of Acoustics*, fourth Edition, chap. 1, 1-26. New York: Wiley.

Martinez, R., Chen, K., Santos, R., Hill, A. D., and Zhu, D. 2014a. Laboratory Investigation Acoustic Behavior for Flow from Fracture to a Wellbore. Presented at the SPE Annual Technical Conference and Exhibition, Amsterdam, Netherlands, 27-29 October. SPE-170788-MS.

Martinez, R., Hill, A. D., and Zhu, D. 2014b. Diagnosis of Fracture Flow Condition with Acoustic Sensing. Presented at the SPE Hydraulic Fracturing Technology Conference, Woodlands, Texas, 4-6 February. SPE-168601-MS.

McKinley, R. M. and Bower, F. M. 1977. Specialized Applications of Noise Logging. Presented at the SPE AIME 52nd Annual Fall Meeting, Denver, Colorado, 9-12 October. SPE-6784.

McKinley, R. M., Bower, F. M., and Rumble, R. C. 1973. The Structure and Interpretation of Noise from Flow behind Cemented Casing. Presented at the SPE AIME 47th Annual Fall Meeting, San Antonio, Texas, 8-11 October. SPE-3999.

Molenaar, M. M. and Cox, B. E. 2013. Field Cases of Hydraulic Fracture Stimulation Diagnostics Using Fiber Optic Distributed Acoustic Sensing (DAS) Measurements and Analyses. Presented at the SPE Middle East Unconventional Gas Conference and Exhibition, Muscat, Oman, 28-30 January. SPE-164030-MS.

Molenaar, M. M., Hill, D. J., Webster, P., Fidan, E., and Birch, B. 2011. First Downhole Application of Distributed Acoustic Sensing (DAS) for Hydraulic Monitoring and Diagnostics. Presented at the SPE Hydraulic Fracturing Technology Conference and Exhibition, Woodlands, Texas, 24-26 January. SPE-140561-MS.

Pal P. B. 2006. Principles of Fiber Optic Sensors. In *Guided Wave Optical Components and Devices*, Chap 24, 371-387. Burlington, MA: Elsevier Academic Press.

APPENDIX A

EXPERIMENT PROCEDURES

Overview:

All of the procedures to conduct experiments are listed below. The 3 main steps to conduct the acoustic experiments are prepare the fracture cell, setup and calibrate the data acquisition system, and analyze the measured data. The fracture cell preparation step requires setting up the fracture cell by loading and pressure packing proppant in the cell for experiment. Data acquisition system setup step requires system calibration and taking measurement during the experiment. After data is taken, post signal analysis step involves analyzing the experimental data.

Table 7: Fracture Cell Preparation Steps

STEPS	DETAILED PROCEDURE
1	Laying the bottom assembly of the fracture cell on a flat surface and load appropriate amount proppant into the facture cell. Making sure outlet screen is in place and top lid can close properly with proppant in the fracture cell.
2	Making sure O-ring is sealed in place and no proppant in the O-ring groove. Slowly close the top lid.
3	Once top lid closed properly, start the screw in the upper middle of the fracture cell first then goes diagonal pattern to start the screw across from the started one. Make sure this step is done on a flat surface,

	otherwise proppant gets in between the top lid and bottom assembly. Once screws in the middle section of the fracture cell are all started, then work on the 2 sides. Start all of the screws in the fracture cell assembly before tightening them up. (Note: the pattern of starting screw is important to ensure no leak occurs in the fracture cell when conduction high pressure experiment)
4	Once all of the screws are started, tightening up all the screws in the same pattern.
5	Rotate the fracture cell with inlet facing up, tape the 2 side inlet ports and threaded holes to prevent proppant drops in. Using a funnel to gravity feed the proppant into the fracture cell through the middle inlet port until the fracture cell is filled with proppant. (Note: it's recommended placing tape on all of the threaded holes to prevent proppant gets in during this process)
6	Remove all of the tapes over threads holes but keep the tape over the 2 side inlet ports. Screwing down inlet adapting piece with O-ring properly seated in the O-ring groove.
7	Flowing compressed gas from inlet to the outlet allowing proppant to pack toward the outlet. This process is called proppant pressure packing process.
8	After pressure packing the proppant, remove the center inlet port adapter piece. Using a funnel to pack more proppant into the cell.

9	Repeat the proppant packing and add proppant process 3 times. The purpose of proppant packing process is to ensure facture cell is fully filled with proppant.
10	Once fracture cell is filled with proppant, screw on the outlet adapter piece.
11	Test for leaks by injecting high pressure through the fracture cell and check around the fracture cell for leaks
12	If leak is found around the fracture cell, fix the leak problem
13	If proppant packed fracture cell passes for the leak test, load the cell onto the experimental station and move onto the next step of the experiment, setup the data acquisition system

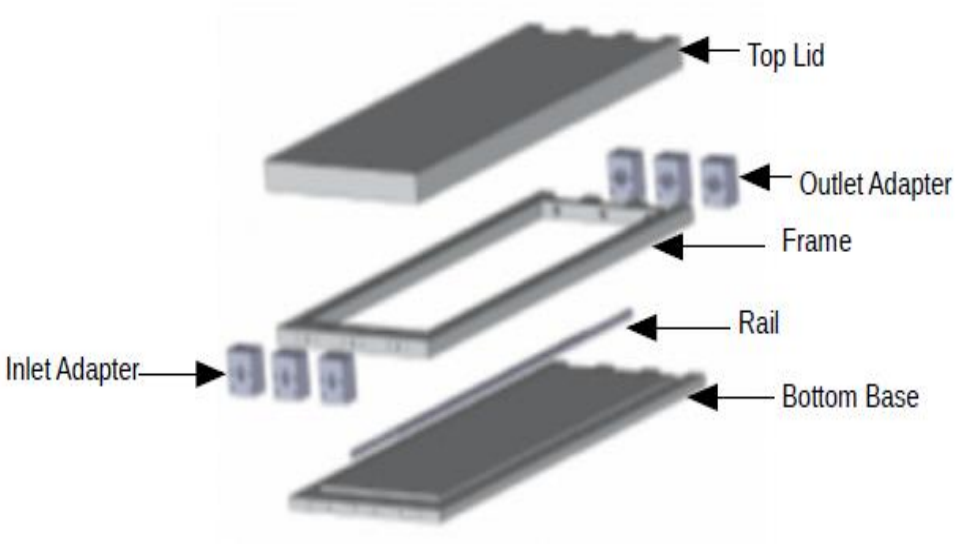

Figure 70: Fracture Cell Assembly Parts

In Figure 69, all of the fracture cell assembly parts are labeled. To assembly it together, screw together the bottom base and frame first. Then fill the fracture cell with proppant and screw down the top lid. Finally, assembly the outlet adapter and inlet adapter piece.

Table 8: Data Acquisition System Setup Steps

STEPS	DETAILED PROCEDURE
1	Ensure National Instrument LabVIEW and software drivers are installed. (Note: software drivers can be found on the official National Instrument website)
2	Locate where the LabVIEW software files are and open the appropriate application software files in LabVIEW. (Note: A total of 3 application files are written for single hydrophone setup, distributed setup, and time step generation)
3.1	If running the single hydrophone setup, open appropriate LabVIEW application software, click on the open file icon. Once open file icon is clicked, a dialog box shows up. Select the name of the file data is saving to; click ok. Dialog box should close down. Change the name to desired name with .csv file extension in the end of the name. (Note: There has to be a .csv file pre-exist the first time; there has been trouble with LabVIEW generating .csv file when no file exists in the directory specified)

3.2	If running the distributed hydrophone & microphone setup, similar procedure is followed as the single hydrophone setup with an exception. The file name has no .csv file extension, the .csv file extension is automatically added to the file name at the end. The file name also has ch0 to ch4 in the end to save each sensor's data into separate .csv files. The ch0 is associated to the physical channel 0 on the NI 9234 data logger. The same rule applies to channel 1 to 3. (Note: Do not conduct experiments with water on the distributed microphone experimental setup)
4	Once the name and location of measurement data saves to is entered, start the experiment process and click on run button on the upper left corner of the LabVIEW GUI.
5	Check if the .csv file is generated in the desired folder
6	Click on stop button on the upper left corner of the LabVIEW GUI
7	Make desired physical change on the experimental station and change the file name, then start and stop experiment again
8	Iterate this measurement process to obtain a set of data containing different flow rates.
9	Once all of the data is taken, back the data up at a secondary location
10	Generate the time step .csv file by running the time step generation LabVIEW application. (Note: Time step .csv file only needs to be generated once) Open the LabVIEW application and select saved file

name and location then enter sample rate and buffer size. Click on run button then stop button. A time step .csv file should be generated in the desired directory. (Note: sample rate and buffer size should match the condition when conducting experiments)

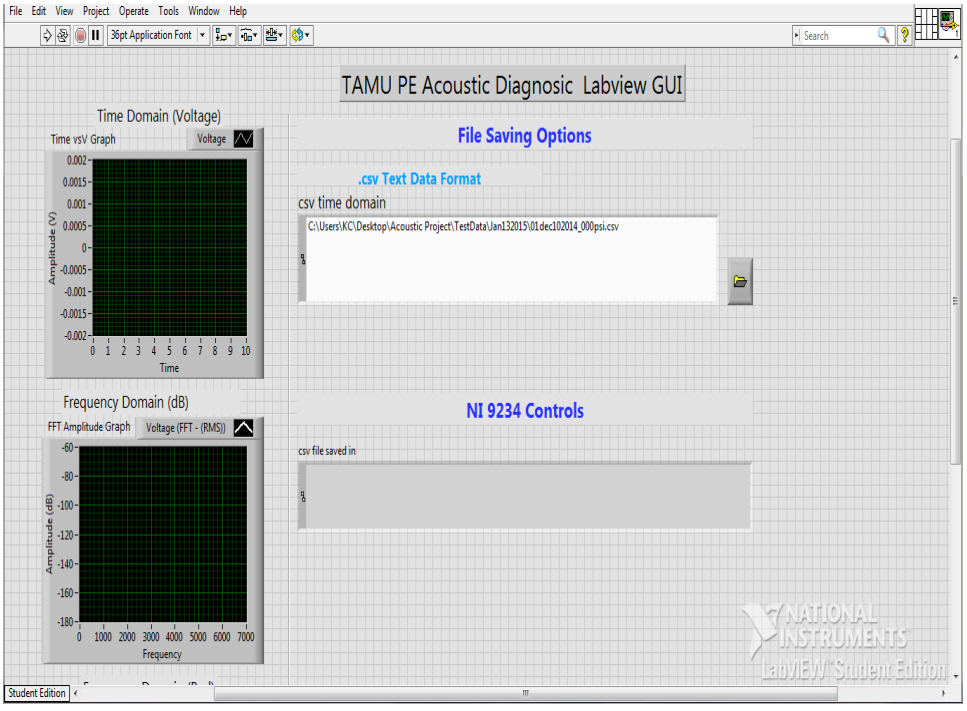

Figure 71: Screen Shot of Single Hydrophone Setup Software User Interface

Screen shot of the LabVIEW application used in the single hydrophone experimental setup is shown In Figure 70. Once clicking on the open file icon, a dialog box shows up. User can select the pre-existing file with .csv extension. Measurement data will be saved to the selected directory with specified file name.

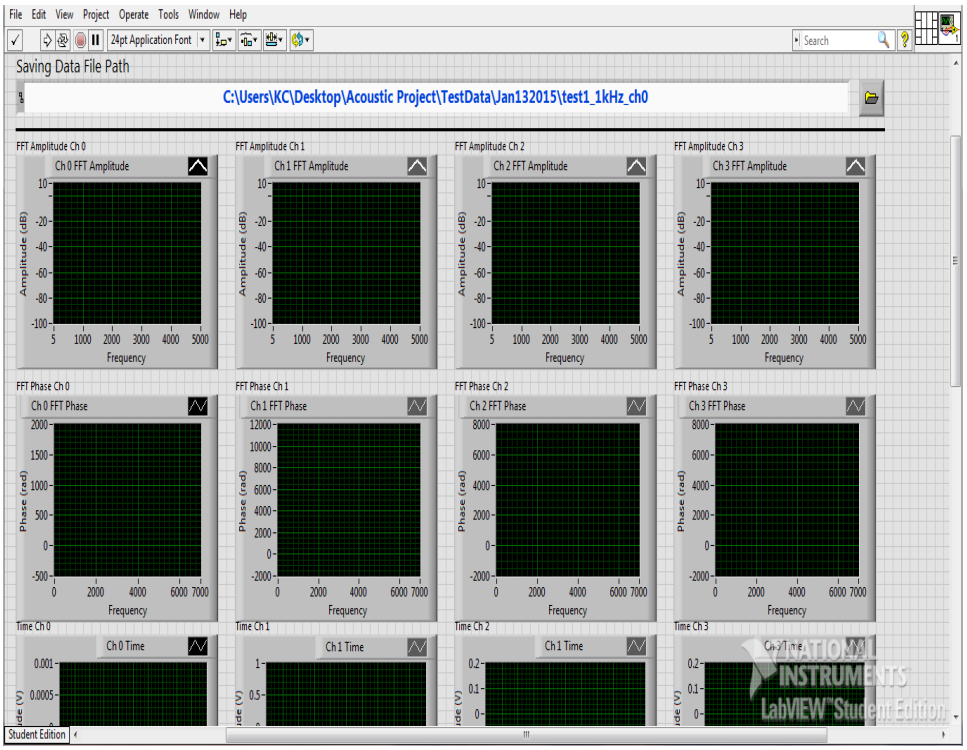

Figure 72: Screen Shot of Distributed Sensor Setup Software User Interface

Screen shot of the LabVIEW application used in the distributed hydrophone and microphone experimental setup is shown In Figure 71. Once clicking on the open file icon, a dialog box shows up. User can select the pre-existing file without .csv extension. The .csv extension is added to the file name automatically. Measurement data will be saved to the selected directory with specified file name.

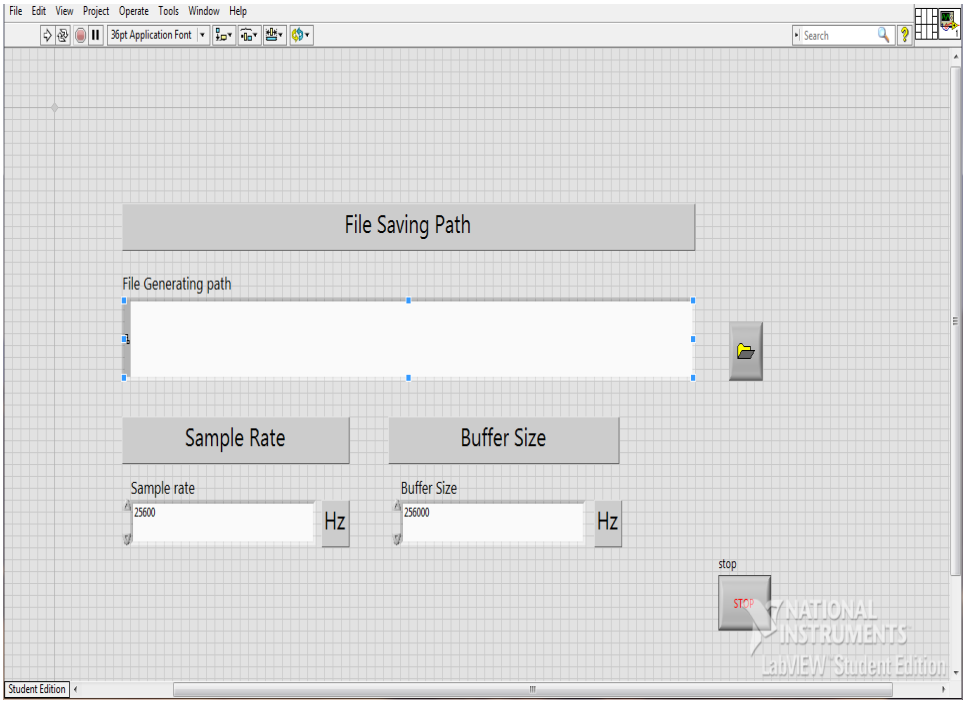

Figure 73: Screen Shot of Time Step Generation Software User Interface

Screen shot of the LabVIEW application used to generate the time step is shown In Figure 72. Enter sample rate and buffer size first. Once clicking on the open file icon, a dialog box shows up. User can select the pre-existing file with .csv extension. Time step data will be saved to the selected directory with specified file name.

Table 9: Post Signal Analysis Steps

STEPS	DETAILED PROCEDURE
1	Open and run the Matlab application file, a graphical user interface with title DAS Data Evaluation Tool shows up.
2	Enter all of the information such as time step file and measured data file directory, sample rate, preamp setting, # of seconds of data to evaluate, bandpass filter range, comments, and axis labels. (Note: Do not leave any input space blank)
3	Once all of the information is entered, click buttons in the following sequence: import .csv => apply => apply filter/none => FFT Amplitude Preview/calculate SPL/other function button
4	Data should be plotted in the preview window. Range of the window can be adjusted by using the "Rescale" button
5	"Generate #1 Data Report" button can be used to generate plot in a separate window for documentation purpose
6	Once finished plotting click on "Clear Memory" button
7	To analyze another data set, start all over from "Import .csv" button
8	If plotting multiple data sets, after plotting the 1st data set, input a name to the textbox above "Save Data to #1" button then click on the button. The "Save Data to #1" button saves the data as data set #1 with the name in the input box when plotting multiple data sets.

9	Click on the “Clear Memory” button, change the input file directory to import another data set, click all of the button sequence as running a single data set.
10	Repeat the above process for other data sets
11	To preview the multiple data set plot, click on “Data 1&2&3” button for 3 sets of data or any other combination
12	Click on “Generating #1&#2&#3 Report” button to generate report for 3 data set plot
13	Import: periodically check the Matlab command window for error messages, the software application doesn’t display any error messages, all of the error messages are displayed in the command window
14	Make sure click on “Clear Memory” button after each evaluation process

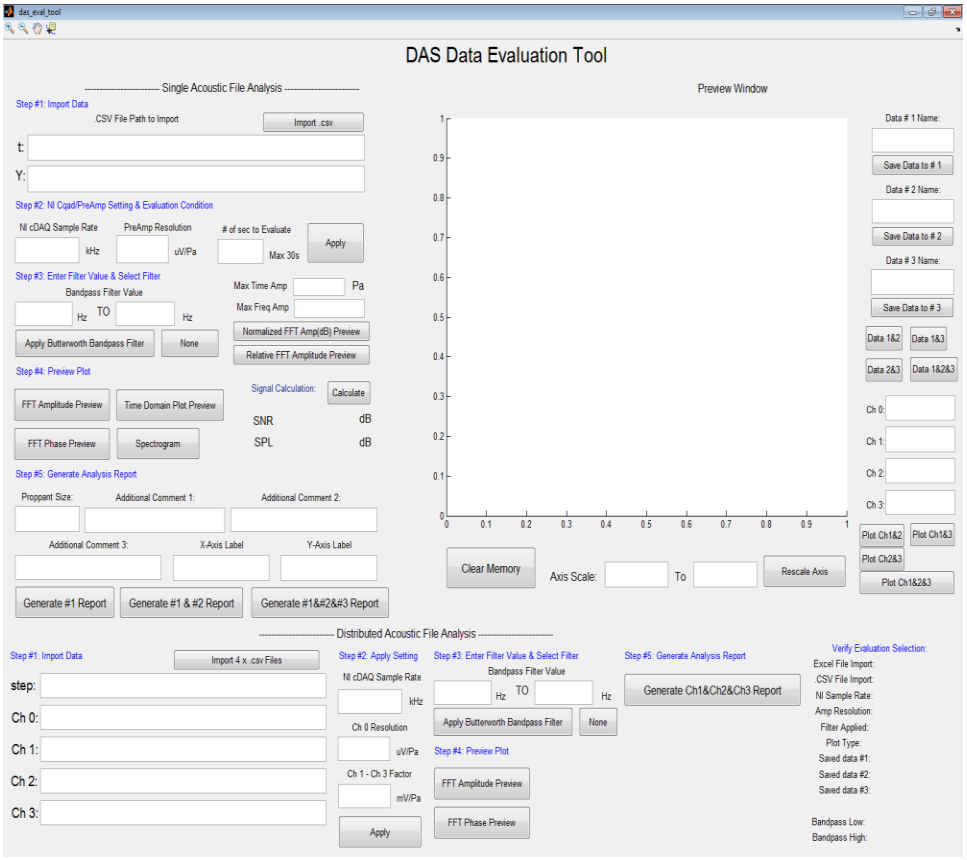

Figure 74: Screen Shot of Opening in DAS Evaluation Tool

Once the Matlab application is started, a startup window shows up. A screen shot of the startup screen is shown in Figure 73. The DAS data evaluation Matlab application is capably of analyzing the acoustic data collected by running the LabVIEW data acquisition software application.

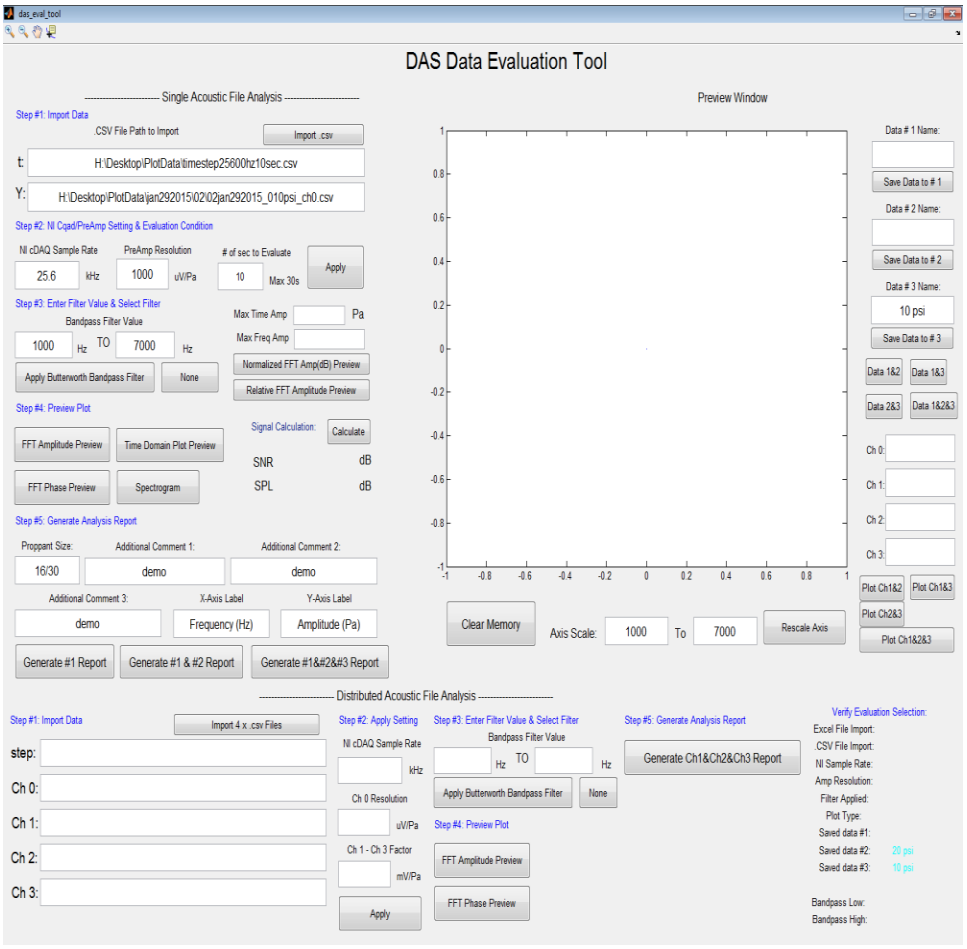

Figure 75: Screen Shot of Information Entered in DAS Evaluation Tool

A screen shot of the DAS evaluation software application with all of the user input information entered is shown in Figure 74. The time step file path is in the textbox labeled “t”. The file path of collected acoustic data is entered in textbox labeled “Y:”; then click on the “import .csv” button. Other user input information such as sample rate should be entered in the “NI cDAQ Sample Rate” textbox. Once all of the user input information is entered, analysis can be performed by clicking on a sequence of buttons.

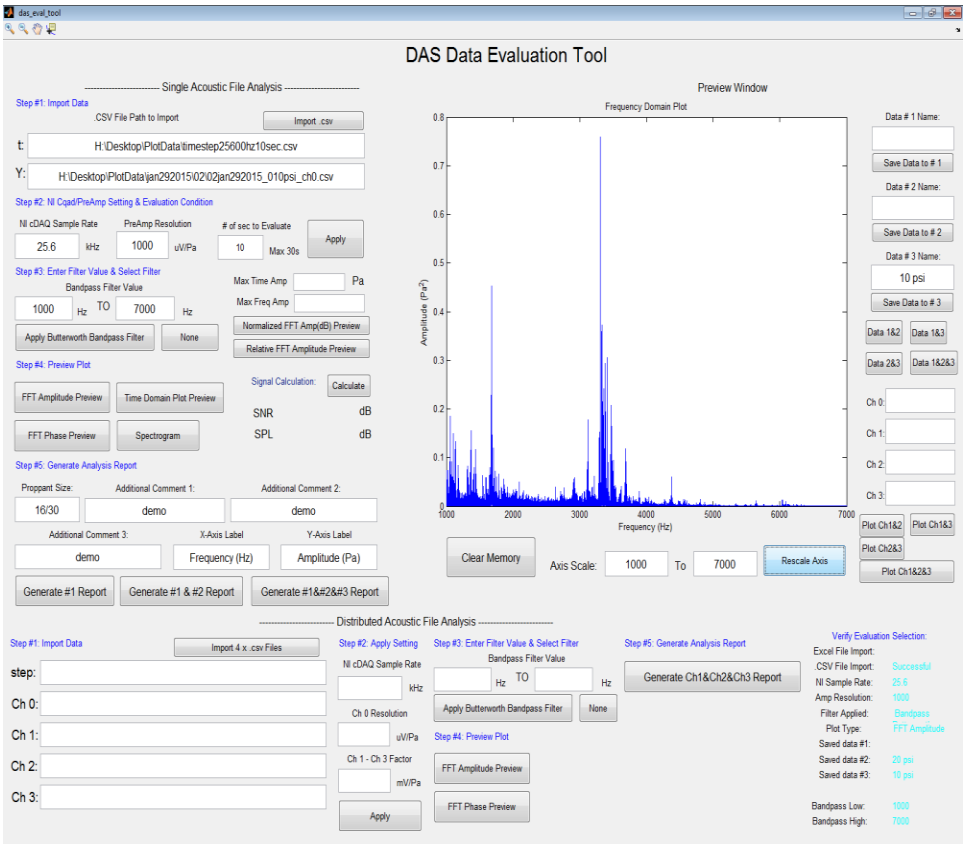

Figure 76: Screen Shot of Preview of Single Data Set in DAS Evaluation Tool

Once all of the user input information is entered and one of the preview plot button is pressed, desired plot should show up in the preview window. A screen shot of the user interface after clicking on the “FFT Amplitude Preview” button is shown in Figure 75. “Rescale Axis” button can be used to change the x-axis scale. “Clear Memory” button can be used to clear the program memory.

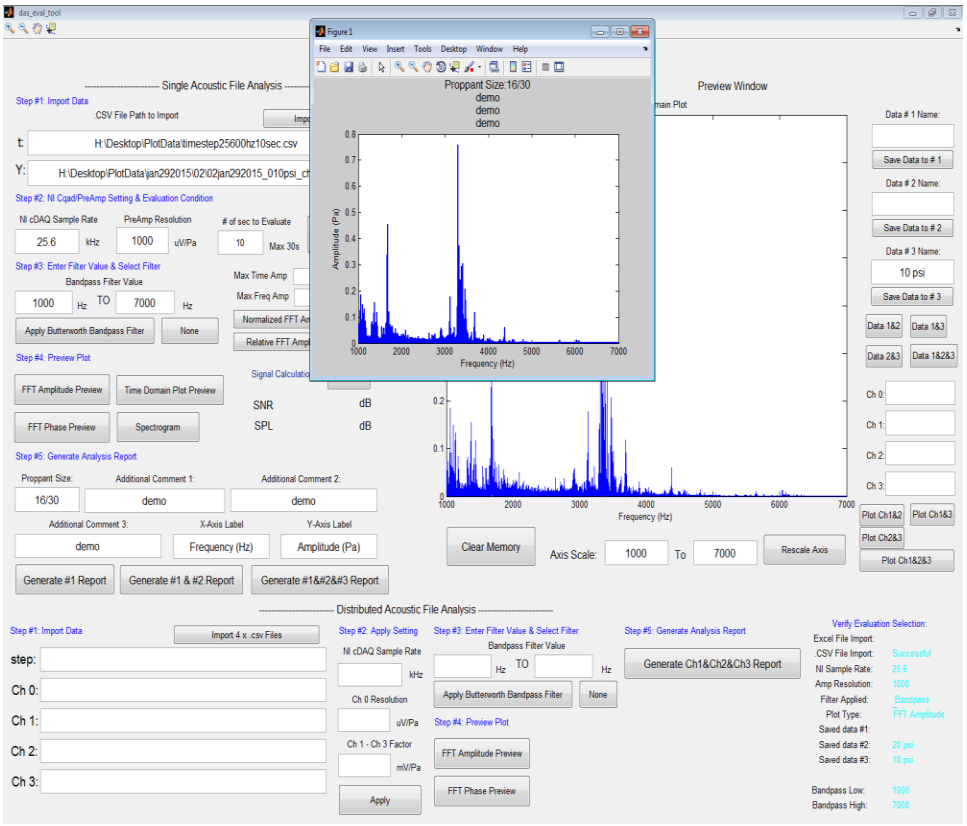

Figure 77: Screen Shot of Generating Report of Single Data Set in DAS Evaluation Tool

When desired plot is generated in the preview window, the same plot can be generated in a separate window for exporting purpose. The preview widow plot can be shown in a separate window by clicking the “Generate #1 Report” button. A screen shot of the plot generated in a separate window is shown in Figure 76. The plot generated in the separate window can be copy and paste into another document for publication purpose.

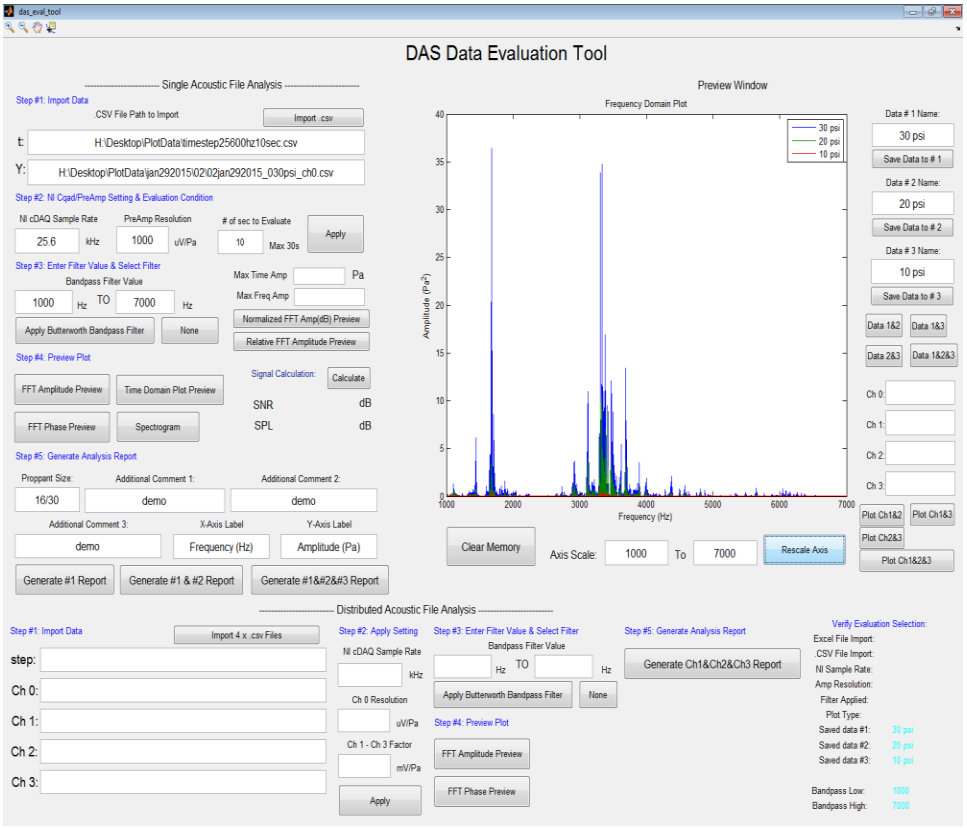

Figure 78: Screen Shot of Preview of Triple Data Sets in DAS Evaluation Tool

When comparing multiple sets of data, a single plot can be generated with multiple data sets shown in different colors. The names of the data sets are entered in the textbox named “Data #1 Name”, “Data #2 Name”, and “Data #3 Name”. Button labeled “Data 1&2&3” is used to plot all 3 sets of data in different colors.

APPENDIX B

FREQUENCY DOMAIN PLOT ON DECIBEL SCALE

Selected figures below are plotted on decibel scale instead of linear scale. Different dynamic range is selected in each figure to accommodate the swing of the amplitude of each frequency components. Data set is taken on the baseline vertical wellbore setup.

Background noise is plotted on the dB scale in Figure 78 from DC to 1 kHz. The Plot shows significant background noise below 200 Hz. The dynamic range is selected from 10 dB to 80 dB for the plot.

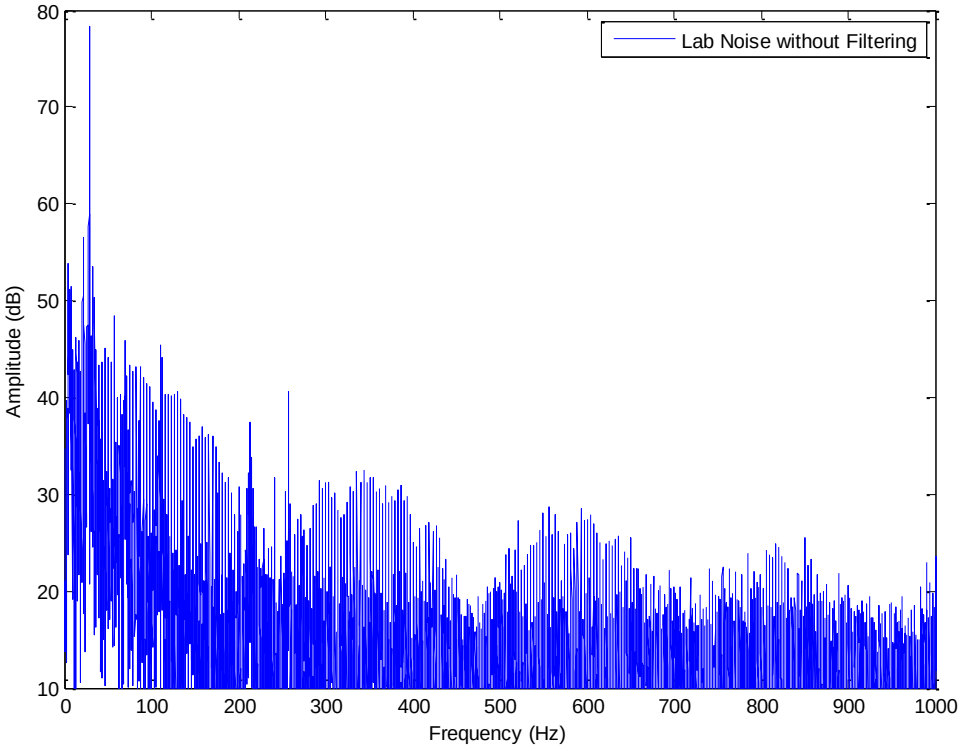

Figure 79: Baseline Setup Lab Noise on dB Scale in Frequency Domain

In Figure 79, nitrogen gas flows through the fracture cell at 510 scf/hr on the vertical wellbore baseline setup is shown. No 2nd order bandpass Butterworth filter is applied to the data set. The lab noise below 200 Hz still can be seen on the plot. The dynamic range of the plot is increased to 35 dB to 80 dB.

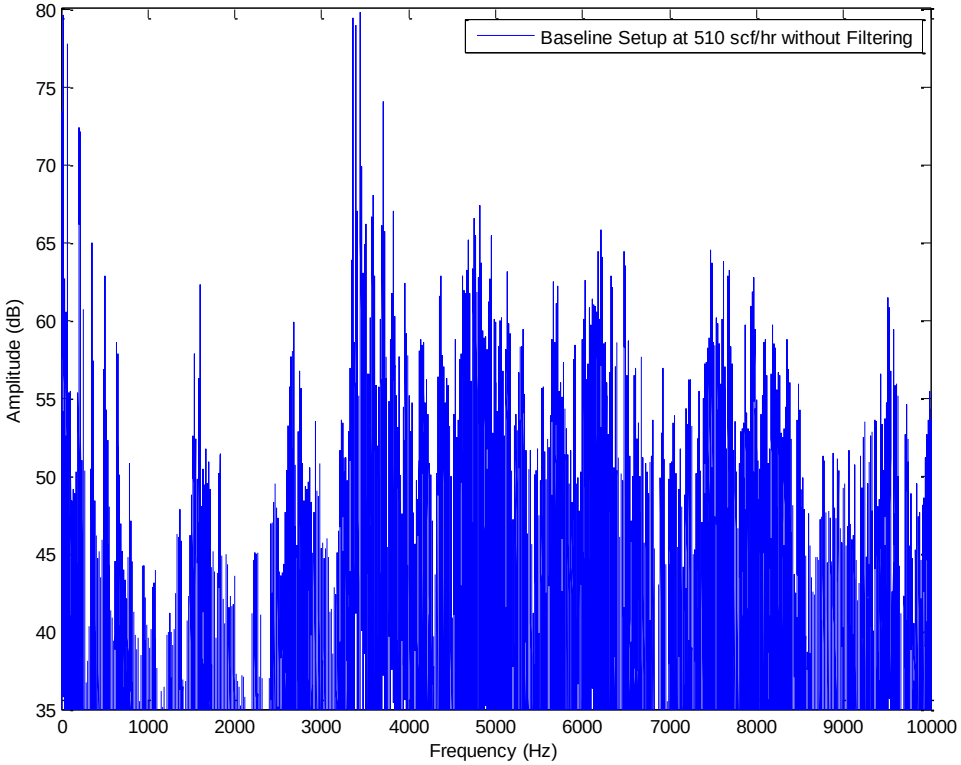

Figure 80: Baseline Setup Flow Rate at 510 scf/hr without Filtering on dB Scale

In Figure 80, nitrogen gas flows through the fracture cell at 510 scf/hr on the vertical wellbore baseline setup is shown. Bandpass second order Butterworth filter is applied to the data set with cutoff frequencies at 1 kHz and 7 kHz. The lab noise below 200 Hz is filtered out on the plot. The dynamic range of the plot is kept at 35 dB to 80 dB.

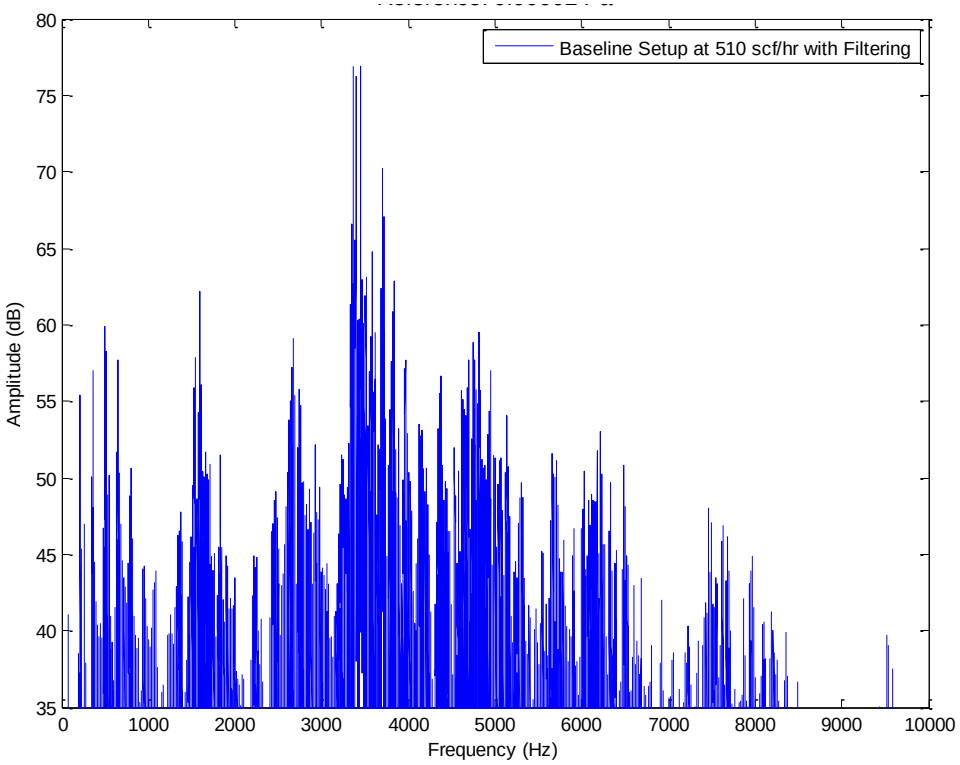

Figure 81: Baseline Setup Flow Rate at 510 scf/hr with Filtering on dB Scale

APPENDIX C

LAB DATA FORMAT DESCRIPTION

All of the lab data taken during the experiments are recorded following a systematic naming convention. To better organize the large number of data sets, a unique data set number is assigned to each data set and the lab experimental setting is recorded in a table. Hydrophone and microphone data are saved in folders with hierarchy. The top level fold is named ‘month + date + year”. This level of folders specifies the date experiment took place. An example is show in Figure 81, the folder highlighted with the name “july072014” means the experimental data took on that particular date. Next folder hierarchy is the experiment number. The number means the order of experiments ran on that day. The next level is the measured data in “csv” extension. The naming convention is “experiment number + month + date + year + _ + xxxpsi.csv” for each acoustic data file. The “xxxpsi” is the injection pressure for that particular data set. For each injection pressure setting, corresponding flow rate measurement is taken.

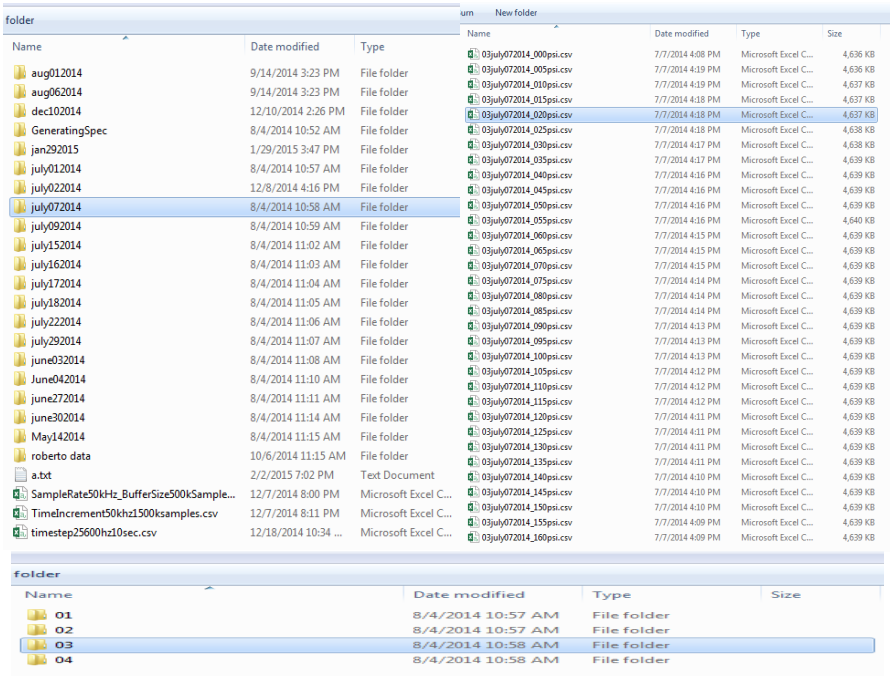

Figure 82: Screen Shot of Experimental Data Folder Hierarchy

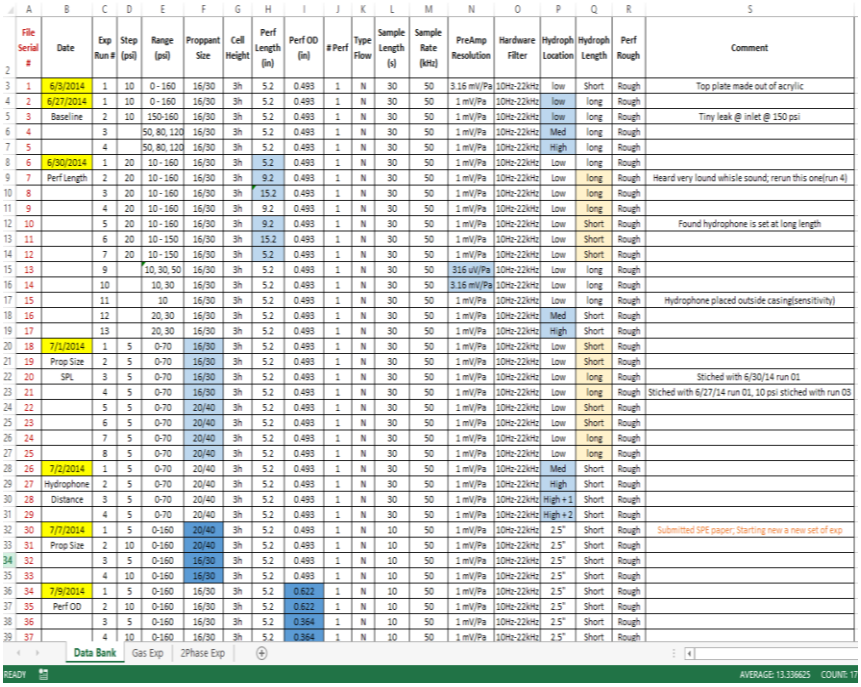

File Serial #	Date	Exp Run #	Step (psi)	Range (psi)	Proppant Size	Cell Height	Perf Length (in)	Perf OD (in)	# Perf	Type Flow	Sample Length (s)	Sample Rate (kHz)	PreAmp Resolution	Hardware Filter	Hydroph Location	Hydroph Length	Perf Rough	Comment
1	6/3/2014	1	10	0 - 160	16/30	3h	5.2	0.493	1	N	30	50	3.16 mV/Pa	10Hz-22kHz	low	Short	Rough	Top plate made out of acrylic
2	6/27/2014	1	10	0 - 160	16/30	3h	5.2	0.493	1	N	30	50	1 mV/Pa	10Hz-22kHz	low	long	Rough	
3	Baseline	2	10	150-160	16/30	3h	5.2	0.493	1	N	30	50	1 mV/Pa	10Hz-22kHz	low	long	Rough	Tiny leak @ inlet @ 150 psi
4		3		50, 80, 120	16/30	3h	5.2	0.493	1	N	30	50	1 mV/Pa	10Hz-22kHz	Med	long	Rough	
5		4		50, 80, 120	16/30	3h	5.2	0.493	1	N	30	50	1 mV/Pa	10Hz-22kHz	High	long	Rough	
6	6/30/2014	1	20	10 - 160	16/30	3h	5.2	0.493	1	N	30	50	1 mV/Pa	10Hz-22kHz	Low	long	Rough	
7	Perf Length	2	20	10 - 160	16/30	3h	9.2	0.493	1	N	30	50	1 mV/Pa	10Hz-22kHz	Low	long	Rough	Heard very loud whisle sound; rerun this one(run 4)
8		3	20	10 - 160	16/30	3h	15.2	0.493	1	N	30	50	1 mV/Pa	10Hz-22kHz	Low	long	Rough	
9		4	20	10 - 160	16/30	3h	9.2	0.493	1	N	30	50	1 mV/Pa	10Hz-22kHz	Low	long	Rough	
10		5	20	10 - 160	16/30	3h	9.2	0.493	1	N	30	50	1 mV/Pa	10Hz-22kHz	Low	Short	Rough	Found hydrophone is set at long length
11		6	20	10 - 150	16/30	3h	15.2	0.493	1	N	30	50	1 mV/Pa	10Hz-22kHz	Low	Short	Rough	
12		7	20	10 - 150	16/30	3h	5.2	0.493	1	N	30	50	1 mV/Pa	10Hz-22kHz	Low	Short	Rough	
13		9		10, 30, 50	16/30	3h	5.2	0.493	1	N	30	50	316 uV/Pa	10Hz-22kHz	Low	long	Rough	
14		10		10, 30	16/30	3h	5.2	0.493	1	N	30	50	3.16 mV/Pa	10Hz-22kHz	Low	long	Rough	
15		11		10	16/30	3h	5.2	0.493	1	N	30	50	1 mV/Pa	10Hz-22kHz	Low	long	Rough	Hydrophone placed outside casing(sensitivity)
16		12		20, 30	16/30	3h	5.2	0.493	1	N	30	50	1 mV/Pa	10Hz-22kHz	Med	Short	Rough	
17		13		20, 30	16/30	3h	5.2	0.493	1	N	30	50	1 mV/Pa	10Hz-22kHz	High	Short	Rough	
18	7/1/2014	1	5	0-70	16/30	3h	5.2	0.493	1	N	30	50	1 mV/Pa	10Hz-22kHz	Low	Short	Rough	
19	Prop Size	2	5	0-70	16/30	3h	5.2	0.493	1	N	30	50	1 mV/Pa	10Hz-22kHz	Low	Short	Rough	
20	SPL	3	5	0-70	16/30	3h	5.2	0.493	1	N	30	50	1 mV/Pa	10Hz-22kHz	Low	long	Rough	Stiched with 6/30/14 run 01
21		4	5	0-70	16/30	3h	5.2	0.493	1	N	30	50	1 mV/Pa	10Hz-22kHz	Low	long	Rough	Stiched with 6/27/14 run 01, 10 psi stiched with run 03
22		5	5	0-70	20/40	3h	5.2	0.493	1	N	30	50	1 mV/Pa	10Hz-22kHz	Low	Short	Rough	
23		6	5	0-70	20/40	3h	5.2	0.493	1	N	30	50	1 mV/Pa	10Hz-22kHz	Low	Short	Rough	
24		7	5	0-70	20/40	3h	5.2	0.493	1	N	30	50	1 mV/Pa	10Hz-22kHz	Low	long	Rough	
25		8	5	0-70	20/40	3h	5.2	0.493	1	N	30	50	1 mV/Pa	10Hz-22kHz	Low	long	Rough	
26	7/2/2014	1	5	0-70	20/40	3h	5.2	0.493	1	N	30	50	1 mV/Pa	10Hz-22kHz	Med	Short	Rough	
27	Hydrophone	2	5	0-70	20/40	3h	5.2	0.493	1	N	30	50	1 mV/Pa	10Hz-22kHz	High	Short	Rough	
28	Distance	3	5	0-70	20/40	3h	5.2	0.493	1	N	30	50	1 mV/Pa	10Hz-22kHz	High + 1	Short	Rough	
29		4	5	0-70	20/40	3h	5.2	0.493	1	N	30	50	1 mV/Pa	10Hz-22kHz	High + 2	Short	Rough	
30	7/7/2014	1	5	0-160	20/40	3h	5.2	0.493	1	N	10	50	1 mV/Pa	10Hz-22kHz	2.5"	Short	Rough	Submitted SPE paper; Starting new a new set of exp
31	Prop Size	2	10	0-160	20/40	3h	5.2	0.493	1	N	10	50	1 mV/Pa	10Hz-22kHz	2.5"	Short	Rough	
32		3	5	0-160	16/30	3h	5.2	0.493	1	N	10	50	1 mV/Pa	10Hz-22kHz	2.5"	Short	Rough	
33		4	10	0-160	16/30	3h	5.2	0.493	1	N	10	50	1 mV/Pa	10Hz-22kHz	2.5"	Short	Rough	
34	7/9/2014	1	5	0-160	16/30	3h	5.2	0.622	1	N	10	50	1 mV/Pa	10Hz-22kHz	2.5"	Short	Rough	
35	Perf OD	2	10	0-160	16/30	3h	5.2	0.622	1	N	10	50	1 mV/Pa	10Hz-22kHz	2.5"	Short	Rough	
36		3	5	0-160	16/30	3h	5.2	0.364	1	N	10	50	1 mV/Pa	10Hz-22kHz	2.5"	Short	Rough	
37		4	10	0-160	16/30	3h	5.2	0.364	1	N	10	50	1 mV/Pa	10Hz-22kHz	2.5"	Short	Rough	

Figure 83: Screen Shot of Experimental Data Record Matrix

To obtain information on the conditions when experiment was conducted, an experiment data matrix is maintained for record keeping purpose. All of the experimental conditions are recorded on the matrix. A screen shot of the matrix is shown in Figure 82. Data and experiment number can be used as a guide going into the folder hierarchy to locate a particular data set. The top folder hierarchy level is the date column and the second folder hierarchy level is the experiment number column. A column named “Comment” records any logs occur during each experiment.